UNIVERSITY OF OKLAHOMA

GRADUATE COLLEGE

STRENGTHS AND LIMITATIONS OF NSSL'S EXPERIMENTAL WARN-ON-FORECAST SYSTEM FOR ENSEMBLES IN FORECASTING CYCLIC MESOCYCLOGENESIS

A THESIS

SUBMITTED TO THE GRADUATE FACULTY

in partial fulfillment of the requirements for the

Degree of

MASTER OF SCIENCE IN METEOROLOGY

By

KELSEY BRITT
Norman, Oklahoma
2018

STRENGTHS AND LIMITATIONS OF NSSL'S EXPERIMENTAL WARN-ON-FORECAST SYSTEM FOR ENSEMBLES IN FORECASTING CYCLIC MESOCYCLOGENESIS

A THESIS APPROVED FOR THE
SCHOOL OF METEOROLOGY

BY

Dr. Pamela Heinselman, Chair

Dr. Patrick Skinner

Dr. Steven Cavallo

Dr. Xuguang Wang

Acknowledgments

First, I would like to acknowledge and thank my advisors: Dr. Pamela Heinselman and Dr. Patrick Skinner. Without them this project would not have been possible. They stood behind me throughout this journey and gave me the guidance I needed to complete this research. Thank you for your continued patience, encouragement, motivation, and feedback as I worked on this project. I'd also like to thank my committee members: Dr. Steven Cavallo and Dr. Xuguang Wang. I am very grateful for their feedback on this project and how I could improve it in the future. Thank you for agreeing to be on my committee to help and guide me through this Master's program.

Next, I'd like to thank Kent Knopfmeier for his work in running NEWS-e at 1-km grid spacings, which was a huge part of this research. I appreciate him taking the time out of his very busy schedule to work with me to discuss the best way to run NEWS-e at 1 km, and then running the system to give me the data to work with. I'd like to acknowledge everyone at NSSL and CIMMS for their guidance, feedback, and encouragement on my project. I have had multiple beneficial and fulfilling conversations with many people from these institutions, which have allowed me to improve this work. I know that if I am ever struggling and am in need of help, I could approach anyone in these groups and will receive the guidance that I need.

Also, I'd like to acknowledge all of the great faculty, staff, and other students in the School of Meteorology. I've had many great professors that challenged me throughout my Masters work and made me a stronger student and professional. Thank you to all of the staff who keep their doors open to all of us graduate students and are there for us when we simply need someone to confide in. You have no idea how much we all appreciate it. Your unwavering support has helped me, and many of us graduate students, get through some really tough times and for that I am grateful. Next, to all of my fellow graduate students: thank you for being there for me when I needed help. Whether it was a Python question,

needing feedback on presentation skills, or just needing a shoulder to cry on, I've always had someone that was willing to be there for me.

Lastly, I'd like to thank my family and friends, both in Oklahoma and back home in Ohio. I've had so much support from all of you and it's been the driving factor that has pushed me to finish strong. Thank you for believing in me, even when I didn't believe in myself. I know that no matter what situation I find myself in, my family and friends will have my back. I'd like to make a special acknowledgement to my brother, Connor Britt, for being my guinea pig and taking the time to help me create a color-blind friendly color scheme for some of my research figures. Finally, to my dog, Beau, who loves me unconditionally and is the best stress-reliever (and causer) in the world. He would always remind me to take much-needed breaks from work and kept me sane throughout the whole graduate process.

Table of Contents

List of Tables

List of Figures

Abstract

Cyclic mesocyclogenesis is the process by which a supercell produces multiple mesocyclones with similar life cycles. Supercells that exhibit cyclic mesocyclogenesis (i.e. cyclic supercells) have the potential to produce several tornadoes that could cause widespread damage. Therefore, having the ability to forecast the potential for cyclic supercells may be beneficial for forecasters when issuing watches and warnings. However, idealized simulation studies of cyclic mesocyclogenesis have found the process to be highly sensitive to both environmental and computational parameters. Thus, whether or not short-term, storm-scale numerical weather prediction models can actually resolve and predict cycling has yet to be determined. This study performs three sensitivity experiments using forecasts generated by NSSL's Experimental Warn-on-Forecast System for Ensembles (NEWS-e) for four cyclic supercells occurring on 9 May, 16 May, and 18 May 2017. NEWS-e, created as part of the Warn-on-Forecast (WoF) initiative, is a convection-allowing ensemble with 18 forecast members. The sensitivity experiments included changing the NEWS-e horizontal grid spacing from 3 km to 1 km, examining the effects of each forecast member's different PBL and radiation schemes, and analyzing how changes in the environment across the different storms can affect the cycling process. Analysis of the individual ensemble members is conducted to assess the capability of a NEWS-e to resolve and predict cyclic mesocyclogenesis, and whether this process is physically representative of the current understanding of cyclic supercells. To provide a source of verification for the NEWS-e forecasts, a database of observations was created from manually analyzed WSR-88D radar reflectivity and radial velocities for each supercell.

Based on past research, the coarsest grid resolution thought to resolve cycling was 1 km. However, seven 3-km, NEWS-e forecasts for 18 May 2017 show evidence of cyclic mesocyclogenesis-like processes occurring in both cyclic supercells observed that day. When the NEWS-e grid spacing was changed to 1 km, cycling was observed more frequently than at 3 km, but there was little skill in NEWS-e predicting the timing of cycles compared to observations. Also, PBL and radiation parameterizations showed no clear impact on cyclic mesocyclogenesis. Analysis of storm-relative helicity (SRH) 0–1 km fields show differences between cycling and noncycling forecast members. Noncycling members had higher SRH values than those members that exhibited cyclic mesocyclogenesis. Given the limited dataset, NEWS-e shows promise in forecasting the probability that cyclic supercells can occur on a given day.

Chapter 1

Introduction and Motivation

Forecasting severe weather, especially supercells, has improved significantly since the late 1900s. During this time, models typically had relatively coarse grid spacing, e.g. greater than 4 km. Due to the resolution being too coarse to resolve convective-scale features, convective parameterizations were required. In contrast, convection-allowing models do not parameterize convection as the grid spacing is fine enough to partially resolve it (>4 km). However, deep, moist convection isn't fully resolved until grid spacings are on the order of 100 m (Bryan et al. 2003). Models with these fine grid spacings are referred to as convection-resolving. Until convection-resolving systems can be fully inputed, predictability of finescale storm hazards will be limited (Potvin and Flora 2015). Even though convective-allowing models can only partially resolve the processes within deep, moist convection, the understanding of convective events by enhancing storm structure and evolution has increased (e.g. Adlerman and Droegemeier 2002; Stensrud and Gao 2010; Wheatley et al. 2015; Yussouf and Stensrud 2010; Schwartz et al. 2017).

An increased understanding of the physical processes that form different types of severe weather, such as supercells, lead to the discovery of a subset of supercells. This subgroup of supercells undergoes different processes of formation, evolution, and decay than the 'classic' supercell case. A classic supercell has one persistent, deep, rotating updraft known as a mesocyclone (further explained in 2.1). However, there is a type of supercell that produces multiple mesocyclones with similar life cycles through a process known as cyclic mesocyclogenesis (Darkow and Roos 1970). These supercells are known as cyclic supercells. Cyclic supercells were first documented during the Palm Sunday Outbreak of 11 April 1965 (Fujita et al. 1970), but have been commonly noted in later studies (e.g. Lemon and Doswell 1979; Burgess et al. 1982; Dowell and Bluestein 2002b; Adlerman et al. 1999; Beck et al. 2006; French et al. 2008, etc.). These supercells produce multiple mesocyclones that can have lifespans that last up to an hour or more. Compared to the ‘classic’ supercell case, cyclic supercells have the potential to have longer durations (e.g. Burgess et al. 1982). The longer lifespans of cyclic supercells results in more opportunities to produce damage through high winds, hail, flooding, or destructive tornadoes. On the other hand, rapidly-cycling supercells may have a lower potential in generating long-track tornadoes due to circulations occluding so quickly that tornadogenesis is hindered (Dowell and Bluestein 2002b; Beck et al. 2006; French et al. 2008). Thus, accurate prediction of cyclic mesocyclogenesis can provide more specific guidance of severe thunderstorm threats to forecasters and the public.

The capability of convection-allowing systems to potentially predict the processes of cyclic mesocyclogenesis has not been explored. Since these systems are used by forecasters, this research strives to answer the following question: can these systems be used to resolve and predict cyclic mesocyclogenesis? This question is broken down into two parts: 1) can convection-allowing systems resolve cyclic mesocyclogenesis? and 2) are these processes physically realistic compared to what we already know about cyclic supercells? In other words, is the model able to capture the intensification of the rear-flank downdraft, the surging of the rear-flank gust front, the occlusion of the mesocyclone, and the rearward movement of the mesocyclone into the heavy precipitation core (e.g., Burgess et al. 1982; Adlerman et al. 1999)?

To explore these questions, this research uses the National Severe Storm Laboratory’s Experimental Warn-on-Forecast System for ensembles (NEWS-e; Wheatley et al. 2015), which is a convection-allowing, short-term (0-3 hr) prediction system. Warn-on-Forecast (WoF) is an ongoing paradigm shift that focuses on short-term forecasting and increasing warning lead times for severe thunderstorm hazards (Stensrud et al. 2009, 2013; Wheatley et al. 2015). The ensemble consists of 18 forecast members that each have different combinations of physical parameterizations and boundary conditions. Three sensitivity experiments will be conducted using NEWS-e to better understand which, if any, of the computational parameters tested best enhance the capability to resolve and predict cyclic mesocyclogenesis. In the first sensitivity study, NEWS-e forecasts are produced using 3-km and 1-km grid spacing. These forecasts are then analyzed for evidence of cycling characteristics, and compared to determine the impacts of grid spacing on the evolution of cyclic mesocyclogenesis. Next, individual ensemble members are compared to each other to examine any differences in cyclic supercell evolution based on the associated planetary boundary layer (PBL) and radiation (shortwave and longwave) parameterizations. The last sensitivity experiment analyzes four supercells from three different days, each of which have different environmental conditions, to examine the environmental impact on cyclic mesocyclogenesis.

In addition to the sensitivity experiments, WSR-88D (Weather Surveillance Radar 1988 Doppler) radar reflectivity and velocity data are examined for each of the supercells of interest and serve as verification dataset for the NEWS-e forecasts. The observations from each of the four supercells are compared to the NEWS-e 3-km and 1-km forecasts to see if there is any skill in how cyclic mesocyclogenesis is predicted and resolved with changing grid resolution. Since the eventual goal of WoF is to have NEWS-e on a 1-km grid, this research will help to identify the strengths and limitations of moving to a finer grid spacing, using its current configuration. Differences in how the four supercells evolve and cycle between the three sensitivity experiments will offer guidance in what information is lost or gained when NEWS-e transitions to a 1-km grid in the future.

Chapter 2

Review of Literature

2.1 Supercell Dynamics

2.1.1 Supercell Environments and Visual Features

Supercells are long-lived storms that are characterized by a strong, rotating updraft known as a mesocyclone. Supercells are less likely to occur compared to other convective storms, but they are responsible for a large number of severe weather reports (hail, strong winds, and violent tornadoes; Lemon and Doswell 1979). The reason these storms have a lower probability of occurring than other storms is because supercells require environments with large amounts of vertical wind shear throughout the depth of the troposphere (e.g. Lemon and Doswell 1979 and references therein). Hodographs are plots of the vertical wind shear (both directional and speed) between different height levels. The more directional vertical wind shear in the environment, the more the hodograph will curve. For example, veering hodographs are conducive for supercells because they often indicate there are high amounts of vertical wind shear throughout the depth of the troposphere. The curve of the hodograph is not necessarily required for a supercell to form, but it does aid in the storm's development (Brooks and Wilhelmson 1993). Highly-curved hodographs in the low-levels are reminiscent of a low-level wind maximum or jet. This maximum increases storm-relative flow into the storm, which enhances the updraft and rotation in the midlevels. Increased rotation in the midlevels creates a stronger the vertical perturbation pressure gradient force, which strengthens the updraft further in a positive feedback loop (Brooks and Wilhelmson 1993). The more curvature the hodograph has, the higher the values of storm-relative helicity (SRH). SRH is the measure of the potential for cyclonic updraft rotation in right-moving supercells. The higher the values of SRH the increased threat for strong supercells and tornadoes. Brooks and Wilhelmson (1993) found that storms initialized in environments with higher helicity have stronger updrafts than storms in low-helicity environments. Hodograph curvature also dictates the direction the supercell will propagate from the mean wind shear in the environment. Cyclonic curvature is indicative of warm air advection and large-scale upward motion, which favors the right member of a splitting supercell (Davies-Jones 1984; Rotunno and Klemp 1982; Weisman and Rotunno 2000; Bunkers 2002. This allows for the right-moving supercell to grown upscale, develop and organize its updraft, and form a mesocyclone in the midlevels by ingesting and tilting environmental horizontal vorticity.

Other than the updraft and its associated mesocyclone, a supercell has a few other visual and radar features (Fig. 2.1). One of the most recognizable supercell features is the hook echo seen in radar reflectivities (e.g. Markowski 2002). The hook echo signifies the advection of hydrometeors out of the heavy precipitation region in the core of the storm (to the left of the updraft) by the mesocyclone. The downdraft region (Fig. 2.1) is located near the rear of the supercell and, because of its location, is closely involved with the hook echo. This area is known as the rear-flank downdraft (RFD). It has long been thought that the RFD forms when dry air in the mid and upper levels impinge on the backside of the updraft. This leads to evaporative cooling and negative buoyancy, which causes downward accelerations (Markowski et al. 2002 and references therein). Downward-directed vertical pressure gradient forces may also play a role in the development of the RFD, but the extent to which process affects the RFD more is not yet known. The descending air of the RFD spreads out as it comes in contact with the surface. This produces a surface kinematic boundary known as the rear-flank gust front (RFGF). Lemon and Doswell (1979) showed the presence of another downdraft they named the forward-flank downdraft (FFD) because of its location on the forward-flank of the supercell. However, recent research (e.g. Dowell and Bluestein 2002b; Beck et al. 2006; French et al. 2008, etc.) has found that the FFD and its associated forward-flank gust front (FFGF) are either weak or nonexistent. Therefore,

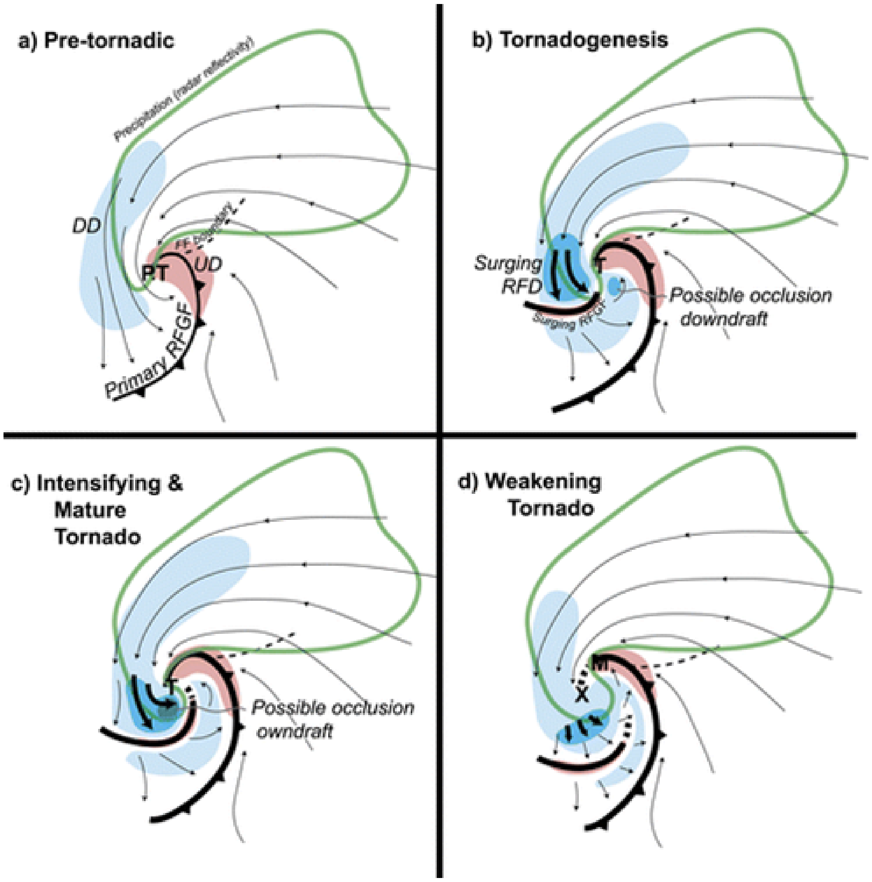

Figure 2.1: Diagram of the low-level structure of a tornadic supercell. Areas of downdraft are marked in blue (DD), updraft core in red (UD), the boundaries of the rear-flank and forward-flank outflow are labeled, precipitation core is in green, and the horizontal flow is depicted as streamlines. PT, T, M, and X denote pretornadic vortex, tornado, location of newly forming low-level mesocyclone, and a dissipating tornado, respectively (adapted from Marquis et al. 2016, their Fig 3).

the RFGF is the most important for providing a source of lift for new updrafts and mesocyclones to form, such as in the process of cyclic mesocyclogenesis as discussed later in Section 2.2.

2.1.2 Mid-level and Low-Level Mesocyclogenesis

Understanding what causes mid-level and low-level mesocyclogenesis in a supercell is important for identifying the differences when analyzing cyclic supercells. As mentioned in the previous section, strong vertical wind shear is important in creating a favorable environment for supercells. The horizontal vorticity generated by the vertical wind shear is crucial to the formation of the mid-level mesocyclone. When this horizontal vorticity comes in contact with the updraft, it is tilted into the vertical. This tilting of vorticity causes the updraft to spin and forms a mesocyclone in the mid levels. There are two components of horizontal vorticity to be considered: streamwise and crosswise vorticity. Streamwise vorticity is the component of the horizontal vorticity that is parallel to the storm's inflow, whereas crosswise vorticity is the perpendicular component to the inflow (Davies-Jones 1984; Brooks and Wilhelmson 1993). These components can be visualized by picturing a thrown football. Streamwise vorticity is a correctly-thrown football that spins like a spiral. Crosswise vorticity would be a football that is thrown so that it rotates end over end. Streamwise vorticity is readily available to be ingested into an updraft and tilted into the vertical, whereas crosswise vorticity has to be turned so that it is parallel to the storm inflow before being tilted into the vertical by an updraft (Davies-Jones 1984). It is for this reason that streamwise vorticity is preferred over crosswise, because it can create a mesocyclone quicker than an environment dominated by crosswise vorticity. Once the streamwise vertical vorticity is ingested and tilted by an updraft, it can then be stretched by the updraft causing the vorticity to be amplified, which in turn leads to the intensification of the mid-level mesocyclone (Davies-Jones 1984).

Not only does the environment supply some horizontal vorticity that can be tilted and stretched to form the mid-level mesocyclone, but outflow boundaries produced by the RFD also generates horizontal vorticity due to gradients in buoyancy (e.g. Klemp and Rotunno 1983; Rotunno and Klemp 1985). The RFD and its associated cold pool is most important to the creation of low-level rotation. The cold outflow from the RFD is due to evaporative cooling of hydrometeors that fall in that region. This creates a baroclinic boundary between the cool air of the outflow and the buoyant, warm air of the storm's inflow. Air moves around this boundary creating baroclinically-enhanced low-level horizontal vorticity. Tilting of this vorticity causes more vertical vorticity in the low-levels than the environmental vertical vorticity does. Therefore, to produce a low-level mesocyclone the supercell needs to have formed a extensive precipitation region and outflow to create baroclinically-generated horizontal vorticity (Rotunno and Klemp 1985). This vorticity is then tilted and stretched by the updraft forming a mesocyclone in the low-levels.

For tornadogenesis to occur, the low-level mesocyclone alone is not sufficient. There needs to be vertical vorticity generated near the surface, which the tilting of environmental horizontal vorticity alone can not accomplish. Since air parcels usually have to rise away from the ground as they are tilted by the updraft, this will not produce vorticity near the surface. Therefore, tornadogenesis needs to have a downdraft near the updraft to generate and tilt vertical vorticity at the surface (e.g. Markowski and Richardson 2014). Air parcels can descend through the RFD towards the surface as tilting creates positive vertical vorticity. The baroclinic generation of vorticity allows for the vertical component of the vorticity to be maintained in the horizontal flow at the surface (Markowski and Richardson 2014). Once the surface vorticity is strong enough, it can he stretched into a tornado. The strength of the cold pool also dictates whether a storm has the potential to form a tornado or not (Markowski et al. 2002). The warmer the cold pool the more buoyant the air parcels, which can be more easily lifted and stretched into a tornado vortex.

2.2 Cyclic Mesocyclogenesis

The first conceptual model of cyclic mesocyclogenesis was developed by Burgess et al. (1982), in which the authors examined various cases of mesocyclones from the National Severe Storms Laboratory (NSSL) Doppler radar archive. They sampled about 100 mesocyclones (only 41 were within the 150-km range of the radar) and found 76% of those mesocyclones were comprised of only a single rotating core throughout their lifetimes, while the other 24% had multiple rotating cores.

According to the Burgess model (Fig. 2.2), during the first mesocyclone's mature phase, strong low-level rotation causes the rear-flank gust front to surge ahead of the mesocyclone's right flank and wrap around the mesocyclone. Once the rear-flank gust front wraps around the mesocyclone, it forms an occlusion with the forward-flank gust front, which signals the occlusion of the mesocyclone from the main updraft and warm inflow leading to the mesocyclone's dissipation. The old mesocyclone moves to the left of storm motion and decays fully in the heavy precipitation region of the supercell. Strong convergence at the occlusion point aids in the development of a new vortex. This second mesocyclone is able to organize rapidly and faster than the first because virtual potential temperature and buoyancy gradients are oriented so that streamwise vorticity generation can occur quickly and without delay (Burgess et al. 1982). The subsequent mesocyclones then go through the same cycling process as the first.

The Burgess model was later modified by Dowell and Bluestein (2002b,a), who performed an observational study of a tornadic cyclic supercell. Dowell and Bluestein's (2002a, b) two-part study was the first of its kind to perform a pseudo-dual-Doppler analysis of cyclic tornadogenesis using aircraft data from NCAR's ELDORA (National Center for Atmospheric Research's Electra Doppler Radar system) at close range. They analyzed data from the 8 June 1995 McLean, Texas supercell that produced at least five tornadoes, one of which caused F-5 damage and persisted for 45 min. Most of the observations of cyclic mesocyclogenesis examined in this study were similar to those seen in the Burgess

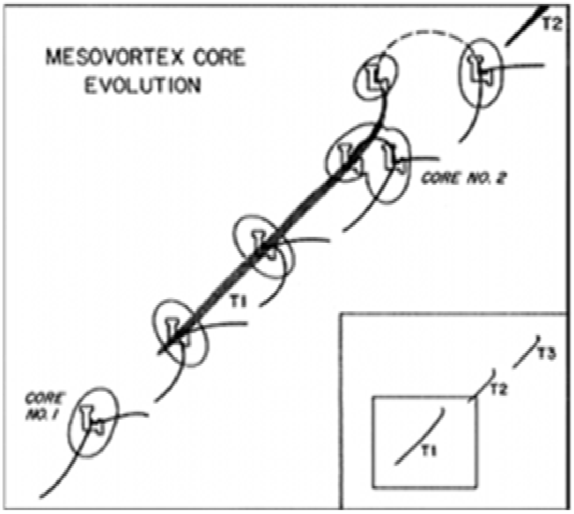

Figure 2.2: Diagram of the Burgess conceptual model for mesocyclone core evolution (adapted from Burgess et al. 1982, their Fig. 3). The inset shows the tornadoes produced by this storm, while the small square in the inset is the area expanded in the figure. The shaded lines represent the tornado tracks and the thin, black lines indicate low-level wind field discontinuities. The ’L’ indicates the circulation core that Lemon and Doswell (1979) mentioned has an evolution similar to that of a synoptic cyclone.

et al. (1982) conceptual model. However, there were a few differences including that low-level mesocyclones and the subsequent tornadoes moved to the left of the mean wind earlier than seen in the Burgess model resulting in more rapid cycling. While Burgess et al. (1982) noted the existence of both the rear-flank and forward-flank gust fronts, Dowell and Bluestein (2002a) found that the forward-flank gust front was either too weak or nonexistent. Thus, any areas of developing vorticity occurred along the rear-flank gust front.

Many of the early observational studies (Burgess et al. 1982; Dowell and Bluestein 2002b,a) did not have high-resolution datasets of cyclic supercells, so numerical studies were performed to get a better understanding of the physical processes contributing to cyclic mesocyclogenesis (e.g. Adlerman et al. 1999; Adlerman and Droegemeier 2002, 2005). Adlerman et al. (1999) used an idealized numerical model with a horizontal grid spacing of 500 m to simulate the process of cyclic mesocyclogenesis. They noted the development of an occlusion downdraft, which is a small-scale intensification of the rear-flank downdraft (RFD). The occlusion downdraft is driven by a downward-directed pressure gradient force that is associated with the intensification of vertical vorticity near the surface, which exceeds that in the midlevels (Klemp and Rotunno 1983; Wicker and Wilhelmson 1995). After its formation, the occlusion downdraft became embedded in the larger-scale RFD and enhanced westerly momentum. This increased momentum causes the RFD gust front to surge ahead of the low-level mesocyclone, to the point where the mesocyclone becomes strongly occluded from the gust front and inflow region. The occluded mesocyclone decays as it becomes completely cut off from the unstable inflow and displaced from the midlevel mesocyclone. This detachment results in a reduced potential for strong, dynamically driven vertical accelerations in the low levels. The old mesocyclone moves to the rear of the storm where it becomes embedded in heavy precipitation and strong buoyancy deficits, which reduce the capacity for upward acceleration of low-level air parcels. As the old mesocyclone decays, a new vortex begins to form along the bulge of the gust front due to enhanced convergence. As this transition from old to new mesocyclone is occurring, the movement of the gust front and cold pool has slowed down, while the RFD decreases in strength in union with the old updraft and its associated mesocyclone decaying. The authors note that the regions of streamwise baroclinic generation are still oriented in a direction favorable for low-level mesocyclogenesis. As the new updraft matures, the inflow increases, and the streamwise baroclinic generation also increases. This set-up is similar to how the first mesocyclone formed, and in this case leads to low-level mesocyclogenesis that creates the second mesocyclone.

Adlerman and Droegemeier (2002) performed experiments using the same case and numerical model as Adlerman et al. (1999) examining the sensitivities of cyclic mesocyclogenesis to horizontal resolution, vertical resolution, numerical diffusion, microphysical parameterization, and surface friction (Fig. 2.3). An important result was that as the horizontal grid spacing became finer, cyclic behavior became more frequent. They also found that cycling was nonexistent at grid spacings coarser than 1 km. Since all of the National Weather Service (NWS) operational convection-allowing models currently used have coarser grid spacing than 1 km, finer grid resolution may be required to provide a forecast of cyclic mesocyclogenesis.

Adlerman and Droegemeier (2005) tested the sensitivity of cyclic mesocyclogenesis to the environmental wind shear and shape of hodographs. This study is the first to define the process of nonoccluding cyclic mesocyclogenesis, which is when the mesocyclones do not go through the occlusion process and instead travel along the gust front. As the weakening mesocyclone moves away from the main updraft, a new mesocyclone forms to the north along the periphery of the forward-flank precipitation region (Fig. 2.4). This study also noted that half-circle hodographs with moderate shear throughout its entire depth were the most favorable for occluding cyclic mesocyclogenesis. Different magnitudes of vertical shear, as well as other hodograph shapes, can dictate if the storm will be steady (i.e., non-cycling) or if it will go through either occluding or nonoccluding cyclic mesocyclogenesis (Fig. 2.5). The straighter the hodograph, the more likely the mesocyclone will go through

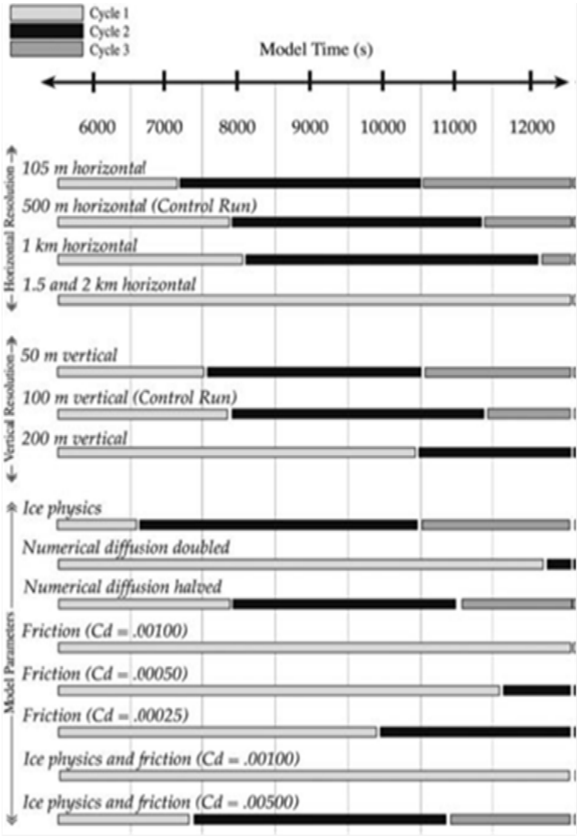

Figure 2.3: Summary of the results from the Adlerman and Droegemeier (2002) numerical study on cyclic mesocyclogenesis and its sensitivity to various computational and physical model parameters (adapted from Adlerman and Droegemeier 2002, their Fig. 2) The figure shows variations in the duration and timing of each cycle for the horizontal and vertical grid resolution experiments, as well as changes in the model physics and parameters.

a nonoccluding cycling process. In contrast, the more curvature the hodograph has with smaller magnitudes of shear, the more likely the storm will exhibit occluding cyclic mesocyclogenesis. High curvature with high amounts of shear will result in storms becoming steady, and therefore exhibit no cycling behavior.

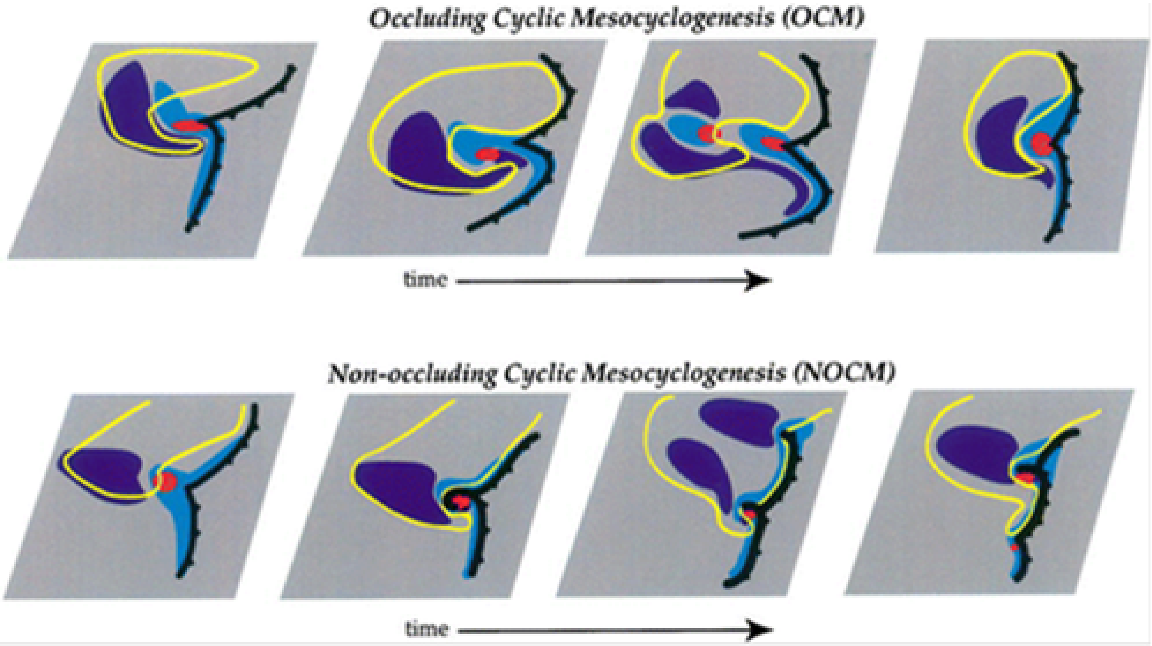

Figure 2.4: Differences in surface patterns between occluding and nonoccluding cyclic mesocyclogenesis (adapted from Adlerman and Droegemeier 2005, their Fig. 3). Dark blue represents downdraft areas, updraft regions are light blue, vorticity maxima are red, and the yellow contour indicates the boundary of the rain area.

As seen from the Adlerman and Droegemeier (2002, 2005) studies, the two modes of cyclic mesocyclogenesis are sensitive to both computational and environmental parameters. This sensitivity presents a challenge in trying to isolate the exact processes responsible for cycling in numerical model output.

Recent observational studies using high-resolution, mobile, Doppler radar data have advanced the understanding of the process of cyclic mesocyclogenesis (Beck et al. 2006; French et al. 2008). Beck et al. (2006) observed a nontornadic, cyclic supercell near Kress, Texas that produced many mesocyclones. The data were collected by Doppler on Wheels

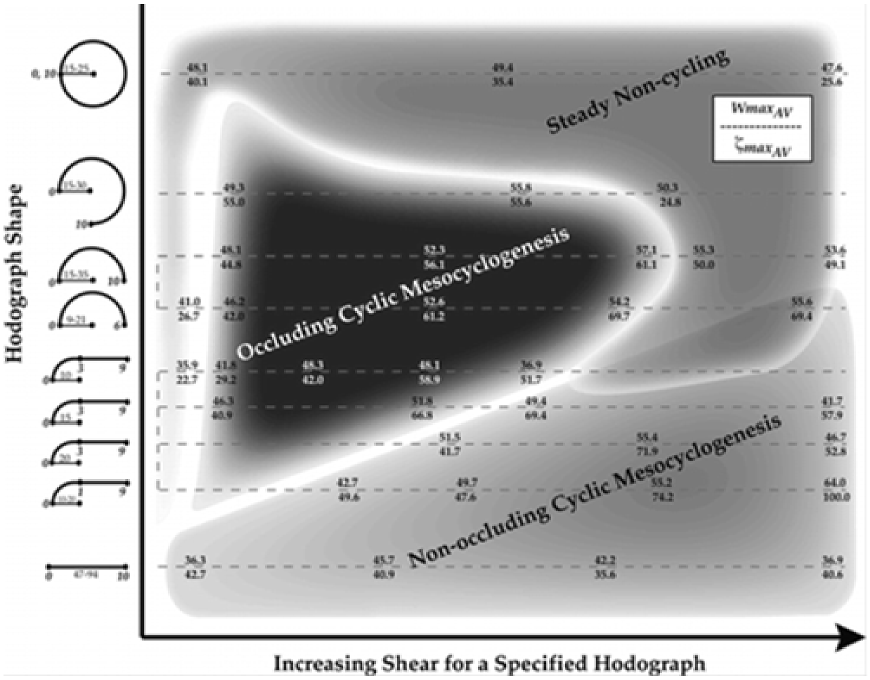

Figure 2.5: Summary of cycling behavior for average shear and hodograph shape (adapted from Adlerman and Droegemeier 2005, their Fig. 22). The numerous simulations are represented by their average vertical velocity maximum (m s^{-1}) and the average low-level vertical vorticity maximum (below 2 km; $\times 10^{-3}$ s^{-1}). The maxima of the values are calculated between 3600 and 14400 s and are domain-wide. The hodographs on the right side of the figure have radii (m s^{-1}) and heights (km; in bold italics) shown.

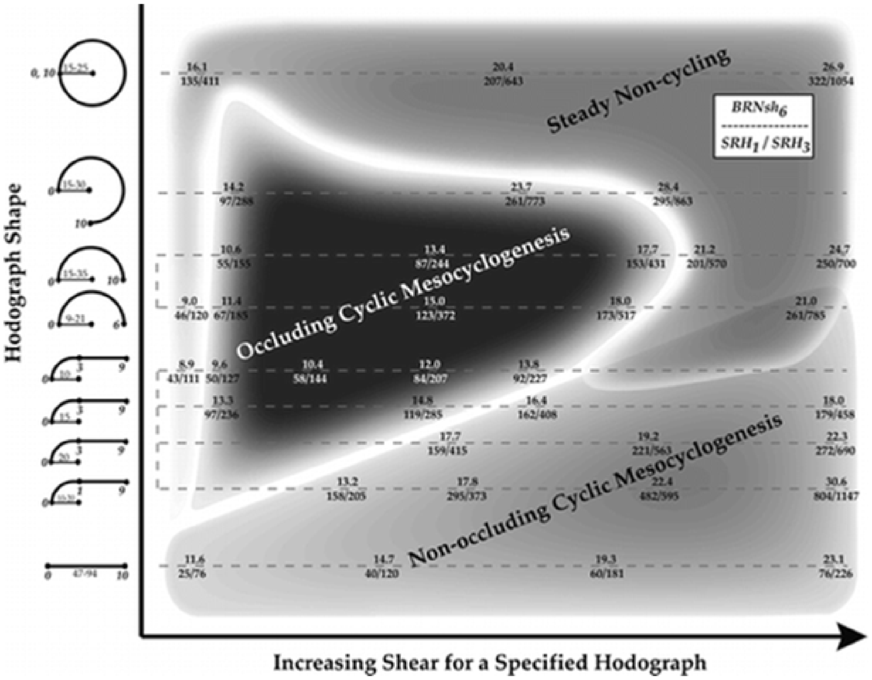

Figure 2.6: Similar to Fig. 2.5, but simulations are represented by Bulk Richardson number shear from 0–6 km, storm-relative helicity from 0–1 km, and storm-relative helicity from 0–3 km (adapted from Adlerman and Droegemeier 2005, their Fig. 21).

(DOW; Wurman et al. 1997) and then used to perform a dual-Doppler synthesis, resulting in the first high-temporal and spatial resolution observational study of a cyclic supercell. They found that the Kress storm exhibited many similarities to previous studies of cyclic tornadic supercells, especially with the conceptual model presented by Dowell and Bluestein (2002b,a). This result suggests there are minimal dynamic differences detected in this study between nontornadic supercells and tornadic supercells analyzed in other studies (e.g. Dowell and Bluestein 2002b). However, there were structural differences between the Kress storm and previous studies. For instance, the cycling frequency of about 6 minutes per cycle was the fastest recorded, which the authors hypothesized may have been due to the slow storm motion and the broad westerly momentum on the southwestern side of the storm. This scenario allowed for the rear-flank gust front to surge far ahead of each of the mesocyclones, leading to rapid cycling. The rear-flank gust front played the major role in the development of the mesocyclones, similar to the Dowell and Bluestein (2002b,a) studies. The rapid cycling was due to an imbalance of the storm's inflow and the rear-flank outflow (Dowell and Bluestein 2002a). The balance between the inflow and outflow also dictated whether vortices would become tornadic or not. When the inflow and RFD outflow were in balance, the vortices could stay close to the RFGF in an area of rich vorticity generation, increasing the potential for tornadogenesis. Finally, Beck et al. (2006) created a hook-echo regeneration model that corresponded to the speed of the cycling frequency and was highly dependent on deformation (Fig. 2.7).

French et al. (2008) also used high-resolution, mobile Doppler radar data to examine the cycling processes of supercells. They found that the majority of the circulations were around 1– 4 km in diameter, had durations around 10–30 minutes, and the tended to dissipate following a decrease in circulation diameter. Mesocyclones of this size and duration could be a constraint on analyzing WSR-88D data in this study. Smaller and short-lived mesocyclones may be missed, while the larger and long-lived mesocyclones will be easier to observe in the data. This study mainly focused on how the low-level circulations

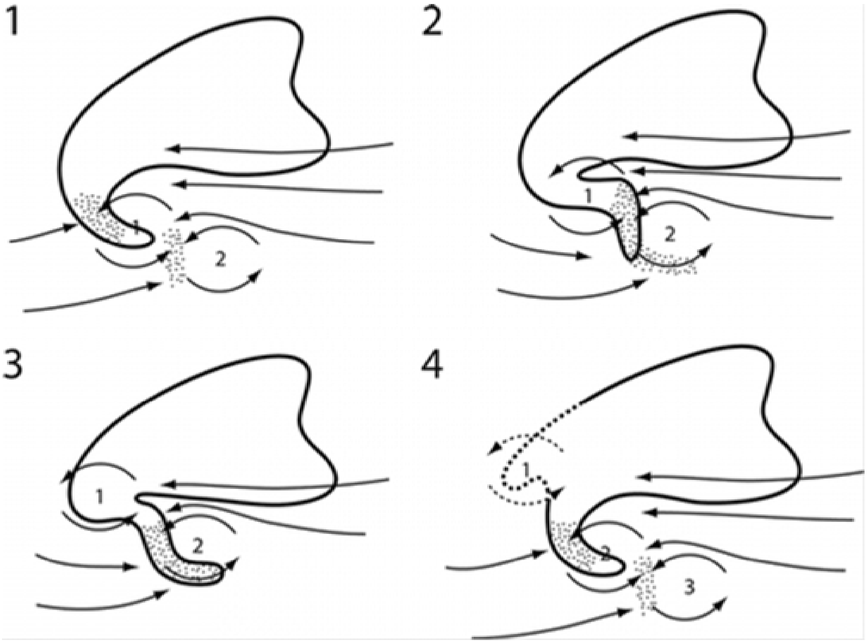

Figure 2.7: Cyclic mesocyclogenesis as related to low-level hook echo regeneration (adapted from Beck et al. 2006, their Fig. 15). The thick, black line outlines the reflectivity echo of the supercell. Strong areas of deformation areas are stippled, while the dashed lines indicate areas of dissipating rotation. Arrows represent the flow of low-level wind field. The mesocyclones are numbered in the order in which they form.

compared with those circulations in the midlevels. Most of the low-level and mid-level mesocyclones were roughly the same mean diameter, and would develop and dissipate at the same time. They noted the regeneration of the hook echo in the radar reflectivity was similar to that outlined in Beck et al.'s (2006) conceptual model.

2.3 Warn-on-Forecast and NEWS-e

NSSL's Warn-on-Forecast (WoF; Stensrud et al. 2009, 2013) initiative strives to produce accurate, probabilistic, short-range (0-3 hr) forecasts for severe convective events. To accomplish this goal, NSSL's Experimental WoF System for ensembles (NEWS-e; Wheatley et al. 2015) uses an ensemble Kalman filter (EnKF; Anderson and Collins 2007; Wheatley et al. 2015) to produce analyses every 15 min by assimilating WSR-88D radial velocities and reflectivities, surface observations from the Oklahoma Mesonet (when applicable), and satellite cloud total liquid water path (Jones et al. 2016). NEWS-e then produces 18-member ensemble forecasts from 1900–0300 UTC for the day of the event.

Many studies have used the EnKF approach with simplified, idealized cloud models and have found that using a storm-scale EnKF to assimilate Doppler radar observations can improve analyses (Snyder and Zhang 2003; Tong and Xue 2005) and forecasts (Yussouf and Stensrud 2010) of supercell thunderstorms. These three studies assumed that the environment was horizontally homogeneous, which is not an accurate representation of the spatial and temporal changes in the real atmosphere. Stensrud and Gao (2010) studied a cyclic tornadic supercell event with an environment that was both horizontally and vertically inhomogeneous. They found that the mesoscale heterogeneity produced more accurate ensemble analyses of a tornadic supercell and improved the forecasts of mesocyclone paths, storm structure, and low-level rotation tracks.

Stensrud and Gao (2010) also examined the influence of grid spacing by running each experiment at 3 km and 1 km. There was improvement in mesocyclone path and storm structure as the horizontal resolution was increased to 1 km. This result suggests that changing the horizontal resolution of NEWS-e from 3 km to 1 km will offer more skill in forecasting supercells. Similarly, Schwartz et al. (2017) found that 3-km ensemble forecasts outperformed the 1-km deterministic forecasts for a mesoscale convective system (MCS). However, 1-km ensembles offer value as they were better at predicting the position and propagation of the MCS compared to the 3-km ensembles. Schwartz et al. (2017) suggested testing the forecasting capabilities of the 1-km ensembles compared to its 3-km counterpart for other severe weather events. Parts of this idea will be addressed in this current research study, as it examines whether using a 1-km ensemble versus a 3-km ensemble will improve the forecast of cyclic mesocyclogenesis in the four supercells examined.

In contrast to idealized simulations, recent studies of a mesoscale convective system (MCS; Wheatley et al. 2014) and a tornadic supercell (Yussouf et al. 2013) have used storm-scale EnKF-based forecast systems together with models that have full physics options, meaning that they include parameterizations for microphysics, radiation, planetary boundary layer, and land surface. The model used in these studies was the Advanced Research Weather Research and Forecasting model (WRF-ARW; e.g. Skamarock et al. 2008), which is the dynamic core used by NEWS-e along with many other convection-allowing models (e.g. HRRR, NSSL-WRF, NCAR ensemble, etc.). The WRF-ARW model in these studies was constructed using boundary and initial conditions from the Global Forecast System (GFS), and then assimilated radar reflectivities, radial velocities and other observations from NOAA's Meteorological Assimilation Data Ingest System (MADIS) using the Data Assimilation Research Testbed software (DART; Anderson and Collins 2007; Anderson et al. 2009). Similarly, Wheatley et al. (2015) used the NEWS-e system with a grid spacing of 3 km, which also applies full model physics, to examine six different severe weather events. They found that NEWS-e produced accurate low-level vorticity swaths, a proxy for mesocyclones, about 30 minutes prior to when the first tornado was observed. Wheatley et al.'s (2015) study noted cyclic characteristics associated with one of the supercell events that occurred on 11 May 2014, but there has yet to be an in-depth analysis using

NEWS-e or any convection-allowing model to examine forecasts of cyclic mesocyclogenesis.

Given that cyclic supercells have longer lifespans (Burgess et al. 1982), NEWS-e forecasts may provide situational awareness of potential storm evolution and cycling to assist forecasters in issuing watches and warnings. Thus, the aim of this study is to test the capability of NEWS-e in resolving cyclic supercells by conducting sensitivity experiments. These experiments examine the influence of grid resolution, environmental conditions like shear magnitude and wind profiles, and PBL and radiation schemes on the physical representation of cyclic mesocyclogenesis. The first experiment tests the sensitivity of cycling to changes in horizontal grid spacing from 3 km to 1 km. Adlerman and Droegemeier (2002) showed that cyclic mesocyclogenesis was only observed when the model's horizontal grid spacing was no coarser than 1 km. Therefore, a hypothesis for this study is that the NEWS-e grid spacing will have to be finer than 3 km to resolve surface small-scale processes such as the surging of the RFGF that triggers cyclic mesocyclogenesis. The second experiment examines the effects of different model parameterizations on cyclic supercells, such as differences between the forecast members' PBL and radiation schemes. The effects that changing these parameterizations will have on the cycling process are unknown. Lastly, differences in the ensemble environmental conditions and their impacts on cyclic mesocyclogenesis will be examined similarly to Adlerman and Droegemeier (2005), who noticed considerable differences in cycling frequency and mode owing to changes in hodograph shape and shear depth. Four supercells from three different days in May 2017 are analyzed that have different environmental conditions (as outlined in 3.1), which may have an impact on whether the supercell goes through occluding or nonoccluding cyclic mesocyclogenesis, or is noncycling.

All of the sensitivity experiments will be compared to observations from WSR-88D radar reflectivities and radial velocities for each supercell on its respective day of the event. The results of these experiments will help guide NEWS-e system development to provide improved short-term, storm-scale forecasts of cyclic supercells, thus furthering the long-term goal of the WoF project.

Chapter 3

Methodology

3.1 WSR-88D Observation Database

To provide verification for the NEWS-e simulations, a radar observation database was created by analyzing WSR-88D reflectivities and radial velocities for each of the four supercells. WSR-88D data were chosen because of its wide availability and use in operations by meteorologists to make their forecasts. Also, WSR-88D radar reflectivities and radial velocities are assimilated into NEWS-e to make the ensemble forecasts. Therefore, WSR-88D data were chosen here as the verification data, and it was the only data available to us at the time.

The Level II NEXRAD (Next-Generation Radar) data were attained from the National Centers for Environmental Information website (NCEI; www.ncdc.noaa.gov/nexradinv), formerly known as the National Climatic Data Center (NCDC). The data were then analyzed using the Gibson Ridge software (GR2Analyst). Since NEWS-e only assimilates radar data up to 150 km in range from a radar site, only data within that radius of the closest radar to the supercell were examined (Table 3.1). One drawback of using WSR-88D data is the temporal frequency at which the radar produces volume scans. Usually these are available every 4–5 min, which can result in the loss of information for processes that can occur quickly, like cyclic mesocyclogenesis and tornadogenesis (e.g., Heinselman et al. 2008; Heinselman and Torres 2011). This temporal problem was mitigated by the incorporation of SAILS (Supplemental Adaptive Intra-Volume Low-Level Scan), in which the lowest elevation scan is completed every 1 min (Tanamachi and Heinselman 2016). These scans are taken halfway through the full volume scan to allow for more information on what is occurring in the low-levels of the storm without having to wait for the full volume scan to complete. SAILSs were available for all three of the case days.

Table 3.1: Radar information for the four cyclic supercell cases.

Case Date	Supercell Name	Radar Site(s) Used	Tilt of Radar Beam (°)	Volume Coverage Pattern(s)
05/09/17	Morton	KLBB	0.445	12, 212
05/16/17	Elk City	KFDR	0.396	212
05/18/17	Corn	KFDR, KTLX	0.396	212
05/18/17	Hennessey	KFDR, KTLX	0.53	212

When interpreting the radar data, only the lowest volume scan angle (Table 3.1) was used to examine each supercell's mesocyclone (Fig 3.1). The exact height of the mesocyclone depended on the distance away from the radar at each time. For cases studied by French et al. (2008), both the mid- and low-level mesocyclones were similar in size and seemed to occlude around the same time. Thus, use of the lowest elevation should provide a representative summary of the cycling process, including the number of mesocyclones, start and end times, duration, intensity, diameter, and cycling frequencies. Two different Volume Coverage Patterns (VCPs) were utilized: 12 and 212 (Table 3.1). VCP 12 was created to meet the demand for faster updates. It has overlapping low-level elevation angles, fast rotation rates to make it useful in viewing severe weather, and samples the vertical structure of storms close to the radar (Brown et al. 2005). VCP 212 is similar to VCP 12, except it works well for distant severe weather. VCP 12 and 212 have update times around 4.5 min.

Radar reflectivities and radial velocities were manually analyzed to locate the mesocyclones in a similar manner to the methods of Thompson et al. (2012, 2017) and Smith et al. (2012, 2013, 2015). Radial velocities were only included if they corresponded to an area of reflectivities $\geq$20 dBZ, to reduce side-lobing and other problems that cause erroneously high and low velocities. Also, velocities were dealiased using GR2Analyst's built-in dealiasing program. In some instances, this dealiasing program would erroneously remove much of the radial velocity data. In those cases, the radial velocities were manually dealiased. Microsoft Excel was used to store all the data and make basic calculations like mesocyclone rotational velocities and diameters. Any problems with the data, such as errors with the dealiasing program or missing radar data bins, were noted for each volume considered.

Even though GR2Analyst has a Mesocyclone Detection Algorithm (MDA) built into the software, it did not reliably identify mesocyclones correctly; therefore subjective analysis based on set criteria was needed for mesocyclone identification. Criteria for the classification of different rotation signatures in WSR-88D data were broken down into four categories (Table 3.2): Mesocyclone, Weak Mesocyclone, TVS (tornado vortex signature) and/or VS (vortex signature). The WSR-88D circulations may have more than one classification (i.e. a circulation can be considered a mesocyclone and a TVS). The mesocyclone criteria were chosen based on past research (Dowell and Bluestein 2002b; Beck et al. 2006; French et al. 2008; Thompson et al. 2012, 2017; Smith et al. 2012, 2013, 2015, and also by keeping in mind the spatial and temporal limitations of the WSR-88D radar data.

Rotational velocities were used as a measure of the mesocyclone's intensity. Rotational velocity is the average of the magnitudes of the maximum inbound and maximum outbound radial velocities within the circulation (Fig. 3.2). Following this definition, rotational velocity was calculated by the equation:

$$RotV = \frac{MaxV_{out} - MaxV_{in}}{2} \tag{3.1}$$

In the above equation, V stands for velocity, and the subscripts "out" and "in" stand for the maximum outbound and maximum inbound velocities, respectively. The maximum inbound and outbound velocities had to be within 10 km of each other to be considered,

Table 3.2: Circulation Criteria

Classification	**Rotational Velocity (ms^{-1})**	**Diameter (km)**	**Other Criteria**
Mesocyclone	≥ 20	1–10	Continuous in time; must be present for at least two consecutive volume scans
Weak Mesocyclone	$15 \leq$ ROT V <20	1–10	Continuous in time; must be present for at least two consecutive volume scans
TVS	≥ 20	<2	Must be associated with tornado report
VS	≥ 20	<2	No tornado report

and had to be within 45° on the beam's centerline to eliminate convergence and divergence signatures.

French et al. (2008) used a rotational velocity threshold of 20 m s^{-1} for a circulation to be considered a mesocyclone when looking at both low- and mid-level mesocyclones. Only one elevation angle was examined in this study, so the exact depth of the mesocyclone is not being considered. Therefore, this study assumes that the mesocyclones are vertically coherent, so the threshold of 20 m s^{-1} was adopted here for a circulation observed on radar to be classified as a mesocyclone. However, there were times when there was a clear circulation present in the radial velocities, but the rotational velocity of this circulation was found to be just below the threshold to be considered a mesocyclone. For these instances, the term "weak mesocyclone" denoted circulations that are under the mesocyclone threshold of 20 m s^{-1}, but greater than 15 m s^{-1}. The rotational velocity threshold of 20 m s^{-1} was adopted by many studies that used mobile Doppler radar data (Beck et al. 2006; French

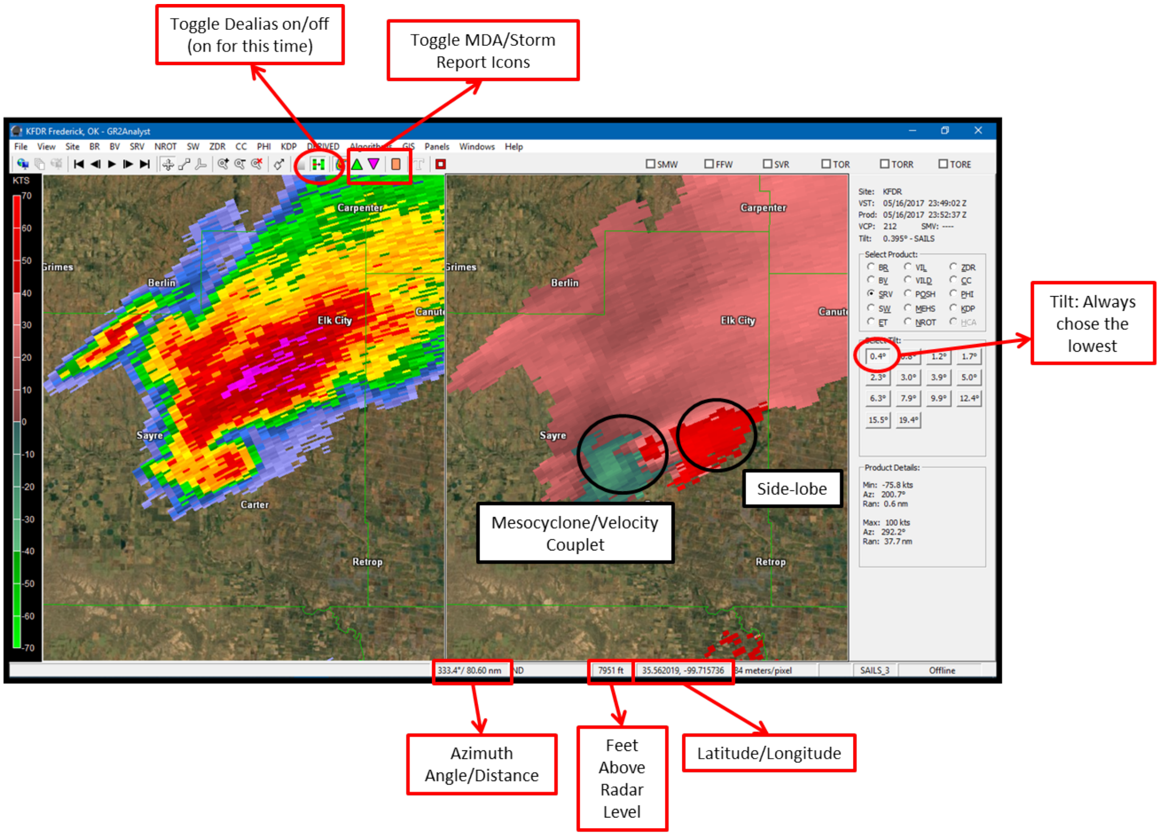

Site: KFDR
VST: 05/16/2017 23:49:02 Z
Prod: 05/16/2017 23:52:37 Z
VCP: 212 SMV: ----
Tilt: 0.395° - SAILS

Product Details:
Min: -75.8 kts
Az: 200.7°
Ran: 0.6 nm

Max: 100 kts
Az: 292.2°
Ran: 37.7 nm

333.4°/ 80.60 nm
7951 ft
35.562019, -99.715736

Figure 3.1: A GR2Analyst screen capture of the 16 May 2017 Elk City supercell at 2352 UTC from KFDR radar site. Numerous parameters were recorded from the subjective assessment of the radar data from each case, including latitude, longitude, feet above radar level of the area of interest, azimuth angle, and distance that were provided or calculated by the GR2Analyst software. This capture also presents features that were used to facilitate finding mesocyclones, such as storm reports.

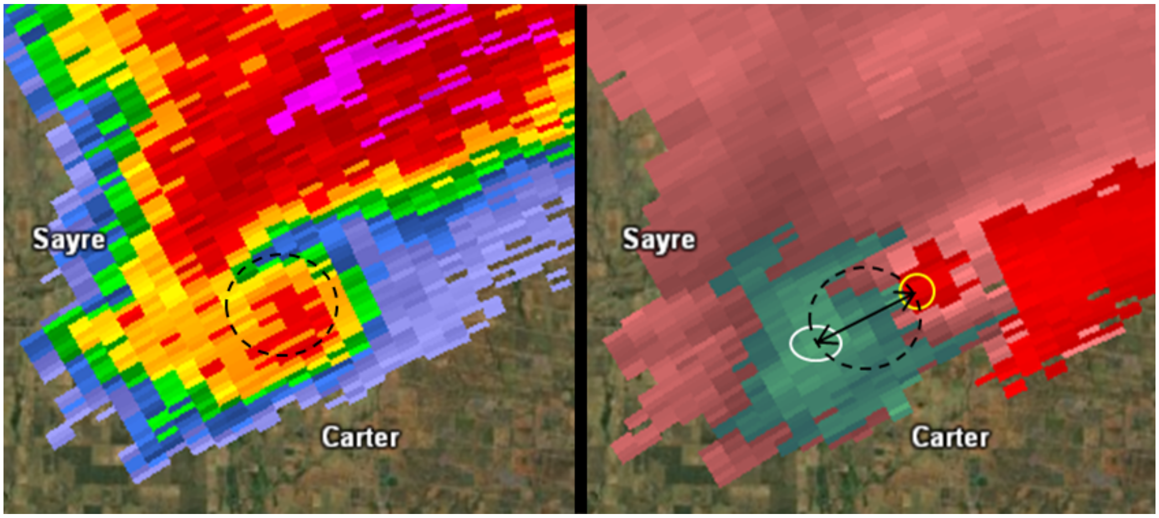

Figure 3.2: Zoomed in version of the hook echo from Fig. 3.1 for the same time. The white circle indicates the location of the maximum inbound velocity, the yellow circle represents the location of the maximum outbound velocity, and the black double arrow shows the distance between the two velocities. The distance of the arrow represents the diameter of the mesocyclone. The dashed black line indicates a rough outline of the mesocyclone.

et al. 2008). The extra classification of "weak mesocyclone" accounts for the lower temporal and spatial resolutions of WSR-88D radar data. Therefore, some mesocyclones may have smaller rotational velocities in WSR-88D data than mobile data because the spatial resolution is coarser.

Another important criteria to classify a circulation as a mesocyclone is the diameter of the circulation. The diameter is found by taking the distance between the maximum inbound velocity to the maximum outbound velocity of the circulation (Fig. 3.2). According to Dowell and Bluestein (2002a), a vortex with a diameter of 2–10 km is considered a mesocyclone. Burgess et al. (1982) found a mean diameter for the mesocyclones they studied to be around 4–5 km. This study uses a diameter threshold for a circulation to be considered a mesocyclone of 1–10 km, which was also adopted by the studies by Beck et al. (2006) and French et al. (2008). Finally, all mesocyclones had to be present for at least two consecutive volume scans (e.g. Thompson et al. 2012; Smith et al. 2012, 2013). Once the circulation lasted for at least two scans, it would be followed in time until it decayed fully (i.e. when it was no longer seen on radar).

Additionally, there were multiple times when a mesocyclone had strengthened and tightened enough to be considered either a TVS or VS. Therefore, another set of criteria were created to highlight these vortex signatures. To be considered a VS, the circulation had to have a rotational velocity $\geq$20 m s^{-1}, a diameter no greater than 2 km, and no tornado reports associated with it at the time and location that the signature occurred (French et al. 2013). A TVS has the same criteria except that it needs to have a corresponding tornado report within 10 min and in the same location that the TVS occurred (French et al. 2013). Depending on the diameters of the TVS or VS, it may also be labeled as a mesocyclone. The extra classification for a TVS and VS was simply to add more information about a tight circulation that may or may not be associated with a tornado.

3.2 NEWS-e Specifications

NEWS-e is an ensemble data assimilation and prediction system that is nested within the experimental High Resolution Rapid Refresh Ensemble (HRRRE) run by the National Oceanic and Atmospheric Administration (NOAA) Earth System Research Laboratory (ESRL). NEWS-e is made up of an ensemble of 36 members from the Advanced Research Weather Research and Forecasting model (WRF-ARW; Skamarock et al. 2008). The 2017 configuration of NEWS-e utilizes various parameterization schemes for longwave and shortwave radiation, and for the planetary boundary layer (PBL; shown in Table 3.4; Wheatley et al. 2015). However, the members all use the NSSL two-moment microphysics scheme (Mansell et al. 2010). NEWS-e is run over a 750×750 km grid with a 3-km horizontal grid spacing. A full list of the physical and computational NEWS-e parameters are shown in Table 3.3.

The High-Resolution Rapid Refresh Ensemble (HRRRE) provides the boundary and initial conditions used to initialize the NEWS-e analyses at 1800 UTC daily. The location of the NEWS-e 3-km domain varies from case to case, and is determined based on the Storm Prediction Center's (SPC) Day 1 Convective Outlook, and is placed over the region that is most favorable for the development of convection. Ensemble analyses are produced every 15 min by assimilating WSR-88D radar reflectivity and radial velocity data, satellite column integrated liquid or ice water path, and Oklahoma Mesonet data (when available) using the Ensemble Kalman Filter (EnKF) technique provided by DART (Anderson and Collins 2007; Anderson et al. 2009). Eighteen member forecasts are issued every half-hour beginning at 1900 UTC and ending at 0300 UTC. The duration of the forecasts is 180 or 90 minutes, depending if the forecast was issued at the top of the bottom of each hour, respectively.

For the purposes of this study, only the last 2 hours of the 3-hr forecasts are used. This is due to the first hour of each forecast containing spurious echoes attributable to imbalance introduced by data assimilation. For instance, if a forecast is initialized at 2000 UTC,

Table 3.3: System Configuration and Physical Parameterizations for NEWS-e

Parameter	**Value/Description**
Horizontal Grid Resolution	3 km
3-km Grid Domain Size	750 x 750 km
Location of Grid	Event specific
1-km Grid Domain Size	Approx. 350 x 350 km
Number of Vertical Levels	51
Vertical Grid Resolution	100 m at surface and 1 km at top (10-hPa)
Grid Points	251 x 251 x 50
Microphysical Scheme (all members)	NSSL 2-moment scheme
PBL Schemes	YSU, MYJ, MYNN
Radiation (shortwave/longwave)	Dudhia/RRTM, RRTMG/RRTMG
Land Surface	RAP Land Surface model
Total number of Ensemble Members	36
Number of Ensemble Forecast Members	18

only the 2100–2300 UTC period of that forecast is examined. The cutoff time of an hour was chosen from results of previous research from Skinner et al. (2018; Fig. 3.3). The results from their research shows that the overforecast of convection at the beginning of each forecast due to spin-up and imbalance usually diminishes within the first hour of the forecast. The overforecast is apparent as a positive bias in the reflectivity objects in the first hour of the forecast (Fig. 3.3b), which arises when spurious echoes in the forecast causing more storms than are observed. After the first hour, however, that bias starts to decrease towards a value of 1, which indicates it is now nearly unbiased. The forecast remains nearly unbiased for the remaining two hours. However, just because the first hour is ignored in this project doesn't discount the usefulness of that first hour. As seen in Fig. 3.3, there is a

Table 3.4: The physics options for NEWS-e ensemble forecast members 1–18 (Wheatley et al. 2015). The NSSL dual-moment microphysics scheme and RAP land surface model are used for all members. For PBL schemes, Yonsei University (YSU), Mellor-Yamada-Janjic (MYJ), and the Mellor-Yamada-Nakanshi-Niino (MYNN) are listed. The radiation parameterizations include Dudhia, Rapid Radiative Transfer Model (RRTM), and Rapid Radiative Transfer Model-Global (RRTMG) schemes.

Parameterizations by Ensemble Member			
Member	*PBL Scheme*	*Shortwave Radiation*	*Longwave Radiation*
1	YSU	Dudhia	RRTM
2	YSU	RRTMG	RRTMG
3	MYJ	Dudhia	RRTM
4	MYJ	RRTMG	RRTMG
5	MYNN	Dudhia	RRTM
6	MYNN	RRTMG	RRTMG
7	YSU	Dudhia	RRTM
8	YSU	RRTMG	RRTMG
9	MYJ	Dudhia	RRTM
10	MYJ	RRTMG	RRTMG
11	MYNN	Dudhia	RRTM
12	MYNN	RRTMG	RRTMG
13	YSU	Dudhia	RRTM
14	YSU	RRTMG	RRTMG
15	MYJ	Dudhia	RRTM
16	MYJ	RRTMG	RRTMG
17	MYNN	Dudhia	RRTM
18	MYNN	RRTMG	RRTMG

high probability of detection (POD) and a low false alarm ration (FAR), which shows that this forecast is skillful. The 90 min forecasts are not considered as too little forecast time following the first hour is available to identify cyclic mesocyclogenesis.

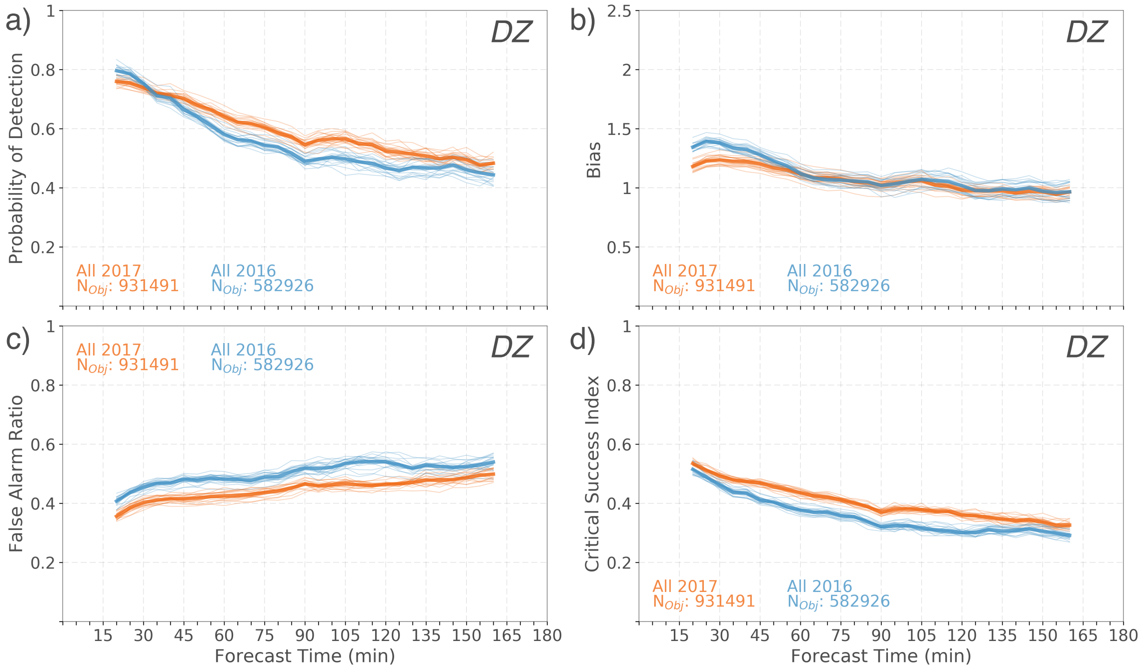

Figure 3.3: Time series of the object-based a) Probability of Detection (POD), b) Bias, c) False Alarm Ratio (FAR), and d) Critical Success Index (CSI) for NEWS-e forecasts of composite reflectivity (DZ; adapted from Skinner et al. 2018, their Fig. 5). The thin lines are each ensemble member, while the thick, bold lines are the ensemble means. The blue lines represent forecasts from 2016, while the orange represent 2017. Bias is a ratio of the amount of convection in the forecast to the amount of observed convection. Bias values greater than 1 indicate the presence of spurious echoes in the forecast. A value closer to 1 indicates forecasts that are unbiased, which occurs just after the first hour of the forecast after the spurious echoes are filtered out of the system.

3.2.1 The Sensitivity Experiments

The first sensitivity experiment consists of running NEWS-e forecasts at a finer horizontal grid resolution of 1 km rather than its standard 3-km grid spacing. The n-down (also know as ndown or nest-down; Skamarock 2004) technique was used to create all of the 1-km forecasts. This process takes the same initial conditions of the 3-km forecast and interpolates them onto a 1-km grid. This method allows for the changes in grid spacing on the forecasts to be more easily seen. If the experiment was rerun at 1 km, then it would include data assimilation at 1 km grid spacing and thus would not be a direct comparison to the 3-km forecasts. The domain size for the 1-km grid is approximately 350 × 350 km and is positioned so that the supercell of interest is close to the center of the domain for all forecast times (Fig. 3.4). Having the supercell in the center of the domain helps limit the impacts of the boundary conditions at longer forecast times.

The last two sensitivity experiments do not require any other changes to NEWS-e. The second experiment will examine differences in each ensemble member's PBL and radiation parameterization schemes (Table 3.4) to see if they have any impact on cyclic mesocyclogenesis. The parameterization schemes for each member remain consistent between the 3-km and 1-km model forecasts. The third experiment will compare the environments between all three cases to examine how the environmental conditions affected cyclic mesocyclogenesis in the model.

3.2.2 NEWS-e Vertical Levels

NEWS-e has 51 vertical terrain-following levels with a spacing of 100 m at the surface and 1 km at the top of the grid, which is also the 10-hPa pressure level. However, out of the 51 levels, 2 of them will be of main interest for this study (Fig. 3.5). French et al. (2008) examined cyclic mesocyclogenesis in the low and midlevels and found that cycling occurred at approximately the same time and frequency. In this study, two vertical levels were chosen to examine cycling in the low and midlevels. These levels are pseudo-constant in height,

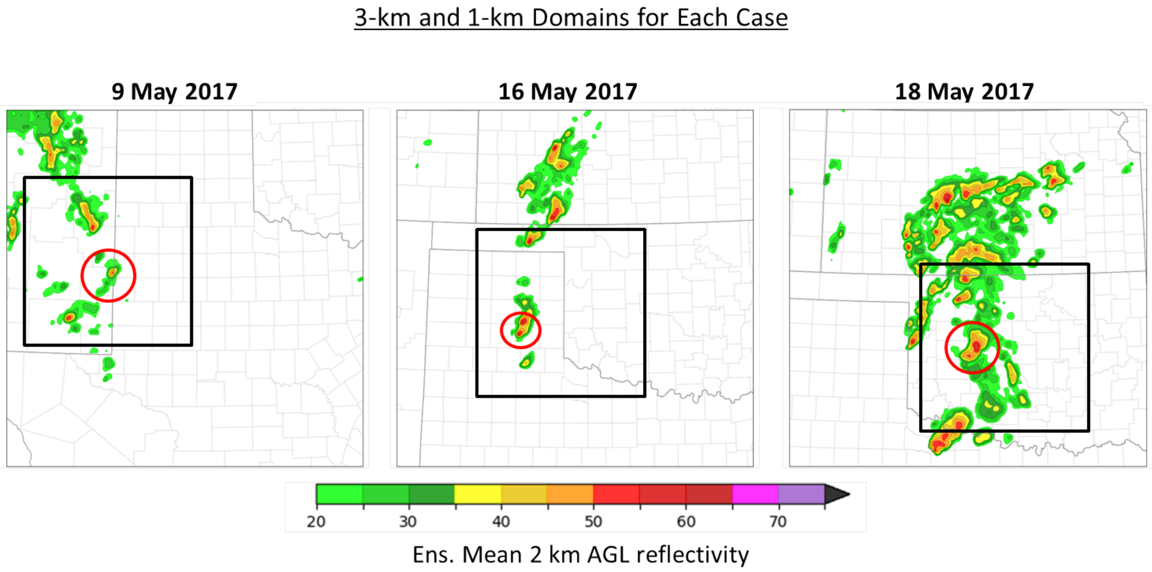

Figure 3.4: Domains for the 3-km and 1-km NEWS-e grids for all three cases. The full domain corresponds to the 3-km grid, the black square indicates the 1-km domain region, and the red circles indicate the supercell of interest. Images for 9 May, 16 May, and 18 May 2017 were taken at the beginning of the 2300, 2100, and 2200 UTC forecasts, respectively. The domains remain constant for all forecast times.

as they have a small range of heights on one level. The tenth vertical level of NEWS-e represents heights of 1–1.2 km AGL (above ground level), and the eighteenth level contains heights of 4.3–4.6 km AGL. However, cycling was found to occur in the low levels at the same time as the midlevels, and the midlevels didn't provide any new information. Therefore, only the low levels will be used to examine cyclic mesocyclogenesis.

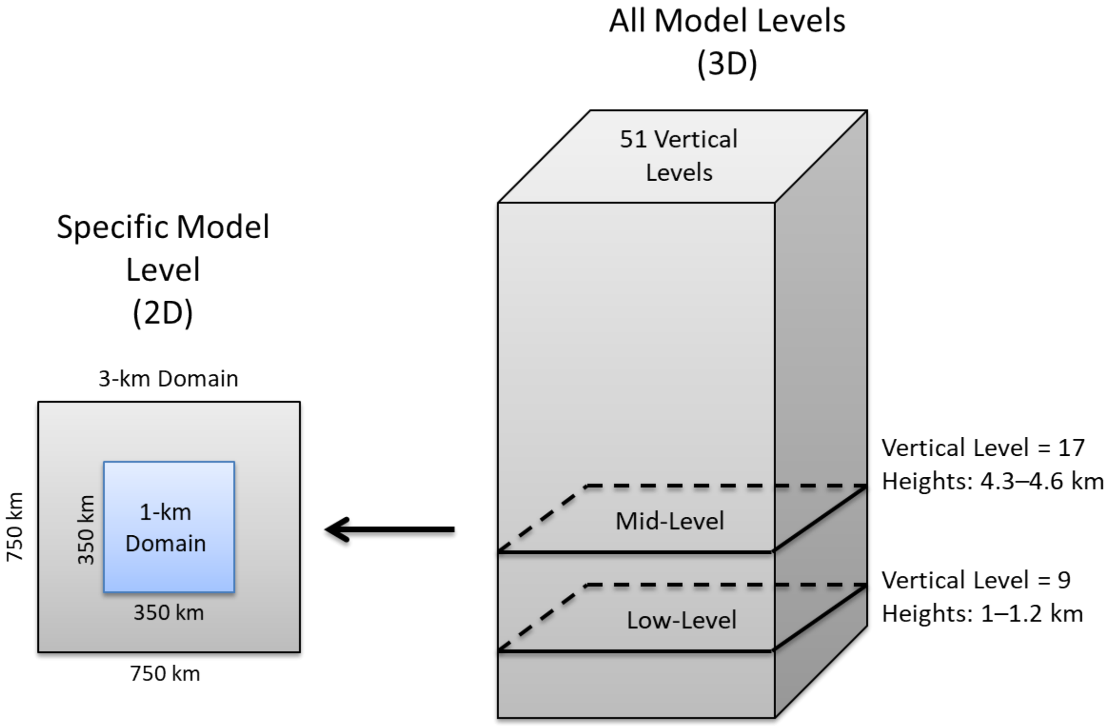

Figure 3.5: Out of the 51 vertical levels in NEWS-e, the 9th and the 17th levels were used the most when plotting model data to to get a representation of both the low and mid levels of the atmosphere. The 9th (17th) level represents the low (mid) levels. The heights AGL (in km) are annotated to the right of the levels.

When plotting the mesocyclone rotation tracks, it was desirable to calculate an average within a specified layer, as was done for multiple variables such as vertical velocity, vertical vorticity, and updraft helicity. When considering a layer to represent the low levels, the variables were calculated between 0.5–1.5 km. For the midlevels, the variables were calculated between 3–5 km. This method was used to smooth over slight disturbances in mesocyclone tracks at each specific level, and get a clearer picture of any cycling that may be occurring.

Chapter 4

Overview of Case Environments

A sample size of four cyclic supercells was chosen to examine if NEWS-e can accurately resolve and predict cyclic mesocyclogenesis (Table 4.1). These four supercells were chosen from three different severe weather days in 2017: 9 May, 16 May, and 18 May. One supercell was analyzed for each day except for 18 May, in which two cyclic supercells formed very close to one another. The first cyclic supercell formed before the first NEWS-e forecast initialization time (around 18 UTC), and therefore NEWS-e only simulated the last half of the storm's evolution before it decayed at 2222 UTC. Another cyclic supercell formed on the first one's rear flank, and merged with the first as it decayed. These supercells were analyzed together because they were both cyclic and provided a long period of cyclic behavior to examine. These two storms also influenced each other. For instance, the storms merged together and the Hennessey storm rained into the rear flank of the Corn storm. This can cause the Corn supercell's RFD to intensify and occlude the mesocyclone. This may also lead to the decay of the Corn storm. Since these supercells are in close proximity and merge with each other, NEWS-e may have a difficult time resolving these storms as two separate cells, especially at coarse resolutions like 3 km. Taking all of these factors into account, both the Corn and the Hennessey supercells storms were analyzed together.

Table 4.1: Overview of the Four Supercell Cases

Date	**Supercell Name**	**Time (UTC) Start - End**	**Total # of Mesocyclones Identified**	**# of Occluding Cycles**	**# of Nonoccluding Cycles**	**# of Tornadoes Reported**
9 May 2017	Morton	2200 - 0548	7	6	0	1
16 May 2017	Elk City	2142 - 0106	3	1	1	5
18 May 2017	Corn	1830 - 2255	9	4	4	2
18 May 2017	Hennessey	2030 - 0015	5	4	0	0

Each of the case days had different environmental conditions, which allows for the environmental impacts on cyclic supercells to be examined, even though the sample size is small. These four supercells occurred in either Texas or Oklahoma, so even though the local environment and terrain were different, the geographic region stayed consistent.

When examining the environmental soundings and other data for each of the supercell cases, various parameters will be examined, such as Convective Available Potential Energy (CAPE), Convective Inhibition (CINH), lifting condensation level (LCL) height, effective bulk wind difference (EBWD), storm-relative helicity (SRH) from 0–1 km, and SRH 0–3 km. Past research on these variables established thresholds that the above are the most favorable for supercell and tornado development (e.g. Davies-Jones 1984, Davies-Jones et al. 1990, Rasmussen and Blanchard 1988, Thompson et al. 2007). The first of these parameters is mixed-layer CAPE, which is the measure of atmospheric instability throughout the mixed layer of the troposphere. The higher the mixed-layer CAPE, the stronger the storm updrafts can be. Forecasters often refer to weak, moderate, high, and extreme instability as CAPE values less than 1000 J kg^{-1}, 1000-2500 J kg^{-1}, 2500-4000 J kg^{-1}, and greater than 4000 J kg^{-1} respectively. CINH is the negative potential buoyancy that vertical motion of air has to overcome to have convection. CINH that is less than -250 J kg^{-1} is often very hard to overcome. Thus, to have convection the environment should have values of CINH closer to zero.

LCL height also plays an important role in determining if the environment is favorable for both supercells and tornadogenesis (Craven et al. 2002; Rasmussen and Blanchard 1998; Thompson et al. 2007). The LCL is the height at which a lifted parcel becomes saturated. Lower LCL heights have been associated with stronger tornadoes (EF2 or greater). The lower the LCL, the higher the relative humidity and thus the lower potential for evaporative cooling. This results in RFDs with higher temperatures, which are more potentially buoyant so the parcels can be easily lifted by an updraft. The warmer RFD also decreases the liklihood of the cold outflow undercutting the mesocyclone and disrupting tornadogenesis (e.g. Rasmussen and Blanchard 1998; Markowski et al. 2002). The approximate threshold for LCL to be considered favorable for tornado development is less than 2 km (Thompson et al. 2012). This is the threshold that is used to calculate the Significant Tornado Parameter (STP; Thompson et al. 2012), in which values that are higher than 2 km will result in lower STPs and thus are less favorable for the development of tornadoes.

Three other environmental parameters that are analyzed are effective bulk wind difference (EBWD), storm-relative helicity (SRH) from 0–1 km, and SRH from 0–3 km. EBWD is the magnitude of the bulk shear vector from the effective inflow base to the most unstable parcel equilibrium level (EL). This variable allows for the identification of elevated and surface-based supercell environments. As the shear increases (greater than 25 kt or 13 m s^{-1}), supercells become more probable (Thompson et al. 2007). Lastly, storm-relative helicity is the measure for the potential that right-moving supercells will develop cyclonic-rotating updrafts. There is no clear threshold for SRH, but larger values are associated with an increased tornado threat. The larger the values for 0–1 km and 0–3 km SRH the better, especially when the values exceed 100 m^2 s^{-2} and 250 m^2 s^{-2} respectively (Rasmussen and Blanchard 1988, Thompson et al. 2007).

The environmental conditions of all three cases are outlined in the following sections. Knowing the approximate inflow environments for each of the supercells, as well as the types of cycling they produced, serve as a comparison to the NEWS-e forecasts. Trends in all three cases are summarized in Section 4.4.

4.1 9 May 2017: Morton Supercell

The Morton supercell of 9–10 May 2017 formed south of Tatum, NM around 2200 UTC (initiation is defined by a reflectivity echo greater than 30 dBZ), but produced its first mesocyclone around 0133 UTC on 10 May 2017 over Gladiola, TX. A total of six cycles and seven mesocyclones were observed in WSR-88D data for the Morton supercell. The main mode of cycling for this supercell was occluding cyclic mesocyclogenesis (Fig. 2.4); hence, all of the mesocyclones went through an occlusion before decaying. Finally, the Morton cell decays just as it passes Edmonson, TX around 0548 UTC.

A sounding from Midland, TX (KMAF) at 0000 UTC on 10 May 2017 (Fig. 4.1) showed an environment with 997 J kg^{-1} of mixed layer CAPE, -94 J kg^{-1} of mixed layer CINH, and an LCL height of 1741 m. The hodograph associated with this sounding has very little cyclonic curvature in the low-levels and is mostly unidirectional in the mid- to upper-levels. Storm-relative helicity (SRH) was around 65 m^2 s^{-2} and 86 m^2 s^{-2} from 0–1 km and 0–3 km, respectively. Lastly, the effective shear, also known as the effective bulk wind difference, for this environment was around 55 kt (29 m s^{-1}). The fact that the LCL height was relatively high might explain why the Morton supercell only produced one tornado throughout its lifetime. Recall that high LCL heights are usually indicative of more evaporative cooling and low relative humidities, which cause the RFD to be colder. This cold air is negatively buoyant and hard to force upwards to its level of free convection (Markowski et al. 2002). The tornado that did form occurred near Morton, TX in Cohran County at approximately 0230 UTC, but fortunately it was very weak and didn't cause any damage.

To supplement the environmental soundings and get an approximate understanding of the near-storm environment for the Morton supercell, SPC mesoanalysis data are examined (archived images were examined from `https://www.spc.noaa.gov/exper/ma_archive/`). In the time period of 2300–0300 UTC, CAPE values are 1000 J kg^{-1} and CIN values are around -25 J kg^{-1} for the entire period. The instability is considered weak, but the low CIN values will favor convective development. The LCL heights are near 1000 m at 2300 UTC but decreases to a more favorable value of 750 m by 0300 UTC. 0–1 km SRH is around 100 m^2 s^{-2} for the beginning of the time frame, but increases to 200 m^2 s^{-2} by 0300 UTC. 0–3 km SRH values are very low (100 m^2 s^{-2}) at 2300 UTC, but increase to 300 m^2 s^{-2} by the end of the time period.

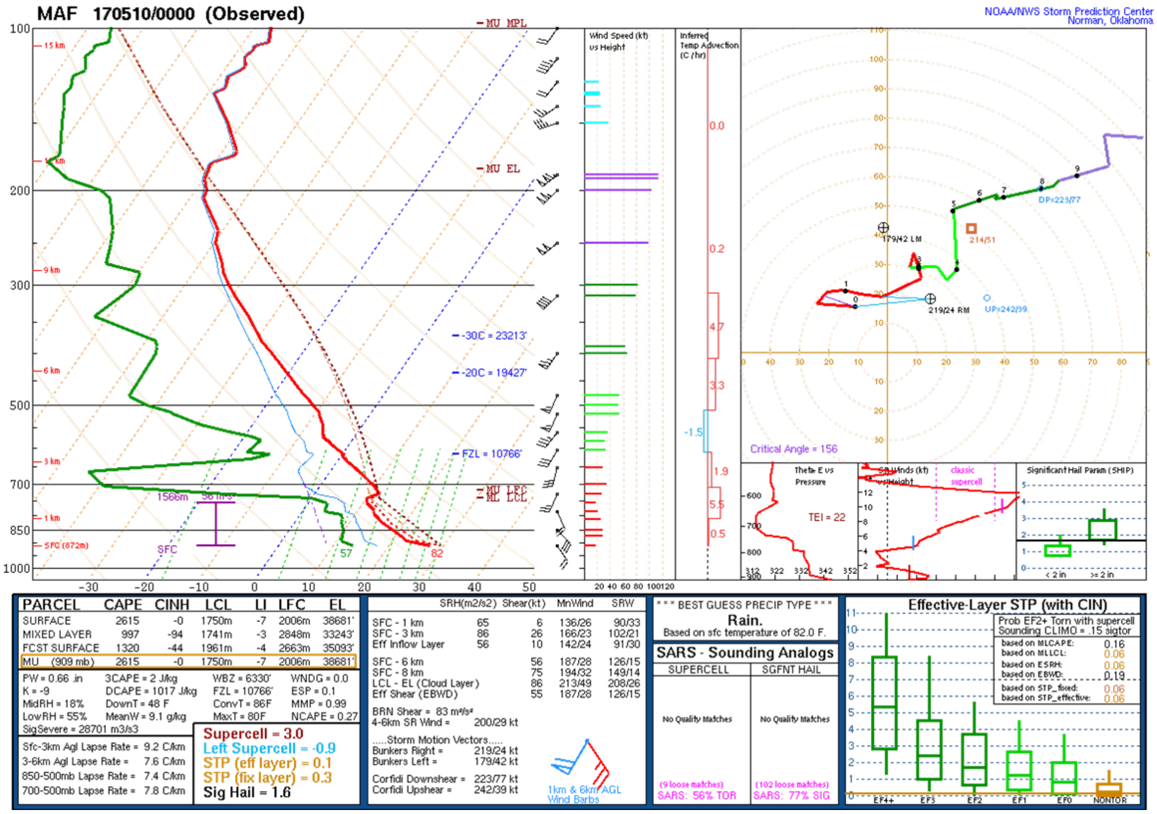

PARCEL	CAPE	CINH	LCL	LI	LFC	EL
SURFACE	2615	-0	1750m	-7	2006m	38681'
MIXED LAYER	997	-94	1741m	-3	2848m	33243'
FCST SURFACE	1320	-44	1961m	-4	2663m	35093'
MU (909 mb)	2615	-0	1750m	-7	2006m	38681'

PW = 0.66 .in
K = -9
MidRH = 18%
LowRH = 55%
SigSevere = 28701 m3/s3
3CAPE = 2 J/kg
DCAPE = 1017 J/kg
DownT = 48 F
MeanW = 9.1 g/kg
WBZ = 6330'
FZL = 10766'
ConvT = 86F
MaxT = 80F
WNDG = 0.0
ESP = 0.1
MMP = 0.99
NCAPE = 0.27

Sfc-3km Agl Lapse Rate = 9.2 C/km
3-6km Agl Lapse Rate = 7.6 C/km
850-500mb Lapse Rate = 7.4 C/km
700-500mb Lapse Rate = 7.8 C/km

Supercell = 3.0
Left Supercell = -0.9
STP (eff layer) = 0.1
STP (fix layer) = 0.3
Sig Hail = 1.6

	SRH(m2/s2)	Shear(kt)	MnWind	SRW
SFC - 1 km	65	6	136/26	90/33
SFC - 3 km	86	26	166/23	102/21
Eff Inflow Layer	56	10	142/24	91/30
SFC - 6 km		56	187/28	126/15
SFC - 8 km		75	194/32	149/14
LCL - EL (Cloud Layer)		86	213/49	208/26
Eff Shear (EBWD)		55	187/28	126/15

BRN Shear = 83 m²/s²
4-6km SR Wind = 200/29 kt

.....Storm Motion Vectors.....
Bunkers Right = 219/24 kt
Bunkers Left = 179/42 kt

Corfidi Downshear = 223/77 kt
Corfidi Upshear = 242/39 kt

* * * BEST GUESS PRECIP TYPE * * *
Rain.
Based on sfc temperature of 82.0 F.

SARS - Sounding Analogs

SUPERCELL	SGFNT HAIL
No Quality Matches	No Quality Matches
(9 loose matches)	(102 loose matches)
SARS: 56% TOR	SARS: 77% SIG

Prob EF2+ Torn with supercell
Sounding CLIMO = .15 sigtor

based on MLCAPE:	0.16
based on MLLCL:	0.06
based on ESRH:	0.06
based on EBWD:	0.19
based on STP_fixed:	0.06
based on STP_effective:	0.06

Figure 4.1: Storm Prediction Center (SPC) sounding taken from KMAF at 0000 UTC on 10 May 2017. Sounding is from the SPC's Severe Thunderstorm Event Archive found at www.spc.noaa.gov/exper/archive/events/

Comparing the values of SRH from 0–1 km, SRH 0–3 km, and basic shape of the environmental hodograph taken from KMAF with the study from Adlerman and Droegemeier (2005; Fig. 2.6), the values are marginally between occluding cyclic mesocyclogenesis and a steady, non-cycling supercell. Of course, caution must be taken when comparing actual environmental observations with Adlerman and Droegemeier's (2005) idealized numerical study because the model background for this study was homogeneous and simple hodograph shapes were utilized to make it easier to interpret the results. Actual environmental hodographs have more variation so they will not be an exact match to the ones used in the numerical study and, therefore, will not have the same results. However, a very basic comparison between the actual environment and the study can be made. The value of 0–1 km SRH fits with the occluding cyclic mesocyclogenesis area, but the values of 0–3 km SRH are extremely low compared to the numerical study. The environmental hodograph shape resembles the four experiments with a veering profile in the low-levels and then a straight hodograph for the rest of the layer. However, the actual hodograph shape was unidirectional with height in the mid- and upper-levels and not straight (i.e. for unidirectional hodographs the wind does not change direction with height and for a straight hodograph the wind does change direction). There was no simulation done with a unidirectional hodograph, so the comparisons between the true environment and this study are, at best, weakly linked.

The evolutions of the observed mesocyclones with the Morton supercell, as well as the durations of each mesocyclone, are shown in Fig. 4.2. Out of the seven mesocyclones observed, the fifth was the strongest and the longest-lived. However, there was no tornado reported with this mesocyclone. Instead, the Morton tornado, the only tornado produced by this storm, occurred during the third mesocyclone. The tornado corresponds to a jump in rotational velocities, as well as a decrease in diameter. The timing of the velocity jump doesn't match exactly with the report of the tornado, but it is important to note that the time of the tornado is estimated based on storm reports from that day. Therefore, there will be some error associated with each time due to how the data was collected (i.e. indicated on

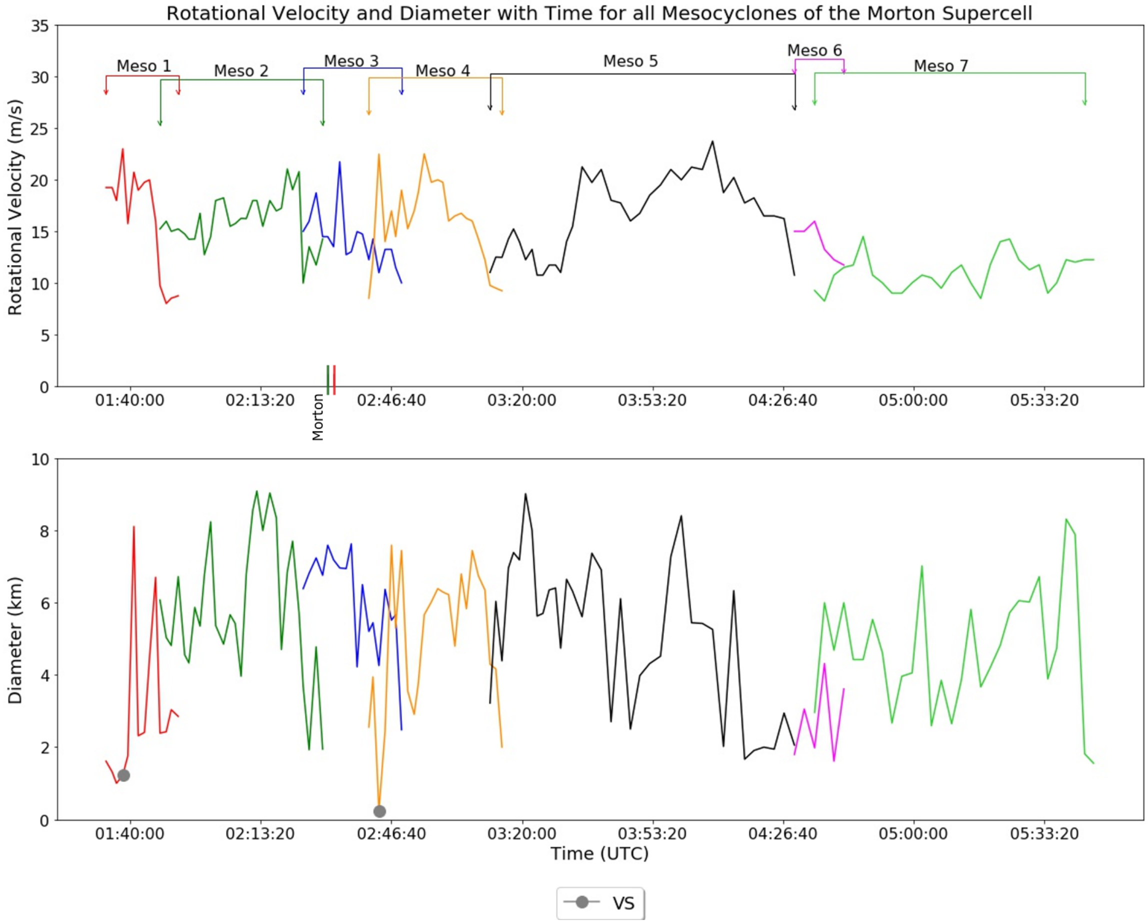

Figure 4.2: Diagram of the evolution of the rotational velocities and diameters for each of the mesocyclones produced by the Morton supercell. The top half of the diagram shows the evolution of the rotational velocities, while the bottom half of the figure shows a time series of each mesocyclone's diameter. Each mesocyclone is color-coded and is labeled from start to finish with a bracket at the top of the figure. The green line on the x-axis of the rotational velocity plot signifies the beginning of the Morton tornado, and the red line indicates the end of the tornado. The gray dots in the diameter plot indicate a VS was observed at that time.

radar vs. human observation; both will have some errors). During the fourth mesocyclone, there was a VS observed on radar just before 0246 UTC. There is also a brief spike in the rotational velocities at this same time. If a tornado did occur, it was most likely brief because the rotational velocities decreased and diameter increased immediately after the VS was observed.

The full path of the Morton supercell compared to the other three supercells is outlined in Fig. 4.3 and the seven mesocyclones that were identified can be found in Fig. 4.4. As stated before, all of the mesocyclones went through an occlusion process, which can be clearly seen in the tracks for the first five mesocyclones. These five tracks have the characteristic left turn towards the end of the track, signaling the occlusion of the mesocyclone from the main updraft and it being swept to the left of storm motion into the heavy precipitation region of the storm (e.g.,Burgess et al. 1982; Dowell and Bluestein 2002b; Adlerman and Droegemeier 2002). Once the mesocyclone is surrounded by this negatively buoyant air it begins to decay, and the track ends. Since the sixth mesocyclone was very short-lived, this left turn is not evident. The last mesocyclone was by far the weakest of the seven identified and decays before it can occlude from the updraft (Fig. 4.2). At this time, the supercell is weakening. This perhaps explains why the last mesocyclone doesn't occlude, and instead just decays with the main updraft.

4.2 16 May 2017: Elk City Supercell

16 May 2017 was a very active weather day across the eastern TX panhandle and into western OK. Two cyclic supercells formed along the border of eastern TX and western OK, which went on to produce multiple tornadoes throughout their lifetimes. Of the two cells, the southern one, which went on to produce the EF2 tornado in Elk City, OK, is of particular interest because it exhibited an interesting cycling pattern.

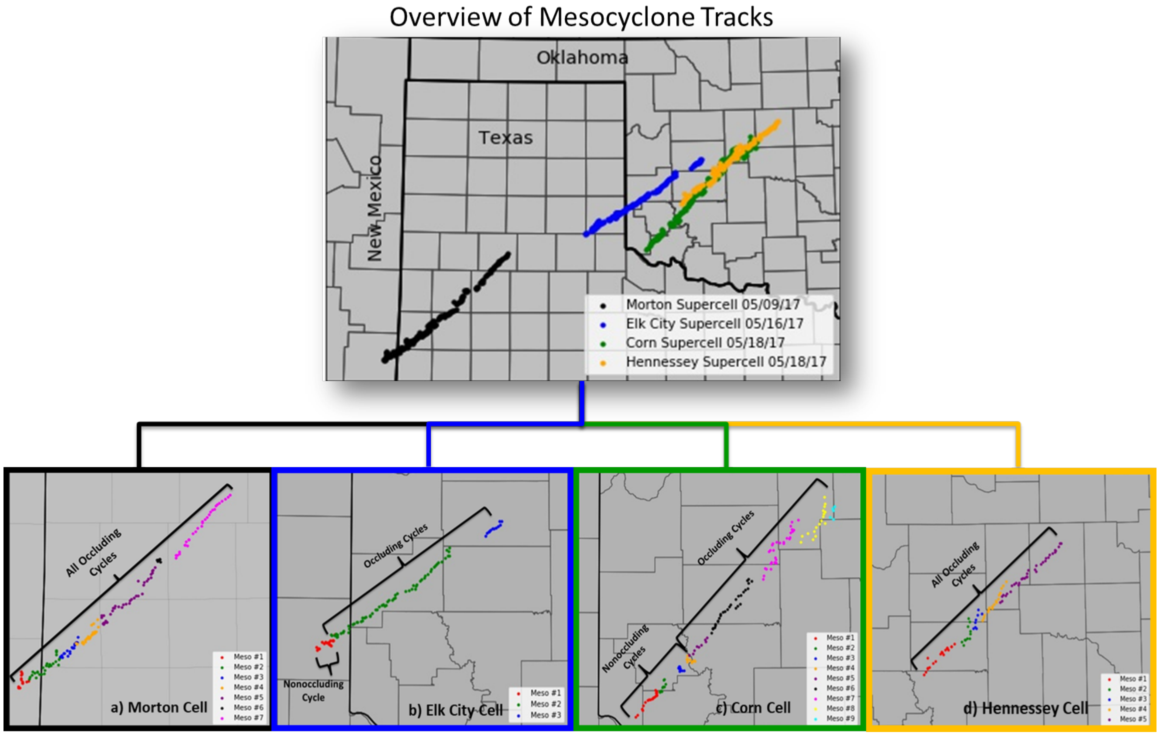

Figure 4.3: Overview of all mesocyclones identified within the four supercells that were analyzed. The top figure shows all the tracks side by side, while each of the lower diagrams shows the individual mesocyclone tracks from a) 9 May 2017 Morton supercell, b) 16 May 2017 Elk City supercell, c) 18 May 2017 Corn supercell, and lastly d) 18 May 2017 Hennessey supercell. The brackets in the lower panels indicate which mesocyclones cycled by occluding or nonoccluding cyclic mesocyclogenesis.

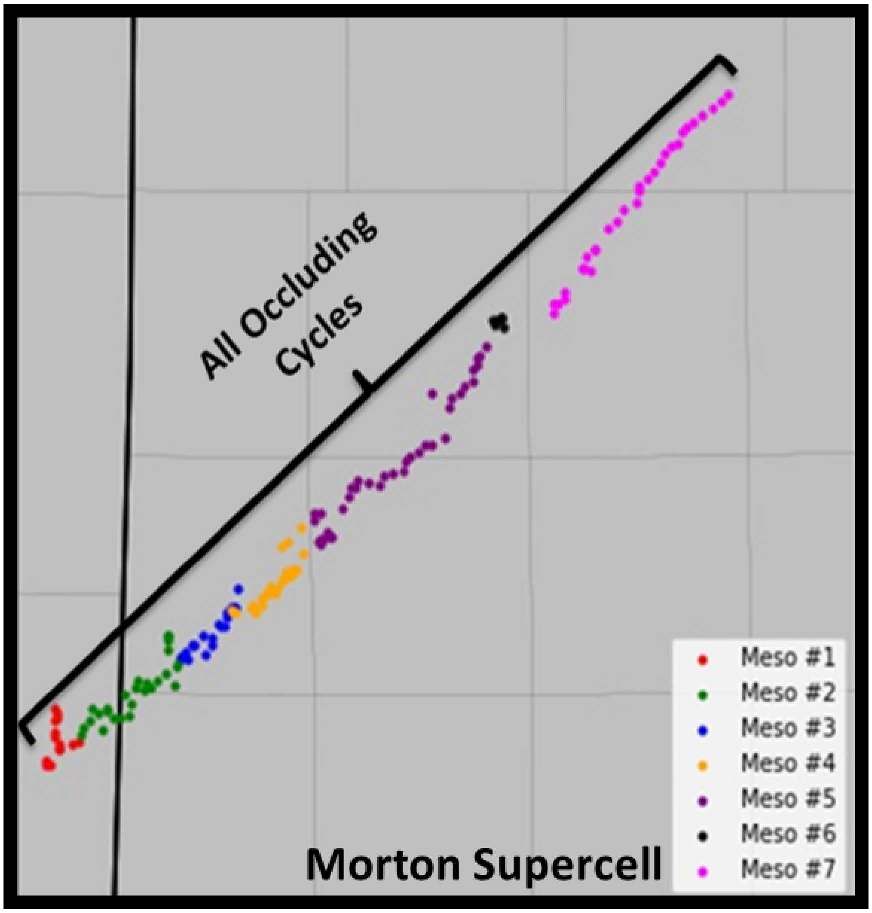

Figure 4.4: Zoomed in version of panel a) Morton Supercell from Fig. 4.8. The seven mesocyclones identified in WSR-88D data are color-coded. All of the mesocyclones went through occluding cyclic mesocyclogenesis.

The Elk City supercell first produced reflectivity greater than 30 dBZ at approximately 2142 UTC south of Turkey, TX. The storm developed its first mesocyclone north of Wellington, TX at 2229 UTC, and three additional mesocyclones were identified in WSR-88D data before it decayed (i.e. no longer had a reflectivity echo on radar) at 0106 UTC on 17 May 2017 west of Hitchcock, OK. This supercell produced five tornadoes, the most tornadoes produced by one storm when comparing all four cases analyzed in this study. The majority of the tornadoes produced were weak, EF0 tornadoes that did little to no damage to personal property. However, the Elk City tornado caused extensive damage to many businesses and homes in and around Elk City. There was also one fatality reported, along with several injuries (NCDC Storm Events).

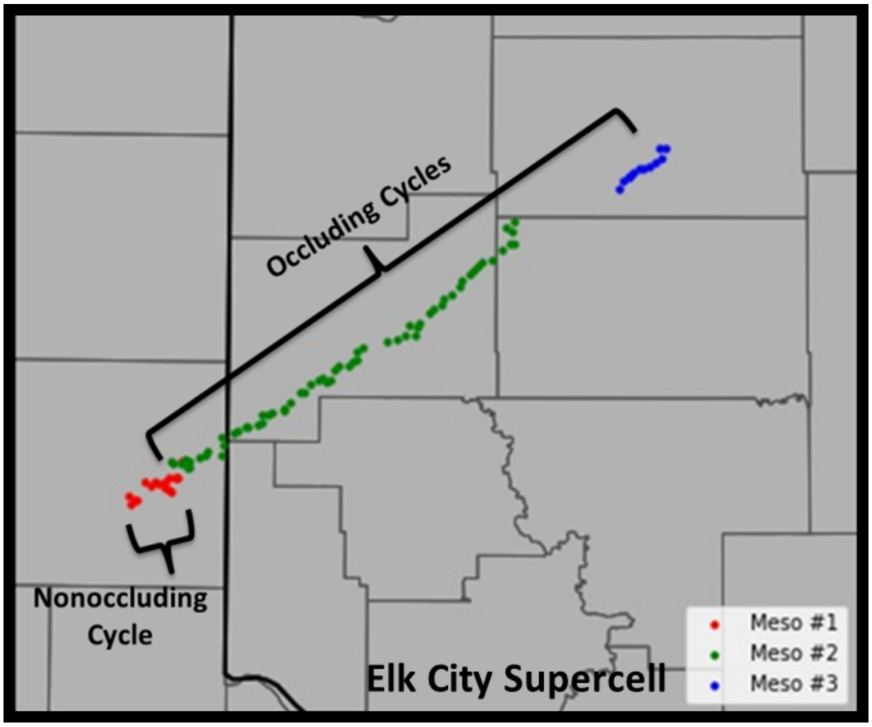

Figure 4.5: Zoomed in version of panel b) Elk City Supercell from Fig. 4.3. All identified mesocyclones are color-coded. The first mesocyclone went through nonoccluding cyclic mesocyclogenesis, while the second went through occluding cyclic mesocyclogenesis.

The Elk City supercell's first mesocyclone goes through nonoccluding cyclic mesocyclogenesis, while the second mesocyclone goes through occluding cyclic mesocyclogenesis (Fig. 2.4, Fig. 4.5). Instead of occluding from the main updraft and being swept into the heavy precipitation region, the first mesocyclone travels south of the storm, down the gust front, and is essentially left behind by the storm while the second mesocyclone matures (Adlerman and Droegemeier 2005; Fig. 4.6). As seen in Fig. 4.5, the first mesocyclone doesn't have the characteristic left turn near the end of its track, as it does not go through the occlusion phase, which is responsible for turning the mesocyclone to the left of storm motion. Instead, the mesocyclone moves slightly south of storm motion as it travels down the gust front and the next circulation matures to its north (Fig. 4.6). On the other hand, the second mesocyclone does exhibit the characteristic left turn because it occludes before decaying (Fig. 4.7). Analyzing this case gives the unique opportunity to look at the processes that caused this supercell to switch modes of cycling, which has yet to be explored.

The environmental parameters observed from a sounding taken from Amarillo, TX (KAMA) at 1800 UTC on 16 May 2017 (Fig. 4.8), well before the Elk City cell formed, shows a very conducive environment for supercellular development. Mixed layer CAPE values were moderate at 2114 J kg^{-1} with very little CINH at -8 J kg^{-1}. The high CAPE and low CINH values already represent an environment that could support the explosive growth of convective storms. The height of the LCL of 1400 m is below the 2 km threshold for an unfavorable tornado environment (Thompson et al. 2007). The 0–1 km and 0–3 km SRH values were 29 m^{2} s^{-2} and 77 m^{2} s^{-2}, respectively. The effective shear was near 46 kt, which according to Thompson et al. (2007) is favorable for the development and maintenance of supercells. However, the 0–1 and 0–3 km SRH values at this time are very low. The effective shear and SRH values are lower than that previously stated for the Morton supercell environment. However, the CAPE values are a lot higher and there is less CINH, as well as a lower LCL height. These factors may have created a more favorable environment for the development of tornadoes produced by this storm. Also, the hodograph for

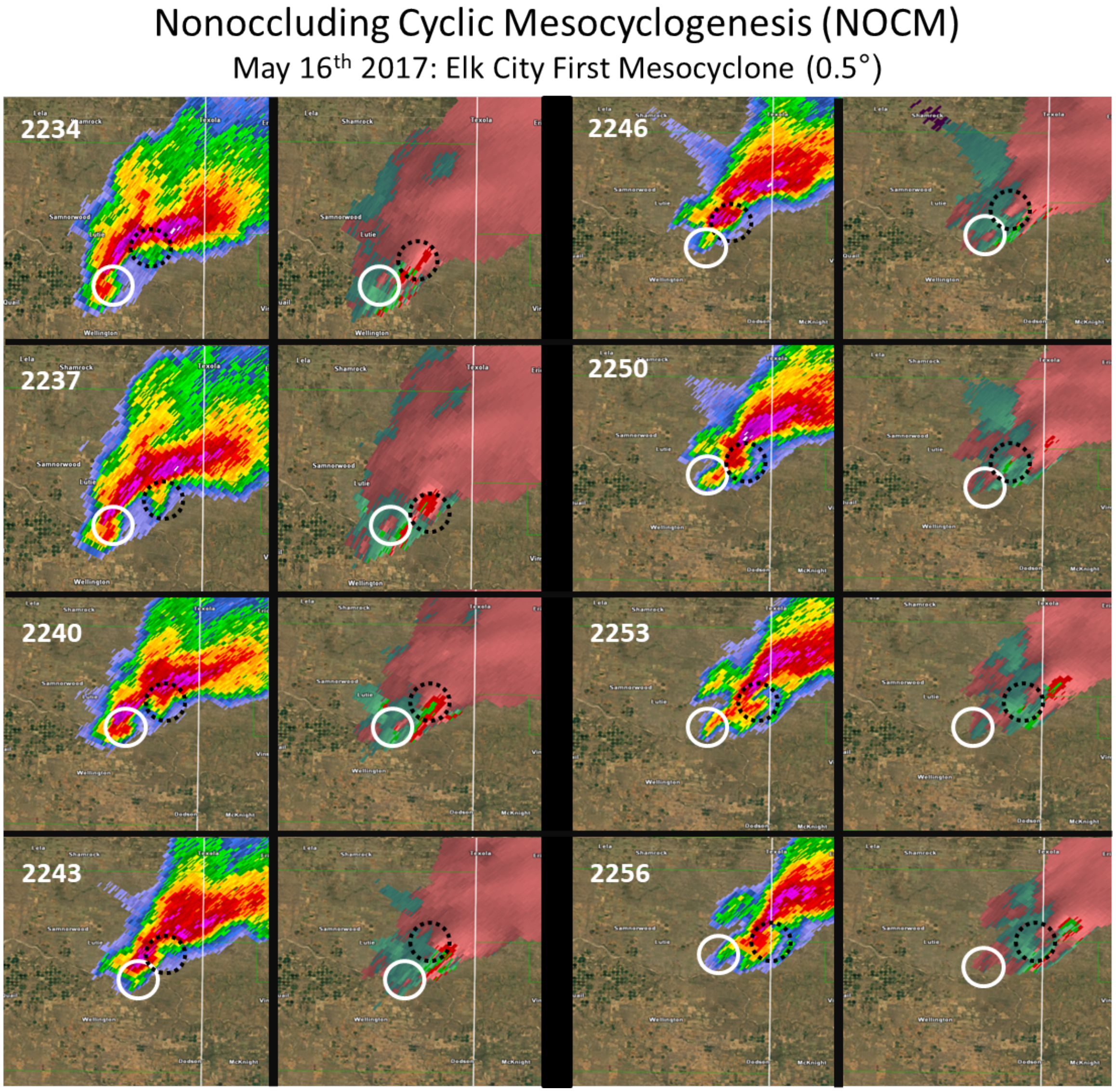

Figure 4.6: Nonoccluding cyclic mesocyclogenesis of the first mesocyclone in the Elk City supercell of 16 May 2017. Reflectivities (left) and radial velocities (right) are taken from KFDR at the lowest elevation angle (0.5°). Time is given in UTC at the top left of each panel. The solid, white circles indicate the first mesocyclone, while the dotted, black circles represent the formation of the second mesocyclone.

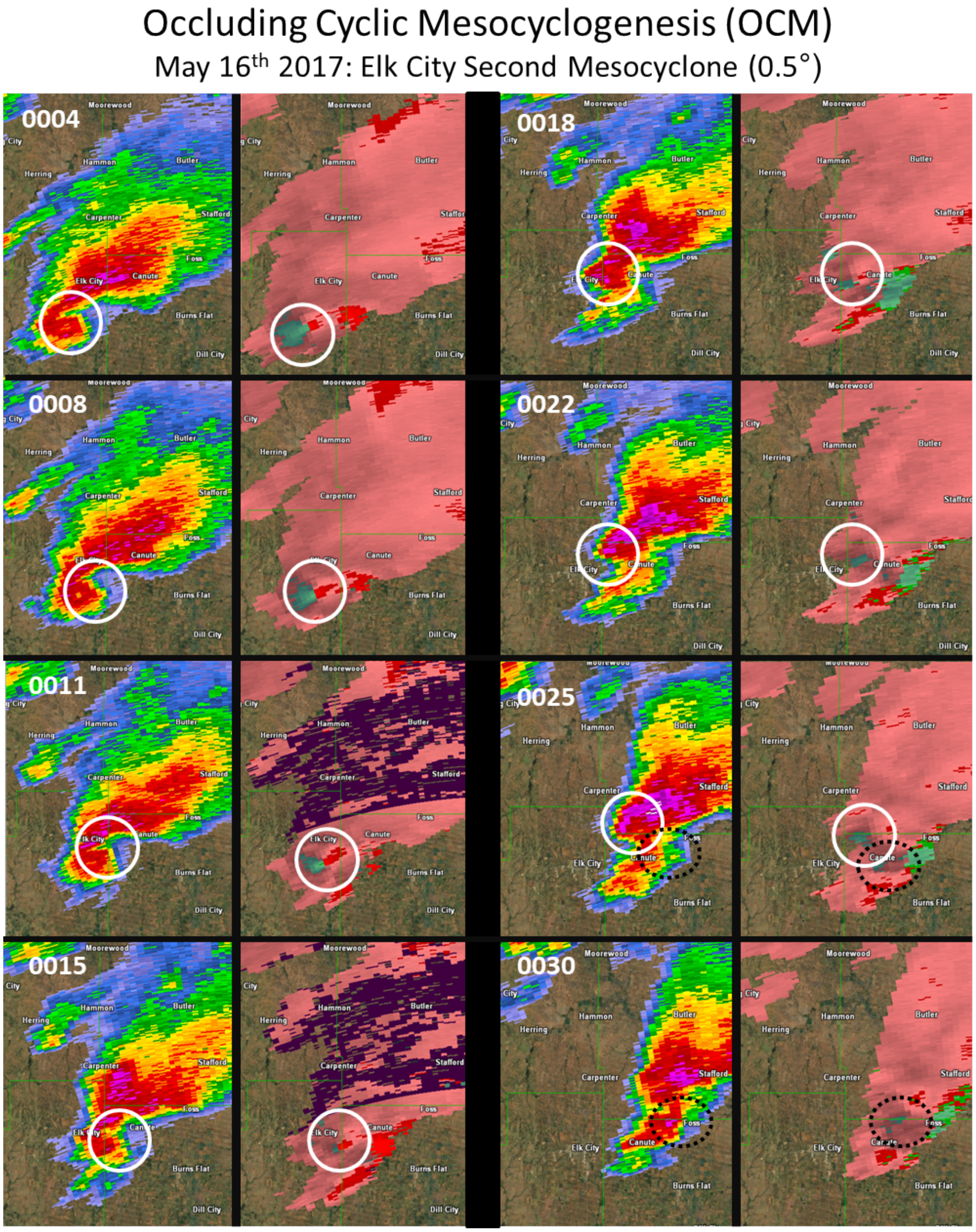

Figure 4.7: Occluding cyclic mesocyclogenesis of the second mesocyclone in the Elk City supercell of 16 May 2017. As in Fig. 4.6, except the white circle indicates the second mesocyclone and the black circle shows the third mesocyclone.

this environment has cyclonic curvature in the mid-levels, but is fairly unidirectional both near the surface and in the upper-levels. However, this sounding was taken about five hours before the Elk City storm and was displaced west of the storm. Therefore, this sounding may not be fully representative of the inflow environment of the Elk City supercell. Obtaining representative observations of all the storm environments for the four cyclic supercells examined is difficult. However, these soundings give a rough estimate of what aspects of the environment may have been like around the time of each supercell.

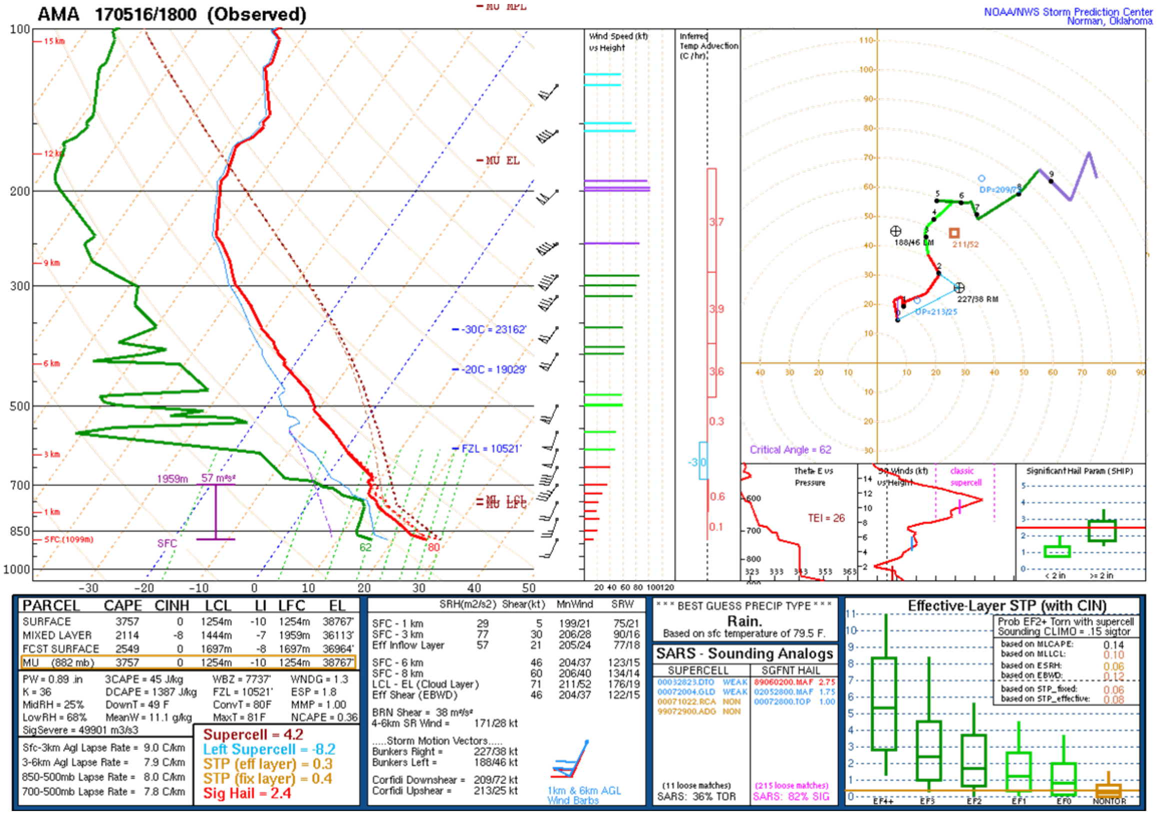

PARCEL	CAPE	CINH	LCL	LI	LFC	EL
SURFACE	3757	0	1254m	-10	1254m	38767'
MIXED LAYER	2114	-8	1444m	-7	1959m	36113'
FCST SURFACE	2549	0	1697m	-8	1697m	36964'
MU (882 mb)	3757	0	1254m	-10	1254m	38767'

PW = 0.89 .in
K = 36
MidRH = 25%
LowRH = 68%
SigSevere = 49901 m3/s3
3CAPE = 45 J/kg
DCAPE = 1387 J/kg
DownT = 49 F
MeanW = 11.1 g/kg
WBZ = 7737'
FZL = 10521'
ConvT = 80F
MaxT = 81F
WNDG = 1.3
ESP = 1.8
MMP = 1.00
NCAPE = 0.36

Sfc-3km Agl Lapse Rate = 9.0 C/km
3-6km Agl Lapse Rate = 7.9 C/km
850-500mb Lapse Rate = 8.0 C/km
700-500mb Lapse Rate = 7.8 C/km

Supercell = 4.2
Left Supercell = -8.2
STP (eff layer) = 0.3
STP (fix layer) = 0.4
Sig Hail = 2.4

	SRH(m2/s2)	Shear(kt)	MnWind	SRW
SFC - 1 km	29	5	199/21	75/21
SFC - 3 km	77	30	206/28	90/16
Eff Inflow Layer	57	21	205/24	77/18
SFC - 6 km		46	204/37	123/15
SFC - 8 km		60	206/40	134/14
LCL - EL (Cloud Layer)		71	211/52	176/19
Eff Shear (EBWD)		46	204/37	122/15

BRN Shear = 38 m²/s²
4-6km SR Wind = 171/28 kt

.....Storm Motion Vectors.....
Bunkers Right = 227/38 kt
Bunkers Left = 188/46 kt

Corfidi Downshear = 209/72 kt
Corfidi Upshear = 213/25 kt

1km & 6km AGL Wind Barbs

* * * BEST GUESS PRECIP TYPE * * *
Rain.
Based on sfc temperature of 79.5 F.

SARS - Sounding Analogs

SUPERCELL		SGFNT HAIL	
00032823.DTO	WEAK	89060200.MAF	2.75
00072004.GLD	WEAK	02052800.MAF	1.75
00071022.RCA	NON	00072800.TOP	1.00
99072900.ADG	NON		
(11 loose matches)		(215 loose matches)	
SARS: 36% TOR		SARS: 82% SIG	

Prob EF2+ Torn with supercell
Sounding CLIMO = .15 sigtor
based on MLCAPE: 0.14
based on MLLCL: 0.10
based on ESRH: 0.06
based on EBWD: 0.12
based on STP_fixed: 0.06
based on STP_effective: 0.08

Figure 4.8: SPC sounding from KAMA taken at 1800 UTC on 16 May 2017. This sounding is the closest representation of the pre-storm environment for the Elk City supercell. Sounding courtesy of SPC Severe Thunderstorm Event archive.

Since the KAMA sounding was taken five hours before the development of the Elk City supercell, another sounding from Norman, OK (KOUN) taken at 0000 UTC on 17 May 2017 (Fig. 4.9) is analyzed since the storms moved into OK shortly after developing in eastern TX, when this storm produced significant tornadoes. This sounding will help to understand the approximate storm environment as the supercell was moving into OK. The KOUN profile has a lower mixed layer CAPE value (891 J kg^{-1}), has a higher CINH (-306 J kg^{-1}), and a lower LCL height at 981 m. SRH and effective shear values have also changed from the sounding taken in KAMA. SRH 0–1 km and 0–3 km was 265 m^{2} s^{-2} and 345 m^{2} s^{-2}, respectively, and effective shear was 53 kt. These values are higher than those in the previous sounding and are above all of the thresholds for a favorable environment to develop supercells (Thompson et al. 2007). The hodograph closely resembles that of a veering, quarter-circle to half-circle hodograph, which is a known profile shape that is extremely favorable for the development of right-moving, strong supercells. These hodographs are favorable because the longer the hodograph, the greater the vertical wind shear, and, in this case, the strong cyclonic curvature indicates the presence of a low-level jet (i.e. wind maximum) that increases the storm-relative inflow.

Even though soundings were available for this day relatively close to where the Elk City supercell occurred, the soundings are still very displaced from the supercell near-storm environment (Thompson et al. 2003; Potvin et al. 2010). To supplement the upper-air soundings analyzed, SPC mesoanalysis data from 2100–2300 UTC are examined to get a better understanding of the near-storm environment of the Elk City supercell. CAPE values in west-central OK rapidly increased from 1000 J kg^{-1} at 2100 UTC to around 3000 J kg^{-1} at 2300 UTC. The CINH values for this time frame are very low (less than 50 J kg^{-1}). These CAPE and CINH values indicate high instability and very low capping, respectively, that will aid in the development and sustainment of supercells. There is a strong gradient of LCL heights in western OK along the dryline that lies along the border of OK and TX. The lower LCL heights are to the east of the dryline in OK, which would be in the inflow environment of the Elk City supercell. EWBD values were approximately 50–60 kt and similar to the KOUN soundings. SRH values in the 0–1 km and 0–3 km layers reached maximum values of 200 m^{2} s^{-2} and 300 m^{2} s^{-2} respectively. These values closely resemble those from the KOUN sounding taken at 0000 UTC. This suggests that the KOUN was the most representative of the Elk City supercell's environment than the KAMA sounding, and was a good estimate of the inflow environment for this storm. All of the variables presented meet the favorable supercell environment thresholds outlined by past research (e.g. Rasmussen and Blanchard 1998; Craven et al. 2002; Thompson et al. 2007, 2012).

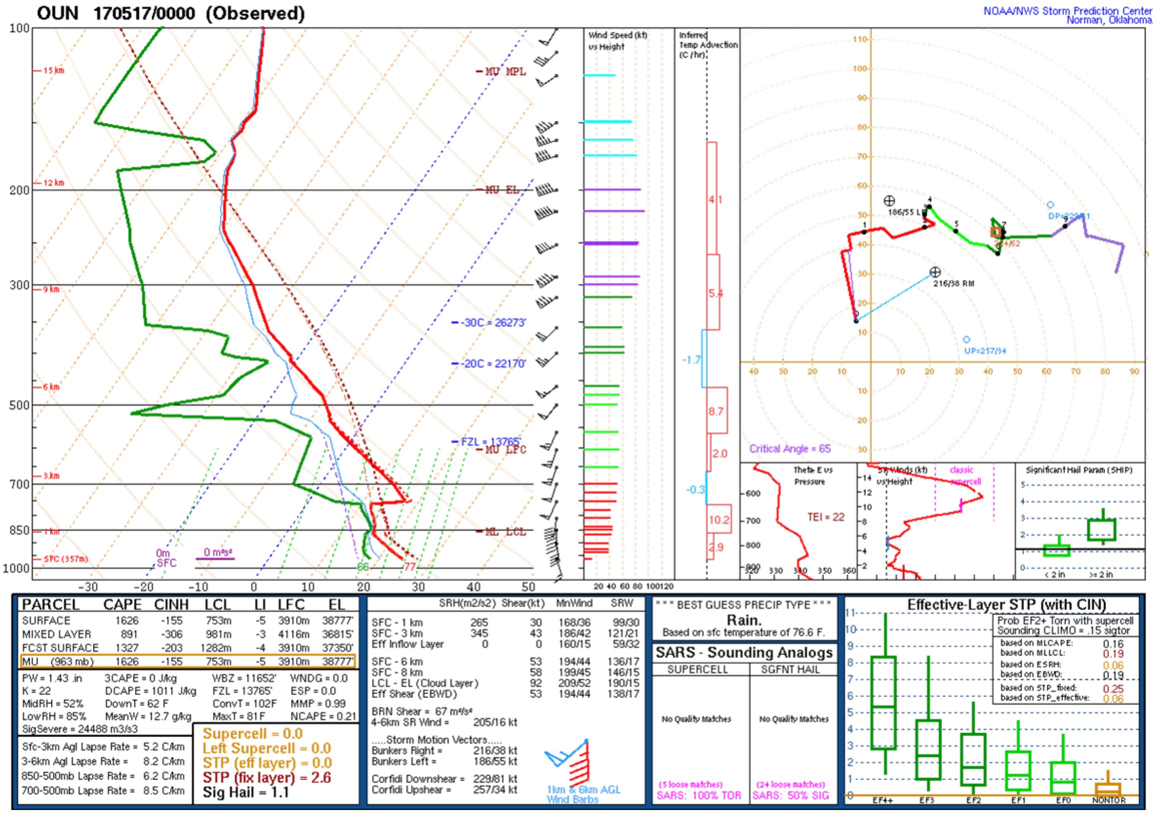

PARCEL	CAPE	CINH	LCL	LI	LFC	EL
SURFACE	1626	-155	753m	-5	3910m	38777'
MIXED LAYER	891	-306	981m	-3	4116m	36815'
FCST SURFACE	1327	-203	1282m	-4	3910m	37350'
MU (963 mb)	1626	-155	753m	-5	3910m	38777'

PW = 1.43 .in
K = 22
MidRH = 52%
LowRH = 85%
SigSevere = 24488 m3/s3
3CAPE = 0 J/kg
DCAPE = 1011 J/kg
DownT = 62 F
MeanW = 12.7 g/kg
WBZ = 11652'
FZL = 13765'
ConvT = 102F
MaxT = 81 F
WNDG = 0.0
ESP = 0.0
MMP = 0.99
NCAPE = 0.21

Sfc-3km Agl Lapse Rate = 5.2 C/km
3-6km Agl Lapse Rate = 8.2 C/km
850-500mb Lapse Rate = 6.2 C/km
700-500mb Lapse Rate = 8.5 C/km

Supercell = 0.0
Left Supercell = 0.0
STP (eff layer) = 0.0
STP (fix layer) = 2.6
Sig Hail = 1.1

	SRH(m2/s2)	Shear(kt)	MnWind	SRW
SFC - 1 km	265	30	168/36	99/30
SFC - 3 km	345	43	186/42	121/21
Eff Inflow Layer	0	0	160/15	59/32
SFC - 6 km		53	194/44	136/17
SFC - 8 km		58	199/45	146/15
LCL - EL (Cloud Layer)		92	209/52	190/15
Eff Shear (EBWD)		53	194/44	138/17

BRN Shear = 67 m²/s²
4-6km SR Wind = 205/16 kt

.....Storm Motion Vectors.....
Bunkers Right = 216/38 kt
Bunkers Left = 186/55 kt

Corfidi Downshear = 229/81 kt
Corfidi Upshear = 257/34 kt

* * * BEST GUESS PRECIP TYPE * * *
Rain.
Based on sfc temperature of 76.6 F.

SARS - Sounding Analogs

SUPERCELL	SGFNT HAIL
No Quality Matches	No Quality Matches
(5 loose matches)	(24 loose matches)
SARS: 100% TOR	SARS: 50% SIG

Prob EF2+ Torn with supercell
Sounding CLIMO = .15 sigtor

based on MLCAPE:	0.16
based on MLLCL:	0.19
based on ESRH:	0.06
based on EBWD:	0.19
based on STP_fixed:	0.25
based on STP_effective:	0.06

Figure 4.9: Sounding from SPC taken at 0000 UTC at KOUN on 17 May 2017. This sounding represents the environment of the Elk City supercell as it crosses into Oklahoma and travels near central OK. Image courtesy of SPC Severe Thunderstorm Event Archive.

Comparing the environmental variables from the KOUN sounding and SPC mesoanalysis to the Adlerman and Droegemeier (2005; Fig. 2.6) numerical study once again places this storm marginally between a steady-state supercell and one that goes through occluding cyclic mesocyclogenesis. The KOUN hodograph was closest to the basic half-circle hodograph simulations in the numerical study. When looking at the values of the 0–1 km and

0–3 km SRH, the Elk City supercell would be placed closer to the steady-state portion of the figure for both the KOUN sounding and the SPC mesoanalysis. The SRH values for the approximate near-storm environment compared to Adlerman and Droegemeier (2005) (Fig. 2.6) are a lot higher for the 0–1 SRH values, but are in the region of occluding cyclic mesocyclogenesis if looking at 0–3 km SRH. Therefore, the environment for this storm suggested either occluding cyclic mesocyclogenesis or a noncycling supercell can occur. Examining the hodographs of the KAMA and KOUN soundings suggest that the main mode of cycling for the KAMA sounding would have been nonoccluding cyclic mesocyclogenesis because the hodograph is relatively straight. The KOUN sounding has high curvature in the lower levels of the storm and would roughly fit in the occluding cyclic mesocyclogenesis parameter space from Adlerman and Droegemeier (2005; Fig. 2.6). The curvature in the KOUN sounding resembles an increase in SRH 0–1 km values from the KAMA sounding, and may be why the Elk City supercell transitioned between nonoccluding to occluding cyclic mesocyclogenesis. However, this is a coarse comparison to the Adlerman and Droegemeier (2005) study, as those hodographs were idealized and lack the variations found in true supercell environments.

The evolution of the three mesocyclones associated with the Elk City supercell is highlighted in Fig. 4.10. All five of the tornadoes produced by this storm were during the second mesocyclone, which was by far the strongest and had the longest duration of all the mesocyclones. Even though the first mesocyclone had a few strong VSs observed on radar, none of them were confirmed to be associated with tornadoes. The first mesocyclone was also nonoccluding, so this raises the question: does mode of cycling have an effect on whether the mesocyclone is tornadic or not? However, the atmospheric conditions show that once the supercell traveled into Oklahoma, the environment became more favorable for tornadogenesis. It was only during the time frame of the second mesocyclone that this supercell moved into Oklahoma, and thus into a more favorable environment for tornadogenesis. This may be why the first mesocyclone was nontornadic and the second mesocyclone produced 5 tornadoes.

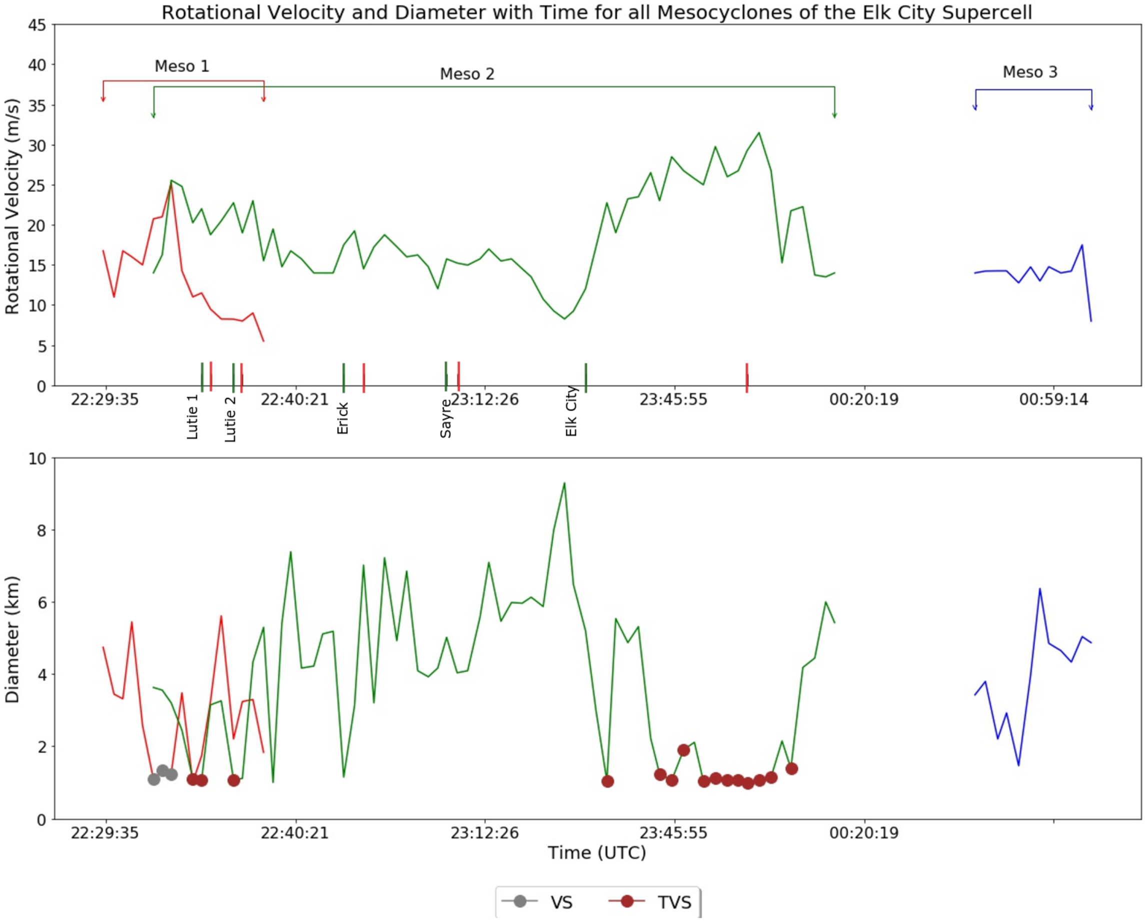

Figure 4.10: Same as in Fig. 4.2 but with the Elk City supercell of 16 May 2017. The red dots indicate a TVS was observed on radar and corresponds to a tornado report.

The first two tornadoes associated with the second mesocyclone occurred outside of Lutie, TX. During both of the tornadoes, the mesocyclone had a fairly tight circulation with strong rotation. The Erick and Sayre, OK tornadoes formed next. They were only a couple minutes long and were both rated EF0. Lastly, the Elk City tornado was the longest-lived and most destructive tornado produced by this storm. This tornado lasted about 40 min and was rated an EF2 because of extensive damage to structures within and around Elk City, OK. During the tornado, rotational velocities peaked around 30 m s^{-1}, and the mesocyclone diameters remained nearly constant around 1 km. There was a period of about 35 minutes that the mesocyclone produced a TVS, which corresponds to the highest velocities in the mesocyclone, as well as the lifetime of the Elk City tornado. Shortly after the decay of the tornado, the mesocyclone moved off to the left of the storm motion (Fig. 4.5) and decayed. There is a pause of about 40 min between the decay of the second mesocyclone and the formation of the third mesocyclone. At this time, the supercell is very weak and close to dissipating, but produces the last mesocyclone before decaying completely. This mesocyclone doesn't go through a cycling process and instead decays with the rest of the storm.

4.3 18 May 2017: Corn and Hennessey Supercells

The severe weather in the southern Plains continued into 18 May 2017 when two supercells developed close to the southwest corner of OK and moved to the northeast. The first supercell formed near East Duke, OK at 1830 UTC and decayed at 2255 UTC around Greenfield, OK. This cell is nicknamed the Corn storm because it was responsible for producing two weak, EF0 tornadoes, one of which occurred near East Duke, OK while the other formed close to Corn, OK a little over an hour later.

The Corn supercell is similar to that of the Elk City supercell in that it goes through both modes of cyclic mesocyclogenesis. The first four mesocyclones identified in this storm went through nonoccluding cyclic mesocyclogenesis, in which the old mesocyclone traveled down the gust front instead of occluding and moving to the left of storm motion into the heavy precipitation (Adlerman and Droegemeier 2005, Fig. 2.4). In Fig 4.11, the first two tracks indicate a "hand-off" between the two mesocyclones, in which the first mesocyclone begins to decay as the second mesocyclone takes over the storm in its place. Radar shows the first mesocyclone traveling down the gust front and being left behind by the storm, while the second mesocyclone forms north of the old one. The transition is less clear for the third and fourth mesocyclones, as they were fairly short-lived. The

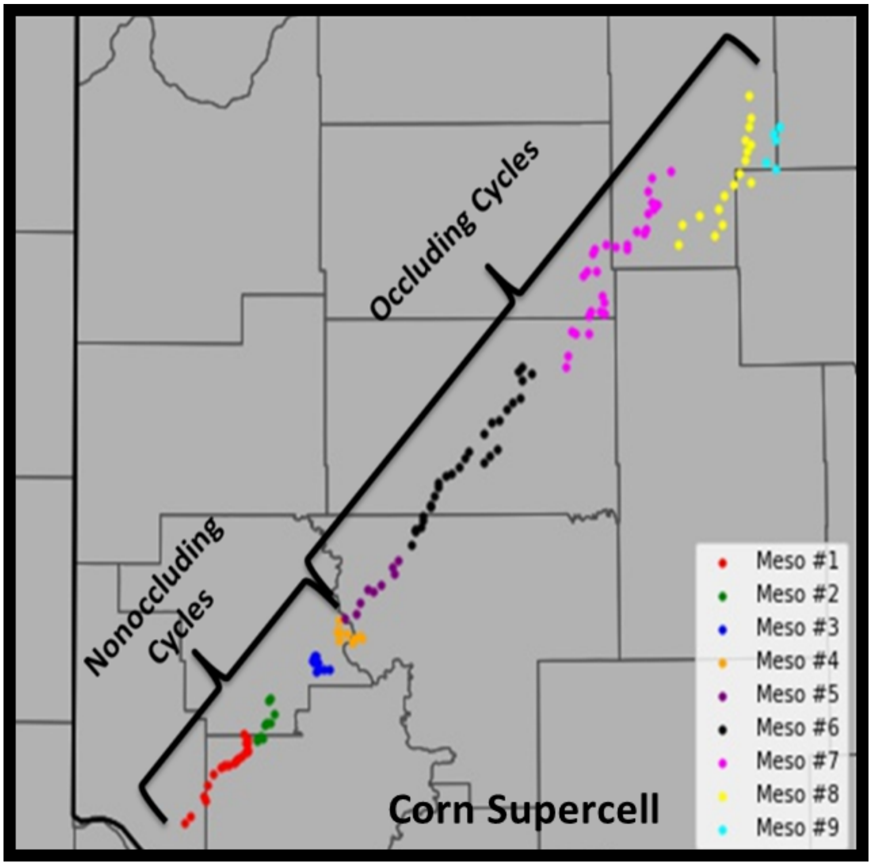

Figure 4.11: Zoomed in version of panel c) Corn Supercell from Fig. 4.3. All identified mesocyclones are color-coded. The first four mesocyclones went through nonoccluding cyclic mesocyclogenesis, while the other five went through occluding cyclic mesocyclogenesis.

remaining five mesocyclones all go through occluding cyclic mesocyclogenesis and most of the tracks show a sharp left turn towards the end. Even though mesocyclone tracks can be very useful in assessing which mode of cyclic mesocyclogenesis may be occurring, there can be considerable uncertainty in determining the exact mode.

The nonoccluding cycles of the Corn supercell occurred before the first initialization time of NEWS-e forecasts and, therefore, are not simulated by the model. Halfway through the lifetime of the Corn storm, another supercell formed on its rear flank. This cell was dubbed the Hennessey storm as it formed close to Mangum, OK at 2030 UTC and the last mesocyclone identified in WSR-88D data decayed near Hennessey, OK at 2328 UTC. This supercell was included in the analysis because it trails the Corn storm and ends up merging with it towards the end of the Corn storm's lifetime. These two storms interacted with each other, so they are grouped into a single analysis since the system sometimes has a hard time deciphering between one, big storm and two individual storms, attributable to NEWS-e's coarse resolution.

The Hennessey storm had a total of five mesocyclones that were identified in WSR-88D data, all of which went through occluding cyclic mesocyclogenesis. Fig. 4.12 shows that the majority of the tracks (mesocyclones 2, 3, and 4) have the characteristic left turn that most occluding cycles display (e.g. Burgess et al. 1982; Dowell and Bluestein 2002b; Adlerman et al. 1999). Fortunately, there were no tornadoes associated with this storm. There were multiple meso-anticyclones that were seen on radar in conjunction with the original mesocyclones, but they are not included in this study. Unlike the Corn supercell, the entirety of the Hennessey supercell life cycle was captured by NEWS-e.

As seen in Fig. 4.13, there is a data gap around 2200 UTC that interrupts the analysis of the Hennessey supercell's fourth mesocyclone. This data gap is a result of poor data quality owing to the radial velocities at this time being removed from the scan entirely or were covered by "purple haze", which is when range-velocity ambiguity causes range-folding to occur. The exact reason why this error occurred is unclear. The longitude and

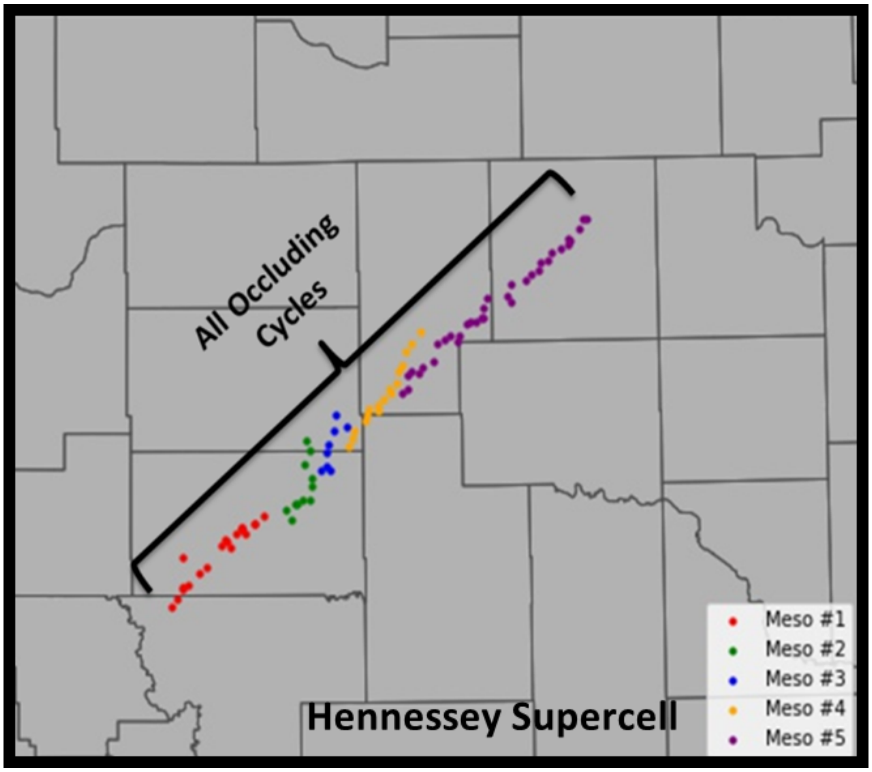

Figure 4.12: Zoomed in version of panel d) Hennessey Supercell from Fig. 4.3. All identified mesocyclones are color-coded. All of the identified mesocyclones went through occluding cyclic mesocyclogenesis.

latitude of the mesocyclone position could be estimated for the times that the radial velocity data were absent. In other words, the fourth mesocyclone track in Fig. 4.12 is complete. The missing data only affected the rotational velocities and the diameters (Fig. 4.13).

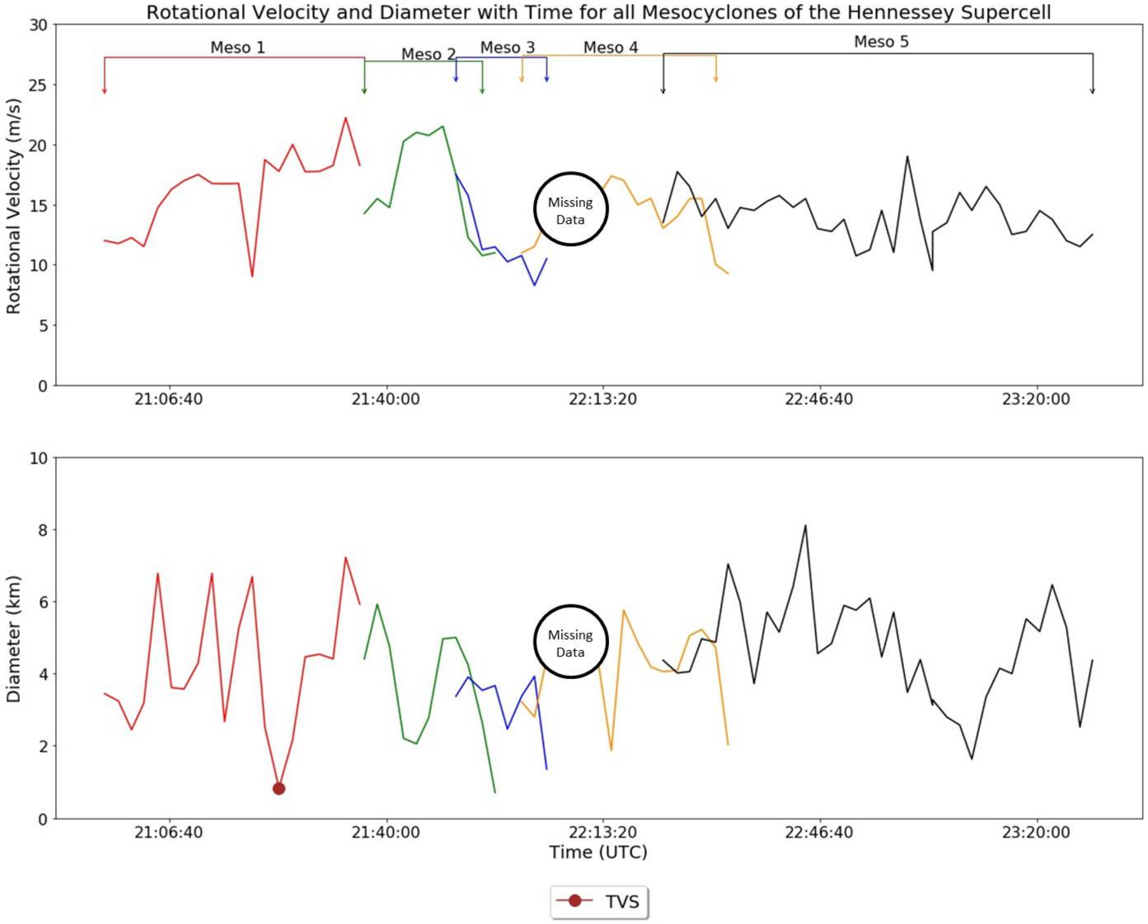

Figure 4.13: Same as in Fig. 4.2 but with the Hennessey supercell of 18 May 2017. The data gap is due to range-folding so there were errors in the velocity data.

There was only one environmental sounding taken around the time of when the two storms formed, close to the area where the supercells occurred. The sounding from Norman, OK (KOUN) taken at 1800 UTC on 16 May 2017 (Fig. 4.14), 30 min before the Corn supercell formed. The sounding shows high mixed layer CAPE of 2590 J kg^{-1} and a very low CINH of -5 J kg^{-1}. The LCL height was around 1146 m. The 0–1 km SRH, 0–3 km SRH, and effective shear values were 60 m^2 s^{-2}, 73 m^2 s^{-2}, and 36 kt respectively.

The hodograph is generally veering with height, which is a favorable shear profile for the formation and maintenance of supercells, similar to the Elk City supercell in Section 4.2.

The 1800 UTC KOUN sounding alone is not representative of the near-storm environment for both the Corn and Hennessey supercells. SPC mesoanalysis data from 1800-0000 UTC is also examined to cover the full evolution of both the Corn and Hennessey supercells to get a better understanding of how the environment changed as the various supercells in the area initiated and interacted with each (Thompson et al. 2003; Potvin et al. 2010). Mixed layer CAPE values at 2000 UTC were near 2000 J kg^{-1} with less than 100 J kg^{-1} values of CINH. As time progresses, CAPE values stay approximately the same, while higher values CINH (greater than 100 J kg^{-1}) enter the area of the two supercells analyzed on this day. LCL heights maintained values of around 1 km for the entire time frame. 0–1 SRH starts out with low values of 50 m^2 s^{-2} at 2000 UTC and increase to 300 m^2 s^{-2} at 0000 UTC. Similarly, 0–3 SRH starts out with 100 m^2 s^{-2} at the beginning of the time frame and ends with values near 400 m^2 s^{-2}. EBWD values stay around 40–50 kt for the entire time frame. SRH values were very low around 1800–2000 UTC, which is when the Corn supercell matured and went through its nonoccluding cycles. According to Adlerman and Droegemeier (2005) and Fig. 2.6, very low values of 0–1 and 0–3 SRH are indicative of nonoccluding cyclic mesocyclogenesis and the SRH values from the 1800–2000 UTC time frame of the Corn supercell would fit into that same area. As time progresses, the SRH values increase and would better fit into the occluding cyclic mesocyclogenesis region of Fig. 2.6, which corresponds to when the remaining part of the Corn and mature phase of the Hennessey supercells were going through occluding cyclic mesocyclogenesis.

The evolution of the nine mesocyclones that were identified in the Corn supercell is shown in Fig. 4.15. The first mesocyclone is fairly strong and has a period with a small diameter, as well as a few TVSs, corresponding to the Duke, OK tornado. The Duke tornado was the first tornado from all four supercell cases that was produced from a mesocyclone that went through nonoccluding cyclic mesocyclogenesis. Mesocyclones 2, 3, and 4 were

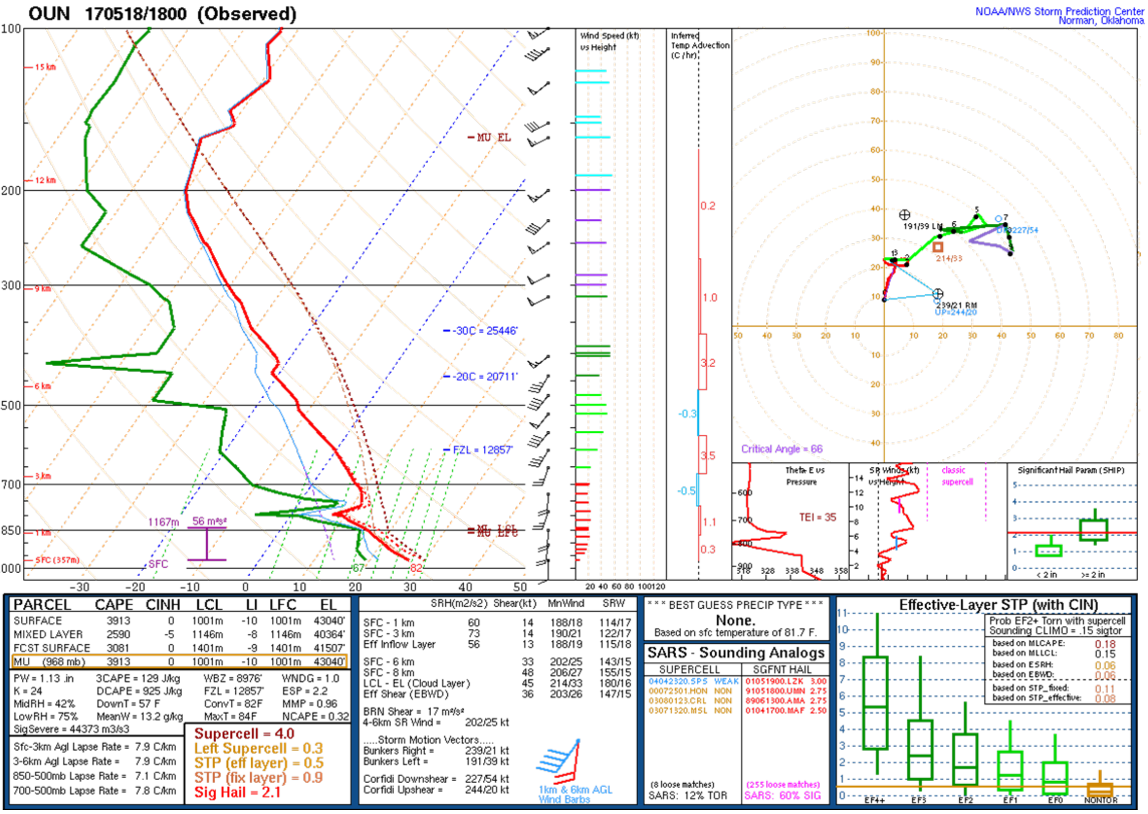

PARCEL	CAPE	CINH	LCL	LI	LFC	EL
SURFACE	3913	0	1001m	-10	1001m	43040'
MIXED LAYER	2590	-5	1146m	-8	1146m	40364'
FCST SURFACE	3081	0	1401m	-9	1401m	41507'
MU (968 mb)	3913	0	1001m	-10	1001m	43040'

PW = 1.13 .in
K = 24
MidRH = 42%
LowRH = 75%
SigSevere = 44373 m3/s3
3CAPE = 129 J/kg
DCAPE = 925 J/kg
DownT = 57 F
MeanW = 13.2 g/kg
WBZ = 8976'
FZL = 12857'
ConvT = 82F
MaxT = 84F
WNDG = 1.0
ESP = 2.2
MMP = 0.96
NCAPE = 0.32

Sfc-3km Agl Lapse Rate = 7.9 C/km
3-6km Agl Lapse Rate = 7.9 C/km
850-500mb Lapse Rate = 7.1 C/km
700-500mb Lapse Rate = 7.8 C/km

Supercell = 4.0
Left Supercell = 0.3
STP (eff layer) = 0.5
STP (fix layer) = 0.9
Sig Hail = 2.1

	SRH(m2/s2)	Shear(kt)	MnWind	SRW
SFC - 1 km	60	14	188/18	114/17
SFC - 3 km	73	14	190/21	122/17
Eff Inflow Layer	56	13	188/19	115/18
SFC - 6 km		33	202/25	143/15
SFC - 8 km		48	206/27	155/15
LCL - EL (Cloud Layer)		45	214/33	180/16
Eff Shear (EBWD)		36	203/26	147/15

BRN Shear = 17 m²/s²
4-6km SR Wind = 202/25 kt

.....Storm Motion Vectors.....
Bunkers Right = 239/21 kt
Bunkers Left = 191/39 kt

Corfidi Downshear = 227/54 kt
Corfidi Upshear = 244/20 kt

* * * BEST GUESS PRECIP TYPE * * *
None.
Based on sfc temperature of 81.7 F.

SARS - Sounding Analogs

SUPERCELL		SGFNT HAIL	
04042320.SPS	WEAK	01051900.LZK	3.00
00072501.HON	NON	91051800.UMN	2.75
03080123.CRL	NON	89061300.AMA	2.75
03071320.MSL	NON	01041700.MAF	2.50
(8 loose matches) SARS: 12% TOR		(255 loose matches) SARS: 60% SIG	

Prob EF2+ Torn with supercell
Sounding CLIMO = .15 sigtor
based on MLCAPE: 0.18
based on MLLCL: 0.15
based on ESRH: 0.06
based on EBWD: 0.06
based on STP_fixed: 0.11
based on STP_effective: 0.08

Figure 4.14: Atmospheric sounding taken from KOUN at 1800 UTC that represents the environment that preceded the Corn and Hennessey supercells on 18 May 2017. Sounding is courtesy of the Severe Thunderstorm Archive from SPC.

relatively weak and short-lived compared to the other mesocyclones this storm produced. The remaining mesocyclones, excluding mesocyclone 9, are strong and long-lived. The fifth mesocyclone contains one VS, but no tornado reported. On the other hand, the sixth mesocyclone produces the Corn, OK tornado during the time where it has some of the strongest rotational velocities, even though the diameters are still quite large. The seventh mesocyclone was another very strong circulation. However, the strongest mesocyclone was the eighth, with a maximum velocity of 38 m s^{-1}. This mesocyclone also had a TVS at one time, but no tornado was reported. The last mesocyclone overlaps with the last mesocyclone, had the shortest duration and decayed at the same time as the mesocyclone before it. After the decay of mesocyclones 8 and 9, the whole storm dissipated.

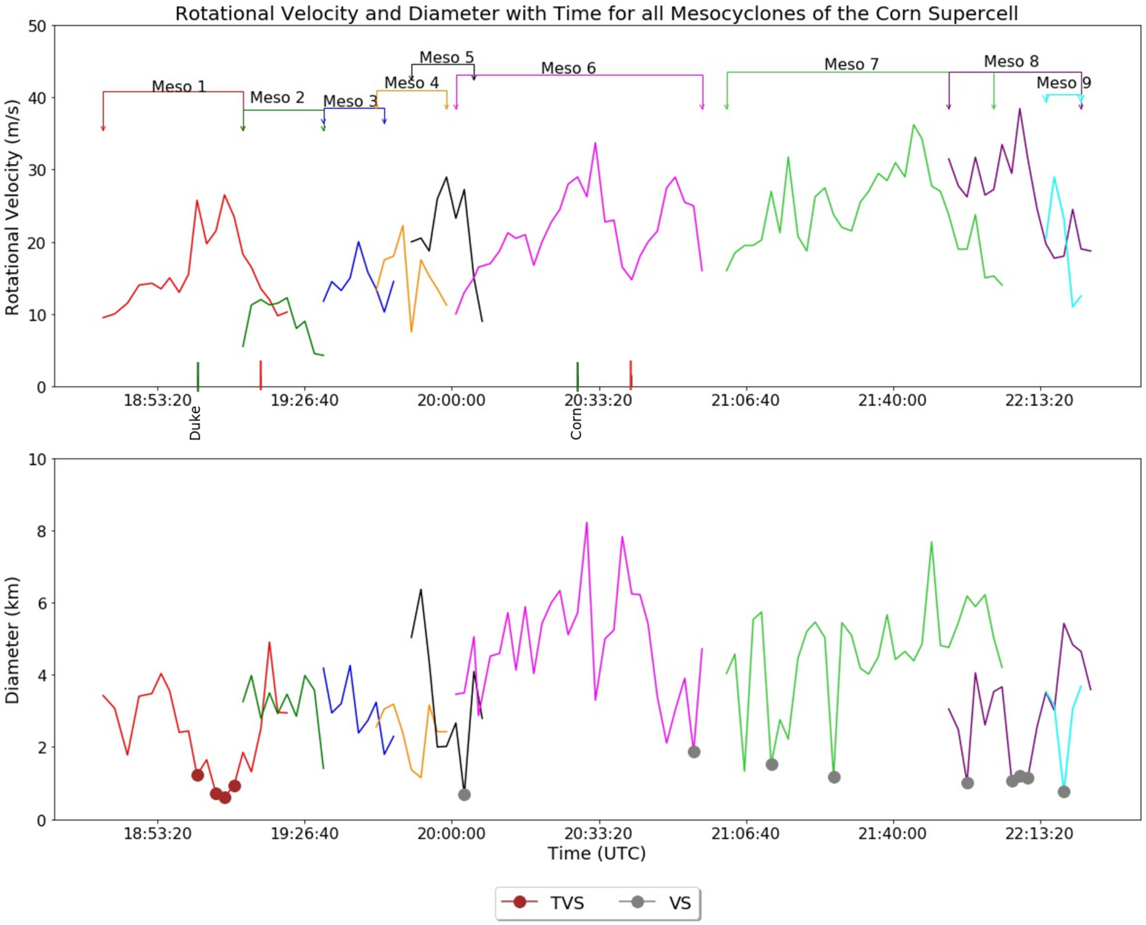

Figure 4.15: Same as in Fig. 4.10 but with the Corn supercell of 18 May 2017.

Similarly, the evolutions of the five mesocyclones produced by the Hennessey supercell are outlined in Fig. 4.13. As mentioned above, all of the Hennessey mesocyclones went through occluding cyclic mesocyclogenesis, and no tornadoes were reported. However, there was a VS observed in the radial velocities during the first mesocyclone. The first and second mesocyclones were the strongest, while the remaining ones were relatively weak. Also, the longest-lived mesocyclones were the first and last produced by this storm. The shortest and weakest mesocyclone was the third. Other than the apparent lack of tornadogenesis with these mesocyclones, this supercell was a classic example of occluding cyclic mesocyclogenesis. Almost all of the tracks have a signature left turn at the end that signifies the mesocyclone has occluded from the main updraft, and is moving to the left of storm motion (Fig. 4.12).

4.4 Summary of Trends Between Cases

When comparing all four supercells to each other, there are a few trends that stand out. First, a minor trend found is the relationship between rotational velocities and the diameter of the mesocyclones (Figs. 4.2, 4.10, 4.15, and 4.13). While it is not always the case, mesocyclone rotational velocities and diameter appear to have an inverse relationship. An inverse relationship would make physical sense because if the diameter of a circulation decreases, the angular momentum increases, and the circulation will rotate faster. Consistent with the conservation of angular momentum. While this trend is often seen in the data, it is not always apparent and, therefore, cannot be labeled as a concrete relationship between the two parameters.

Second, for the Elk City and Corn supercells exhibiting both cycling modes, the nonoccluding phase always occurred first. For each of these two supercells, there was only one transition period between the different cycling modes. Once the transition to occluding cyclic mesocyclogenesis happened, the supercell would stay in this phase until it dissipated. Environmental hodographs taken during the Corn and the Elk City supercells show an increase in curvature and SRH in the low levels when the supercells transitioned to occluding cyclic mesocyclogenesis. These changes in SRH and the impacts on the mode of cyclic mesocyclogenesis is similar to that outlined in Adlerman and Droegemeier (2005; Fig. 2.6). However, and in-depth look at various environmental parameters and how they affect the transition between cycling modes could serve as a future research topic.

Lastly, out of the 24 mesocyclones analyzed from all four supercells, only 5 of them were nonoccluding. Also, out of the 8 tornadoes that formed over all four storms only one of them was produced by a nonoccluding mesocyclone. In Section 4.2, the question was posed of whether or not the cycling mode has any effect on tornadogenesis. While it is not impossible to have a tornado form with a mesocyclone that will go through nonoccluding cyclic mesocyclogenesis (as shown with the Corn supercell), within this sample tornado occurrence within nonoccluding mesocyclone was rare. However, only four supercells were analyzed throughout this research, which is a very small sample size. A larger sample of cyclic supercells would have to be examined to find any substantial relationships between cycling mode and tornadogenesis.

Chapter 5

Results of the Sensitivity Experiments

5.1 3-km vs. 1-km Horizontal Grid Resolution

5.1.1 3-km Cyclic Mesocyclogenesis

According to the idealized simulations performed by Adlerman and Droegemeier (2002), resolving cyclic mesocyclogenesis was sensitive to horizontal grid resolution. The authors found that cycling didn't occur at grid spacings coarser than 1 km. This may be attributed to the small-scale processes occurring at the surface (surging of the gust front to occlude the mesocyclone) that a coarse grid spacing of 3 km cannot fully resolve. Therefore, the preliminary hypothesis for the first sensitivity experiment was there would be no cycling observed on the NEWS-e 3-km grid, but cycling would likely be resolved at the 1 km grid. Analysis of the 3-km forecasts for the Corn and Hennessey supercells of 18 May 2017 found six instances of "cyclic mesocyclogenesis-like" processes in the low levels. These processes are termed "cyclic-like" because they behave like real cases of cyclic supercells, but at grid resolutions that are too coarse to fully resolve them.

Five of the 3-km cycling cases were within the Hennessey supercell (Fig. 5.1), and the last case occurred during the Corn supercell (Fig. 5.2). There were two ensemble members that produced cyclic-like processes during the Hennessey supercell: members 2 and 8 (Fig. 5.1). The Hennessey supercell produced by member 2 cycles once in 3 out of the 4 forecast periods analyzed. Member 2's first mesocyclone is seen at 2245 UTC and is represented by the high vertical velocities and a corresponding area of maximum vertical vorticities (Fig. 5.3). Around the 15–20 min, downdraft air (negative vertical velocities in Fig. 5.3) start to wrap around the first mesocyclone. As the downdraft surrounds the mesocyclone, it begins to occlude from the original updraft and move to the left of the storm's motion. At 40 min,

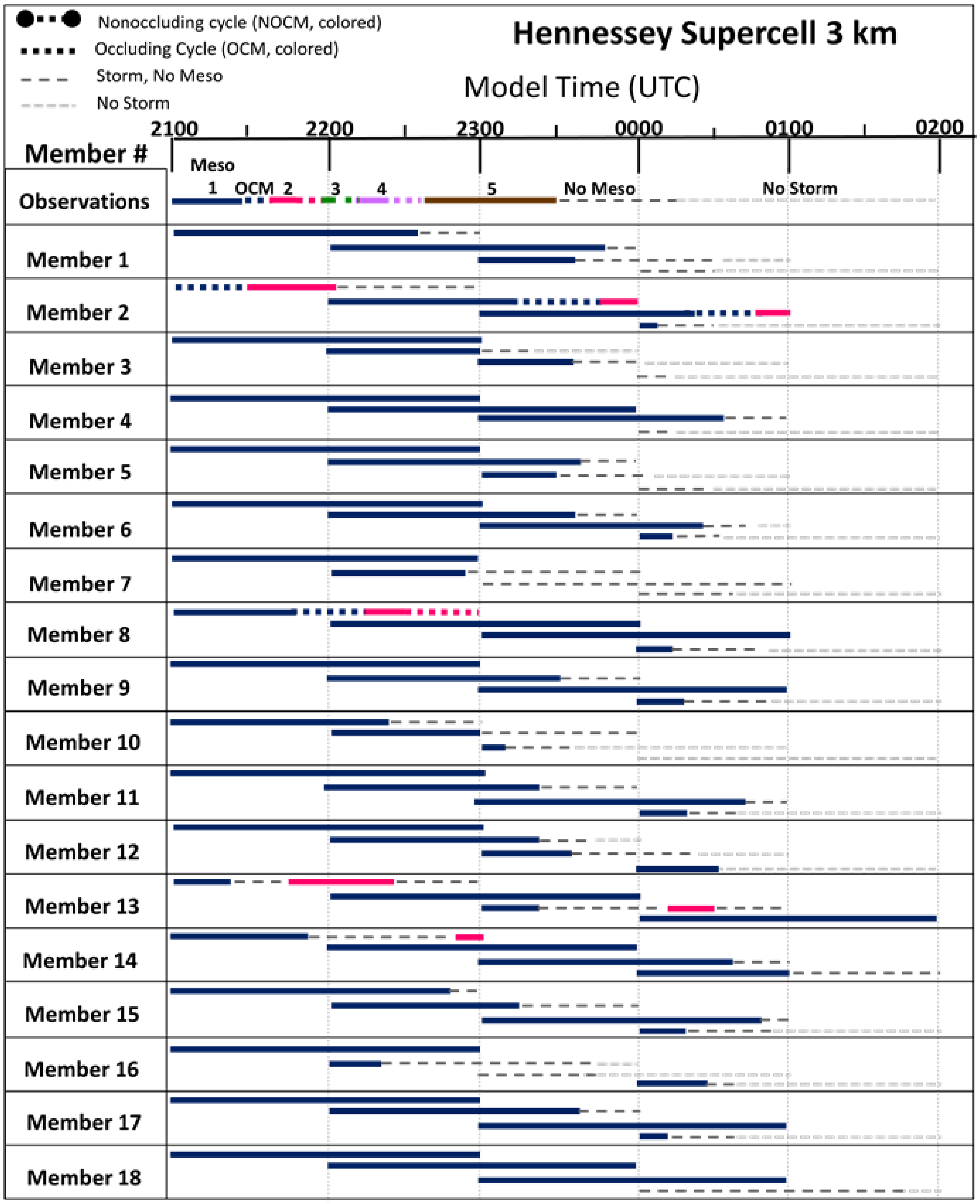

Figure 5.1: Summary of results from 3-km, 18 member forecasts for the Hennessey supercell of 18 May 2017. WSR-88D radar observations are given at the top with the legend overlaid above. For the ensemble members, there were four forecasts (2000, 2100, 2200, and 2300 UTC) analyzed and are displayed as stacked bars. Recall that the first hour is ignored, so if the forecast was initialized at 2000 UTC the bar begins at 2100 UTC.

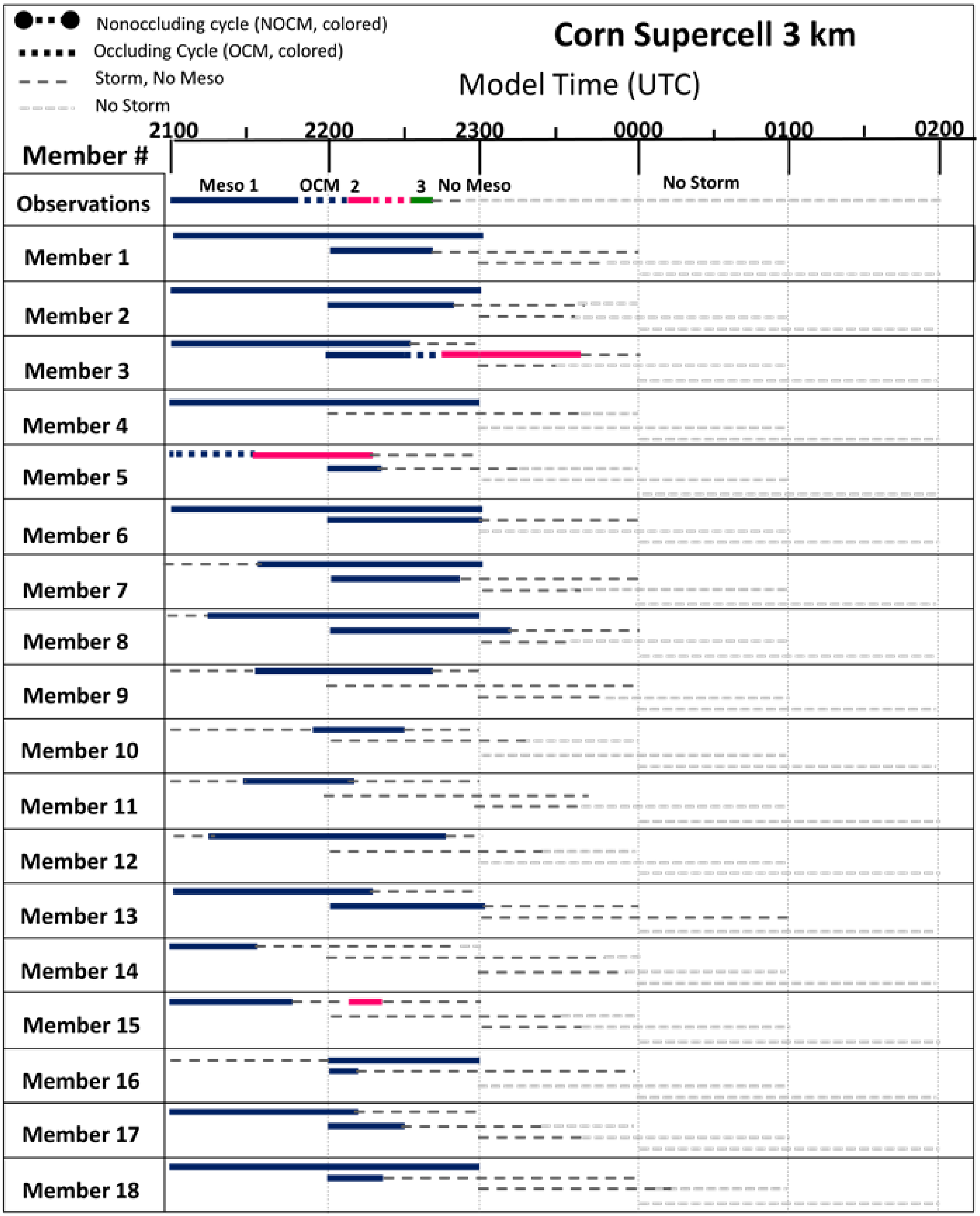

Figure 5.2: Similar to Fig. 5.1, but for the Corn supercell for the forecasts of 2000, 2100, 2200, and 2300 UTC.

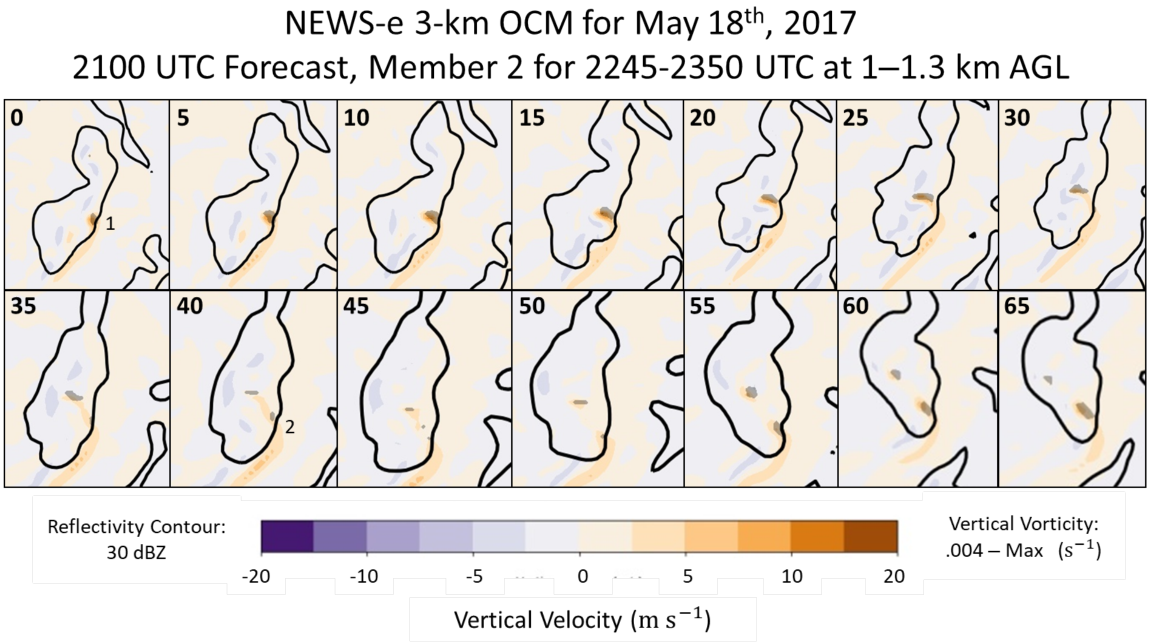

Figure 5.3: Occluding cyclic mesocyclogenesis seen in NEWS-e member 2 at 3 km during the 2100 UTC (2245–2350 UTC) forecast on 18 May 2017 for the Hennessey supercell. Maximum vertical vorticity is shaded in gray, vertical velocities are colored, and the black outline represents the 30 dBZ reflectivity line. The time is shown in the upper left corner of each panel and is in minutes after the start time (2245 UTC). Mesocyclones are numbered as they first appear.

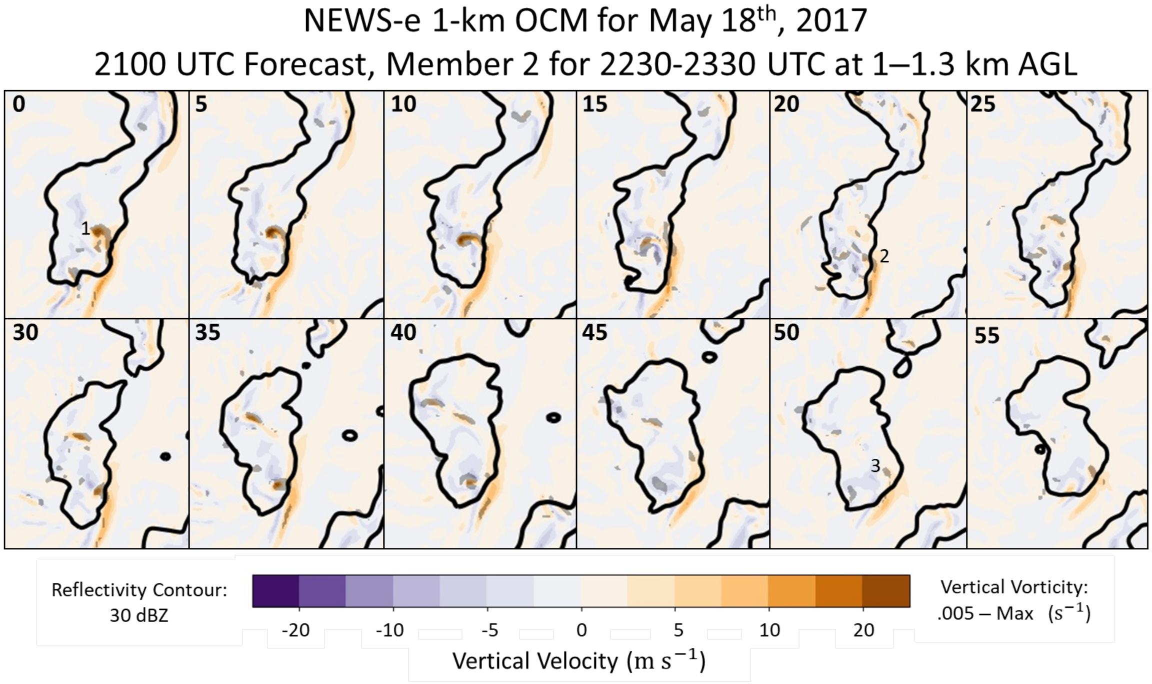

Figure 5.4: Similar to Fig. 5.3 but at 1 km. Note that these images are for a slightly different time frame than that in Fig. 5.3 (2230–2330 UTC).

the second mesocyclone is beginning to form along the gust front as the first mesocyclone decays in the heavy precipitation region of the Hennessey supercell. This process is very similar to that outlined in previous studies (e.g. Burgess et al. 1982; Adlerman et al. 1999; Beck et al. 2006; French et al. 2008).

The remaining cases for 3-km cyclic mesocyclogenesis exhibited similar processes (seen in Fig. 5.3), where the first mesocyclone becomes surrounded by the RFD (20–25 min mark in Fig. 5.3), occludes and moves to the left of storm motion, and decays in the heavy precipitation. The most simple way to identify cyclic mesocyclogenesis at 3 km was to watch the downdraft. For the cycling cases, the downdraft would clearly wrap around the mesocyclone and cause it to break off from the original updraft (25–30 min mark in Fig. 5.3). In cases where the storms were steady-state, or noncycling, the downdraft would stay off to the side of the updraft and would not move to undercut it. Therefore, the occlusion was an important criterion when classifying which storms were cycling and which were not. In the case of a nonoccluding cycle, there had to be development of a secondary mesocyclone to the north while the old mesocyclone moved south along the gust front.

Analyses on the timing of the cycles compared to the actual observations found large differences. For member 2, the first cycle is the closest in timing to the observations for the Hennessey supercell, but is temporally displaced by 30 min. The cycle starts at the beginning of the forecast and ends around the same time that the actual cycle begins for the observations. For the subsequent forecast times (2100 and 2300 UTC), the cycles occur towards the end of the forecast, which corresponds to the decay of the last Hennessey mesocyclone or when there is no longer a supercell present in the observations. Member 8, on the other hand, cycles two times during the 2100 UTC forecast. The first cycle occurs at the same time as the second and third cycles in the observations, and the second cycle happens around the same time as the fourth cycle. The last cycle persists through the end of the forecast period, which is when the fifth mesocyclone is occurring in the observations.

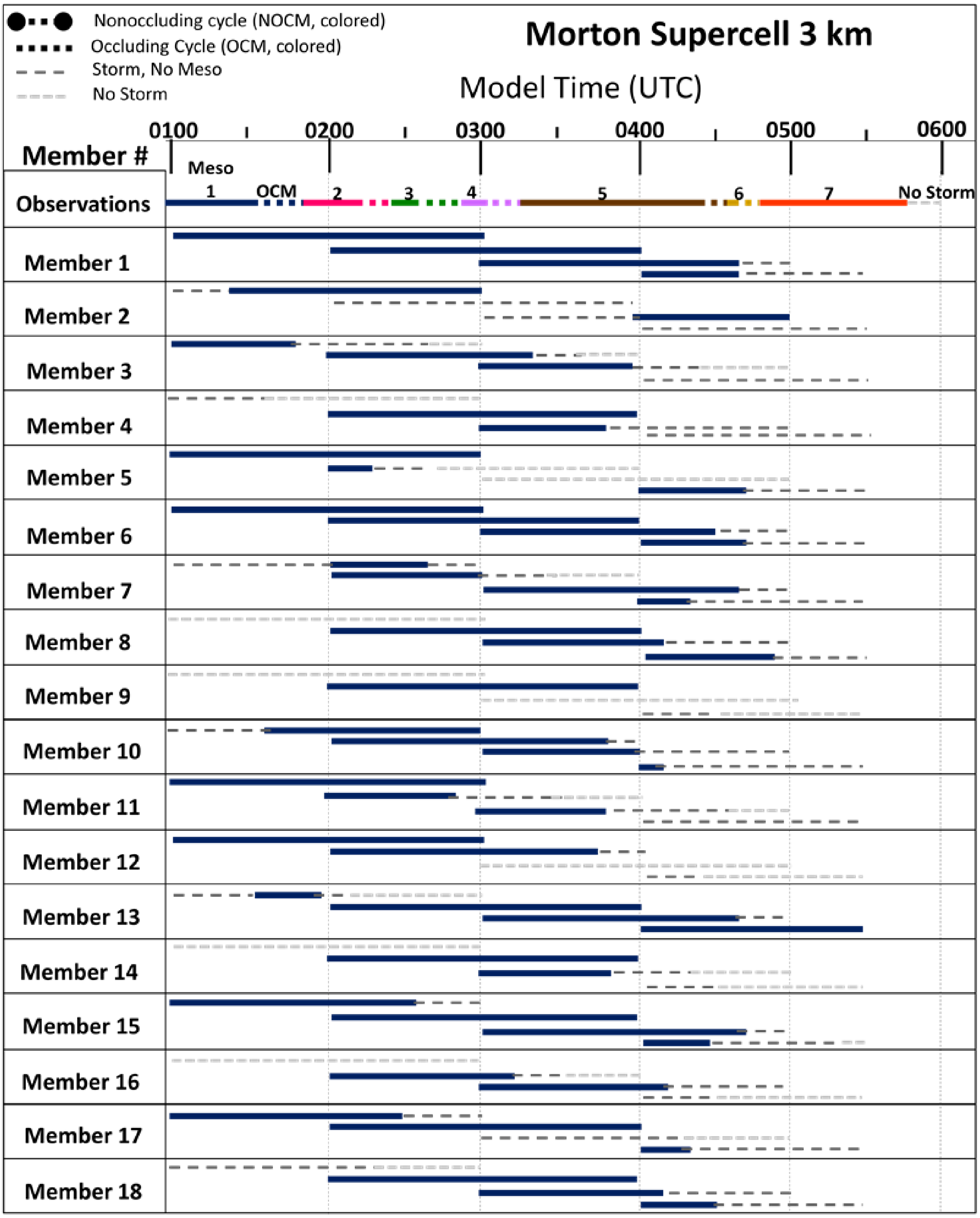

Figure 5.5: Similar to Fig. 5.1, but for the Morton supercell of 9 May 2017 for the forecasts of 2000, 2100, 2200, and 2300 UTC.

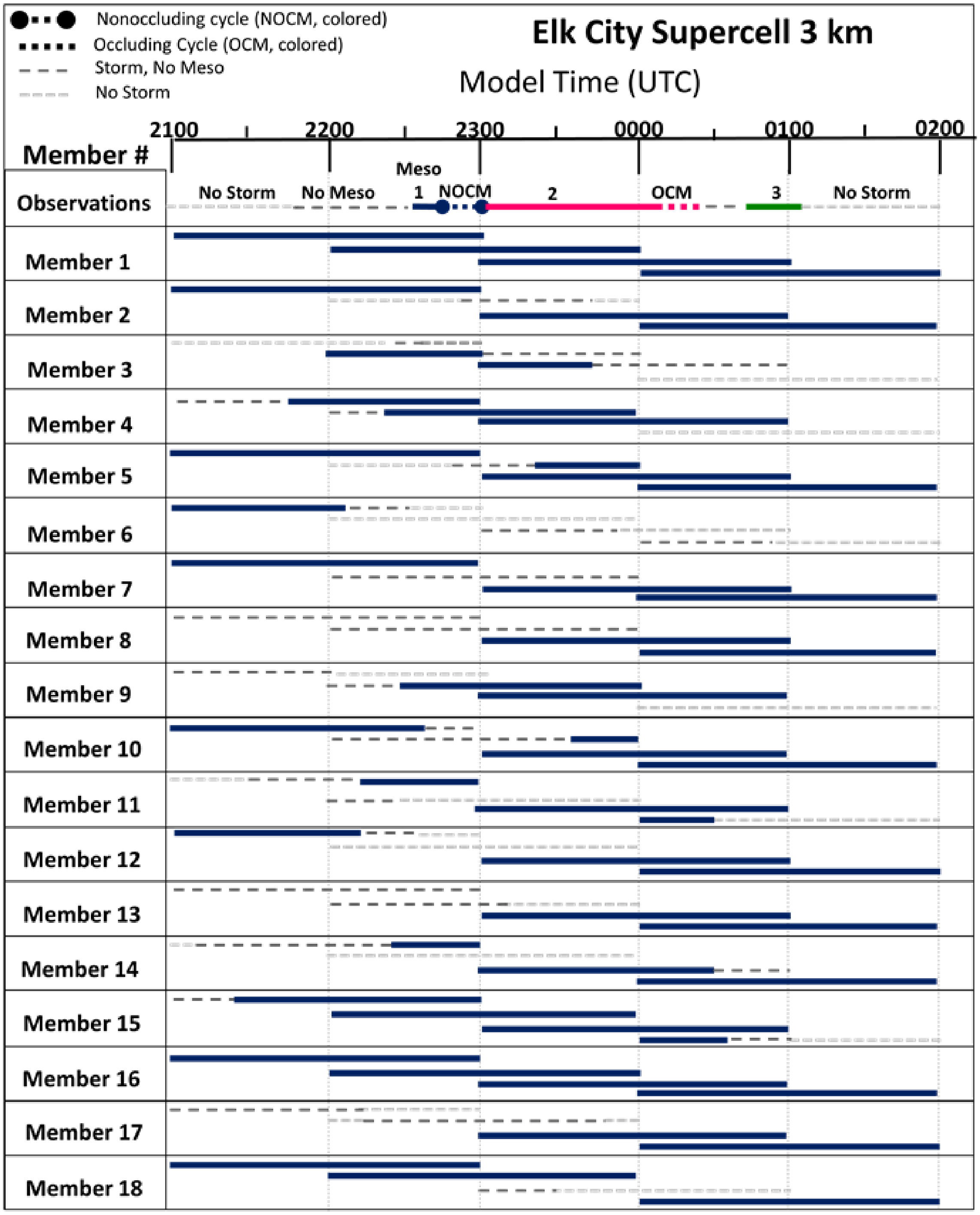

Figure 5.6: Similar to Fig. 5.1, but for the Elk City supercell for the forecasts of 0000, 0100, 0200, and 0300 UTC. The 0300 UTC forecast ends 30 min early because boundary conditions were not available to finish the forecast.

Even though the cycling frequency wasn't predicted, the timing was superior compared to member 2's forecasted cyclic mesocyclogenesis.

The reason why members 2 and 8 forecasted cyclic mesocyclogenesis-like processes and the other members did not is unclear. Interestingly, the forecast members share the same PBL (YSU) and radiation parameterizations (RRTMG for longwave and shortwave radiation). However, the parameterizations themselves wouldn't have caused the cycling-like characteristics to occur because member 14 also has the same parameterizations, but did not cycle. The reasoning as to why the two members cycled and the others did not, most likely has to do with their differences in environmental boundary conditions. A set of different boundary conditions are given to members 1–9, and those are then repeated for 10–18. For instance, members 2 and 11 would have the same boundary conditions but different PBL parameterizations (YSU vs. MYNN, respectively). Although members 2 and 8 have the same physical parameterizations, they have different boundary conditions, and thus are influenced by different environmental conditions.

The last case of cycling at 3 km was from member 3's 2100 UTC forecast of the Corn supercell on 18 May 2017 (Fig. 5.7). There is only one cycle and it starts approximately 10 min after the second control cycle. The duration of the cycle is close to the control, which was about 15 min. Member 3's Corn storm may have cycled because of its interactions with the trailing Hennessey storm. At the beginning of the forecast, the Hennessey storm is trailing the Corn storm, both of which have clear mesocyclones present (Fig. 5.7). As time progresses, the Hennessey storm starts to merge and overtake the Corn storm. At the 30 min mark, Corn's RFD starts to impinge on the first mesocyclone. Within 5 min, the first mesocyclone has fully occluded from the main updraft and begins to move to the left of storm motion. A new mesocyclone develops in its place at t = 50 min (Fig. 5.7). However, with the Hennessey cell so close to the Corn storm, it may have contributed to the cycling process. The forward-flank precipitation region of the Hennessey storm would have precipitated into the RFD area belonging to the Corn supercell. This added

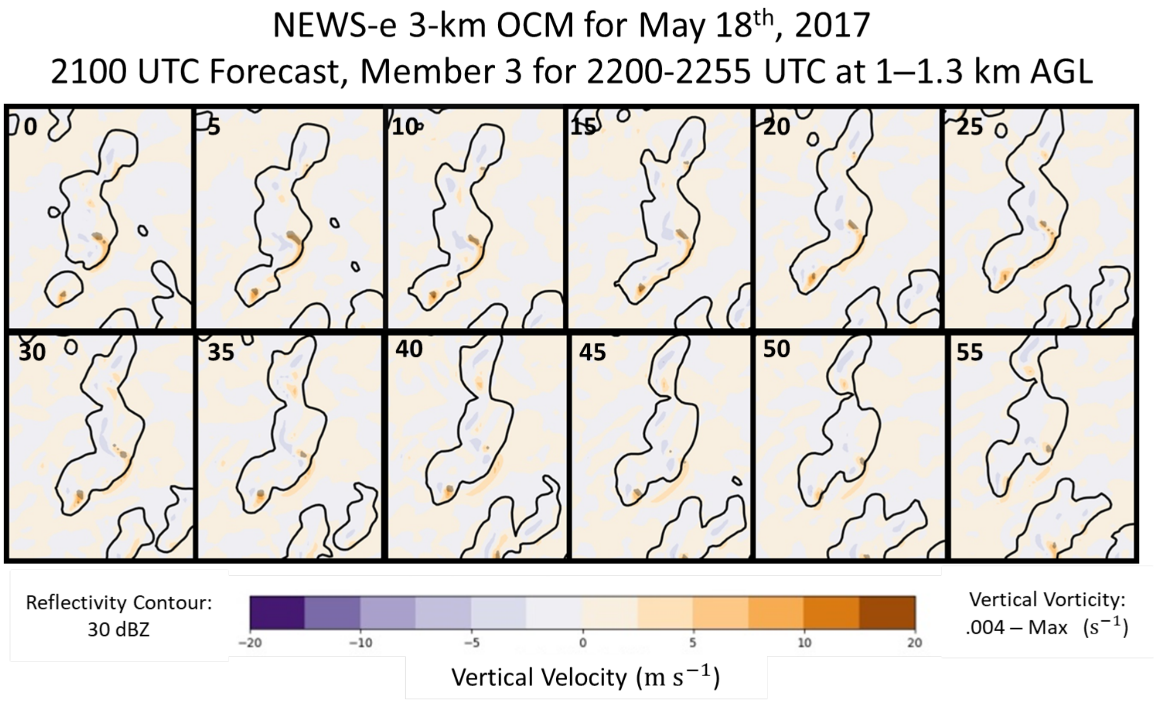

Figure 5.7: Similar to Fig. 5.3, but for the Member 3's 2100 UTC forecast of the Corn Supercell. The Northern cell is the Corn supercell, while the trailing cell is the Hennessey supercell.

precipitation causes evaporative cooling and intensifies the downward acceleration in the downdraft. Amplifying the downdraft causes the gust front to surge further away from the updraft, causing the downdraft air to wrap around the mesocyclone and cut it off from its supply of vorticity-rich, buoyant air. A new mesocyclone forms on the bulge of the gust front as the old mesocyclone decays in the heavy precipitation region of the Corn supercell. This is characteristic of occluding cyclic mesocyclogenesis, but may be occurring because a non-local force (e.g. the Hennessey supercell) is triggering the supercell to cycle.

Non-local forces that trigger cycling weren't the only cases of induced cycling that were seen at 3 km. As was mentioned in the Section 3.2, the first hour of the forecast periods are ignored due to data assimilation-induced imbalance that can cause spurious convection to form. The spurious convection can interact with nearby storms by creating a moisture surge, which can enhance the RFDs of supercells in the domain. This surge of moisture triggers cycling to begin in much the same way that a trailing supercell raining into a storm's downdraft would. This is the main reason why the first hour of the forecast is ignored, as to cut down on cases of data assimilation-induced cyclic mesocyclogenesis that sometimes occur in the 3-km and 1-km domains.

Recalling the Adlerman and Droegemeier (2002) study, cyclic mesocyclogenesis was once thought to be impossible to simulate at horizontal grid resolutions coarser than 3 km. An important result of this research is that NEWS-e was able to resolve a few cases of cyclic mesocyclogenesis-like processes (Figs. 5.1 and 5.2). Adlerman and Droegemeier's (2002) study used an ideal simulation with no PBL or radiation parameterizations. They also used the Kessler warm rain microphysics scheme for their control simulation. However, they found that when ice microphysics was added the model tended to handle cycling better. NEWS-e has multiphysical parameterizations, ice microphysics, and is horizontally heterogeneous. The variation in NEWS-e may have helped the system predict the possibility of cyclic mesocyclogenesis-like processes at coarser grid spacings. However, the cycling at 3 km was still very rare when compared to the very frequent cycling at 1 km.

Therefore, the horizontal grid resolution does have a large effect on the presence of cycling in NEWS-e.

5.1.2 1-km Cyclic Mesocyclogenesis

5.1.2.1 Cycling Duration

As was expected from the results of the Adlerman and Droegemeier 2002 study, cyclic mesocyclogenesis in NEWS-e was observed more frequently at 1-km grid spacings. For the 3-km NEWS-e runs, there were only two storms that exhibited cyclic characteristics: the Hennessey and Corn supercells. On the other hand, all four of the supercells displayed characteristics of cyclic mesocyclogenesis at 1 km. With the exception of the Corn supercell that didn't cycle as frequently due to NEWS-e only simulating the end of the storm. Out of the three other supercells analyzed with 18 forecast members each, only a seven forecast members didn't cycle. Nevertheless, cycling was very common at 1 km whereas at 3 km it was rare to observe.

One aspect of cyclic mesocyclogenesis that Adlerman and Droegemeier (2002) studied was how the duration of each cycle varied with horizontal grid resolution. Cycling duration is the time between when the mesocyclone starts to move to the left of the storm motion and ends with its decay. However, because Adlerman and Droegemeier's (2002) 3-km model runs never cycled, they couldn't examine if there were any cycling duration differences between 3-km and 1-km resolutions. Luckily, there are members at 3 and 1 km that cycle for both resolutions, allowing duration differences to be analyzed. Since most of the 3-km forecast members did not cycle, only the few members that did will be compared to their 1-km counterparts. For the Hennessey supercell, two members cycled at both 3 km and 1 km: members 2 and 8 (Fig. 5.1). For member 2 on a 3-km grid, the first cycle of the 2000 UTC forecast occurs around the same time as the first cycle at 1 km. The 3-km cycle lasts for about 30 min, while the 1-km cycle has a duration of 15 min. For the 2100 UTC forecast, the 3-km cycle also has a duration of approximately 30 min. The 2100 UTC forecast for 1

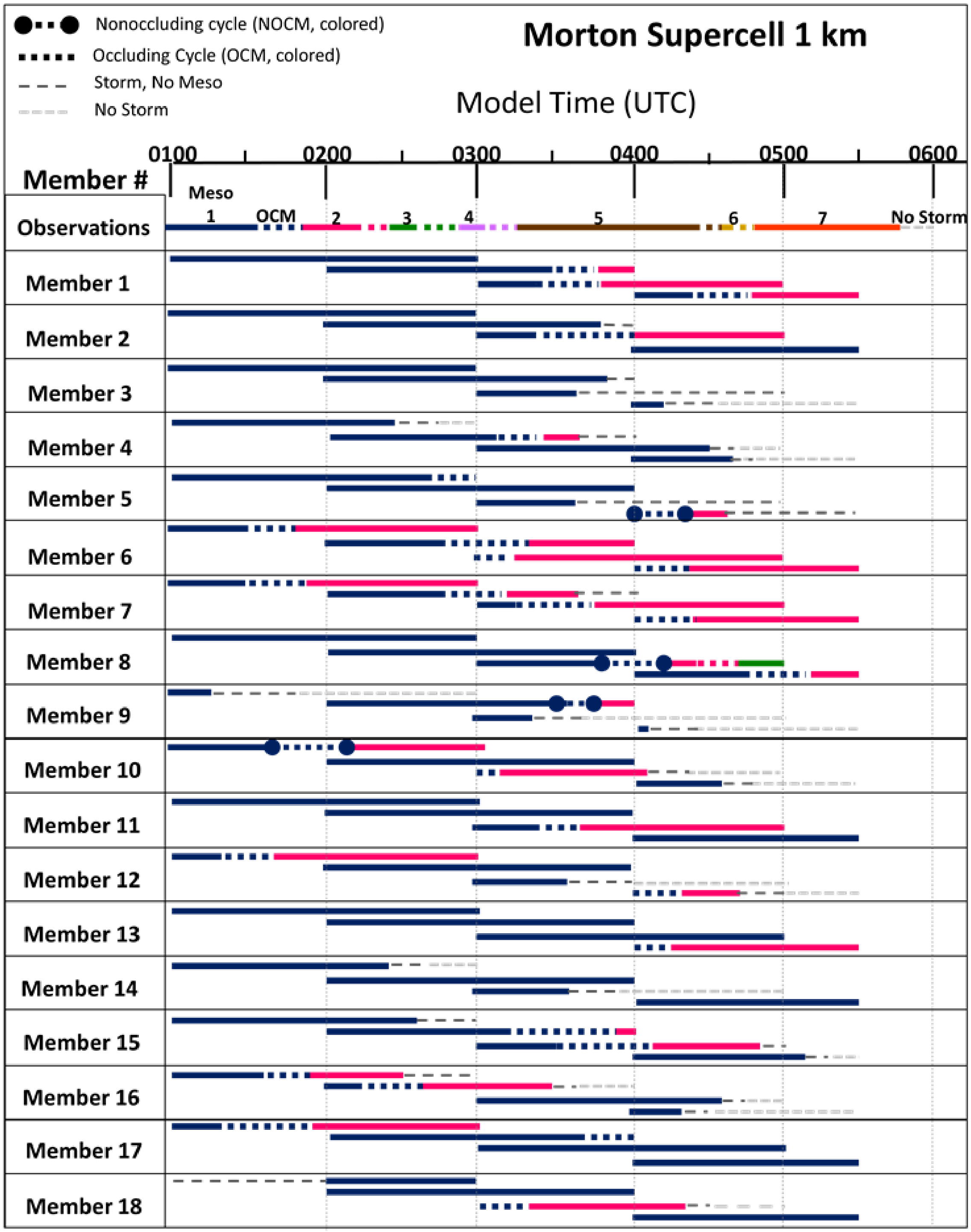

Figure 5.8: Similar to Fig. 5.5, but for the Morton supercell 1-km forecasts.

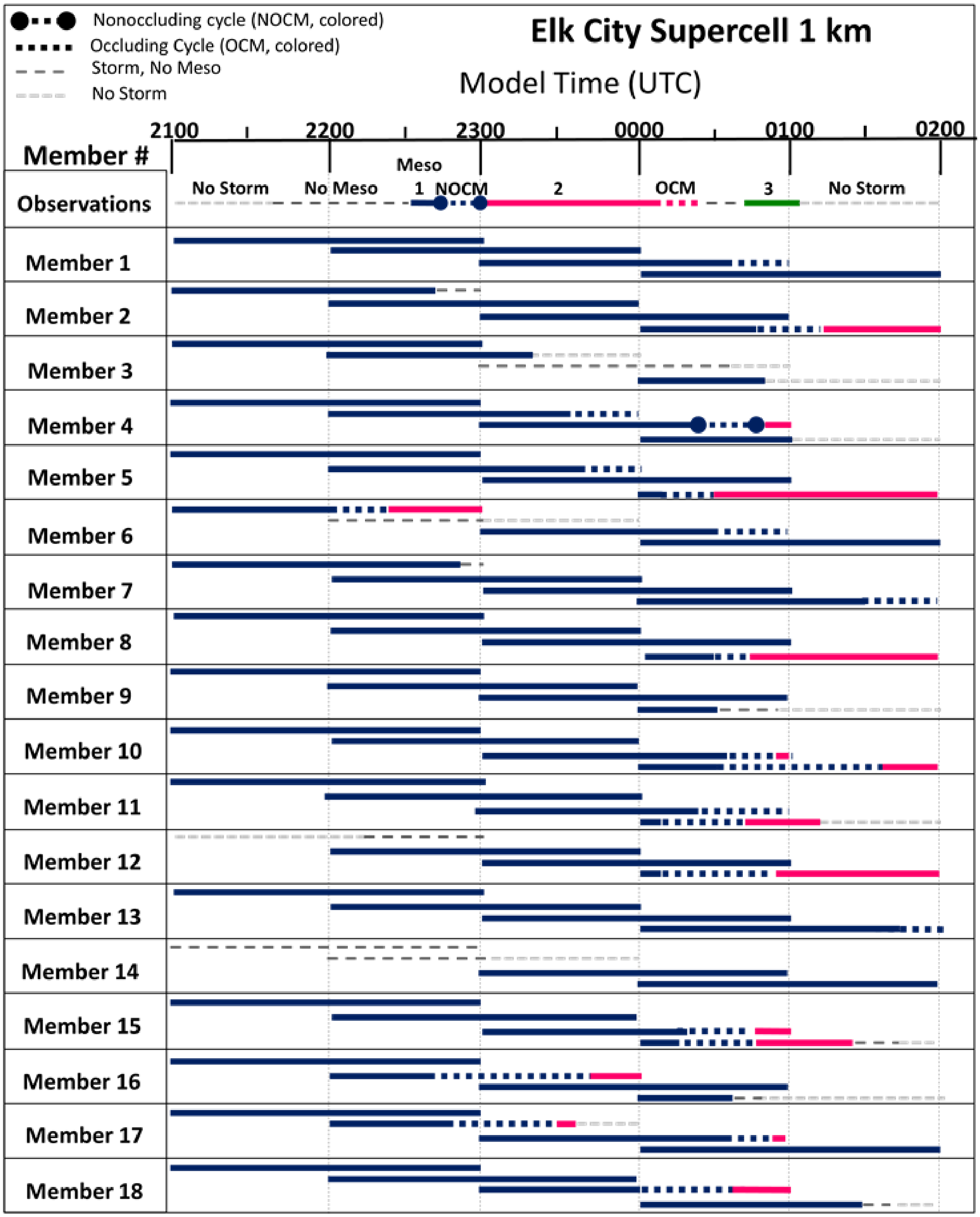

Figure 5.9: Similar to Fig. 5.6, but for the Elk City supercell 1-km forecasts.

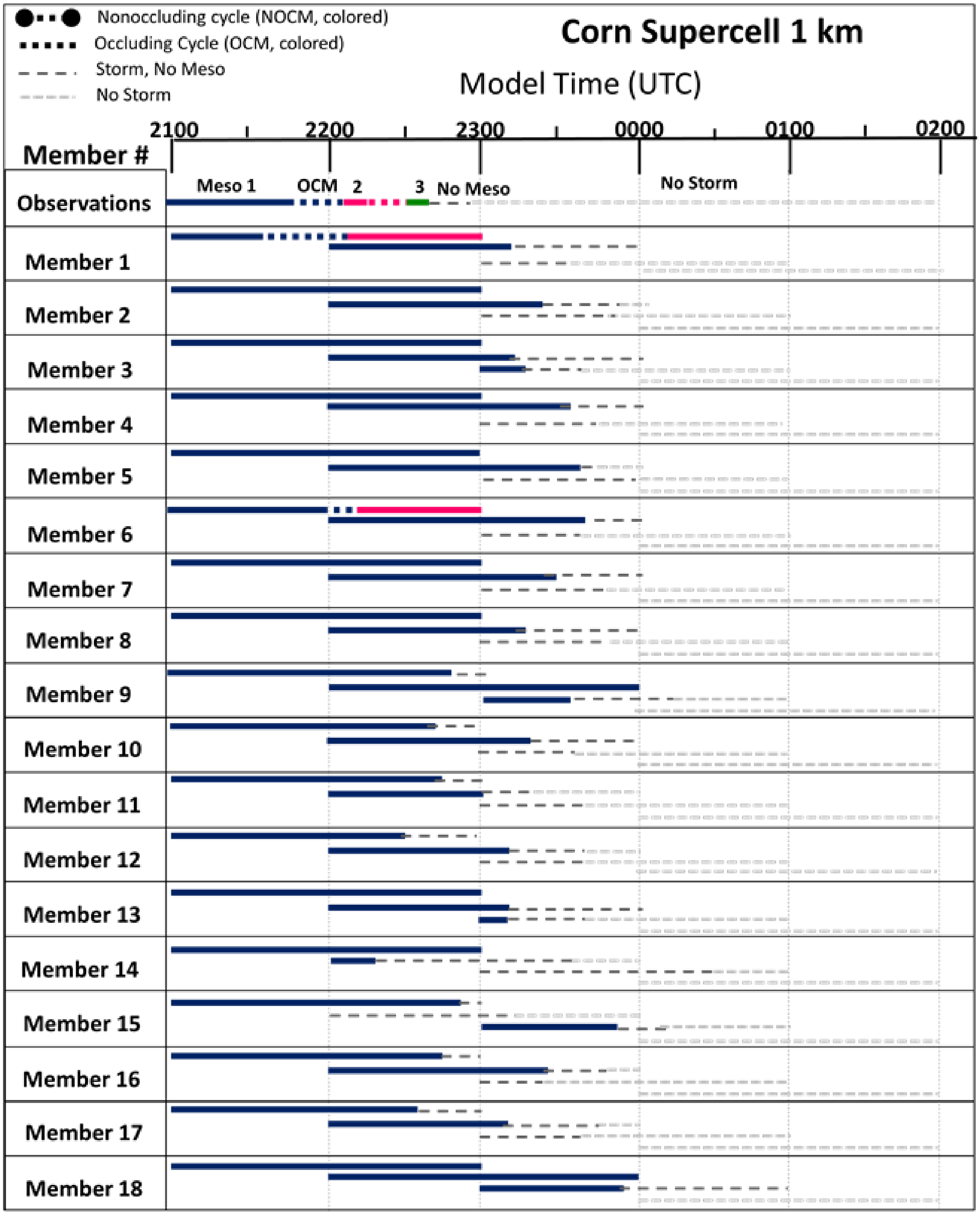

Figure 5.10: Similar to Fig. 5.2, but for the Corn supercell 1-km forecasts.

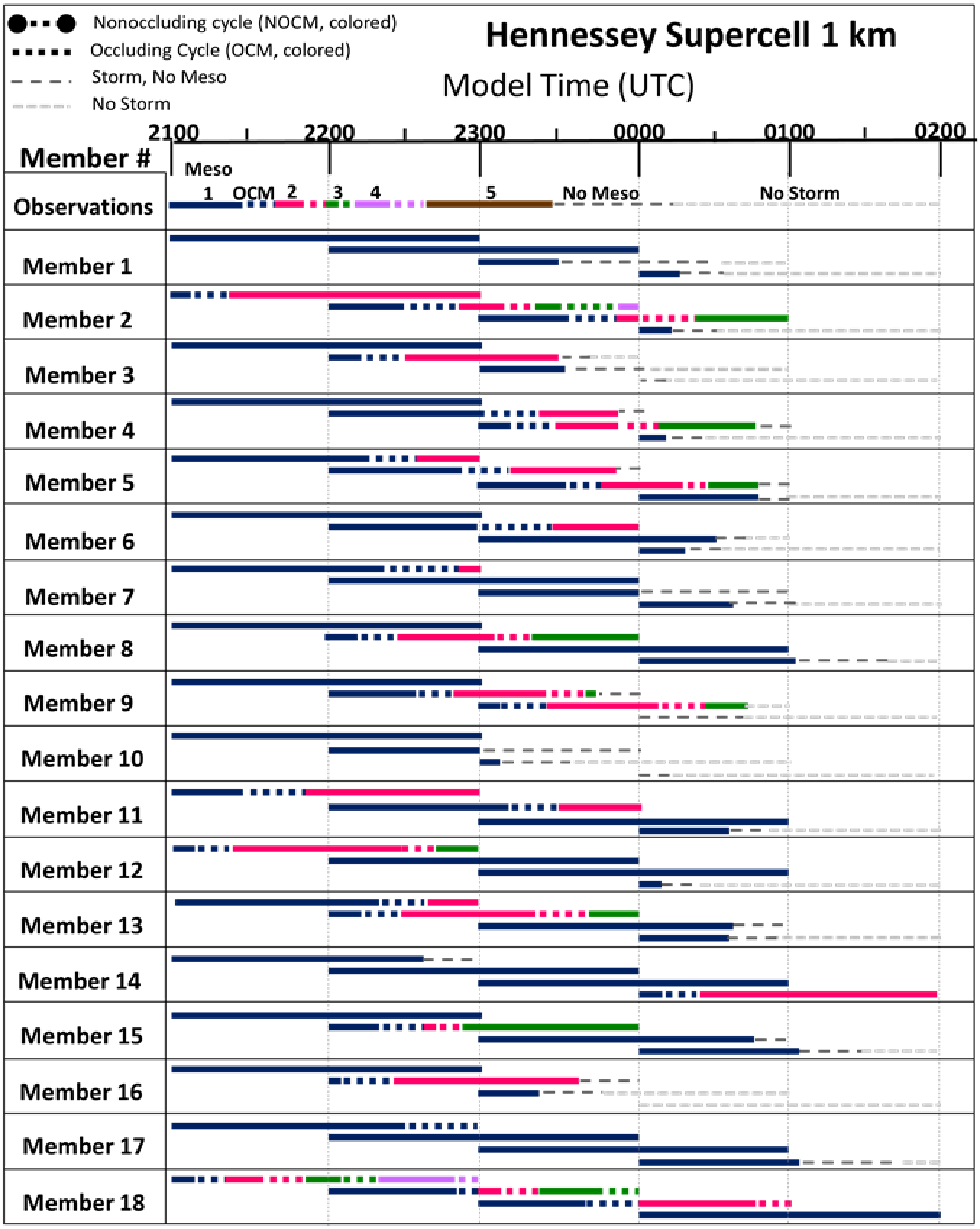

Figure 5.11: Similar to Fig. 5.1, but for the Hennessey supercell 1-km forecasts.

km (Fig. 5.11) has a total of 3 cycles, where the last two correspond to the timing of the 3-km cycle. These last two cycles last about 10 min and 20 min, respectively. Lastly, the duration of the 3-km cycle for the 2300 UTC forecast is 25 min. The 1-km forecast at the same time has two cycles occurring, with the last one closest to the time of the 3-km cycle (Fig. 5.11). This last cycle lasts 20 min. At 1-km, all of the cycles that occur for member 2 are shorter compared to that of its 3-km counterpart. The 3-km cycles are mostly near 30 min in duration, which is almost twice the length of some of the 1-km cycles.

The above analysis assumed that the cycles seen at 3 km are the same cycles that are observed at 1 km. This may not be the case, so the cycling durations for all the 1-km supercells and the two 3-km supercells that cycle are compared. Fig. 5.12 shows a box-and-whisker plot for all of the cycling durations that occur at both 1 and 3 km. First, comparing the Corn supercell cycling durations from 1 km to 3 km shows that, generally, the 3-km cycles may have longer durations even though there is some overlap between the distributions. The same can be seen for the Hennessey supercell from 1 km to 3 km, with the longer durations occurring at 3 km. This result is similar to the conclusion made when directly comparing the cycles that happen at 3 km to the ones that occur at 1 km, assuming they are the same cycles. However, when comparing the Corn and Hennessey cycling durations at 1 km to the Morton and Elk City cycling durations, the Corn and Hennessey supercells have shorter durations overall. There are no 3-km cycles that occur with the Morton or Elk City supercells, so we cannot conclude that the cycling durations will always be longer at 3 km compared to 1 km. Additionally, the short cycling durations for the Hennessey and Morton supercells coincided with a higher cycling frequency than the other supercells (Corn storm didn't cycle much so it is not included). On the other hand, the Elk City supercell had a lower cycling frequency as well as very long durations. Therefore, the supercells that had shorter durations had more cycles occurring, whereas the longer durations were associated with fewer cycles.

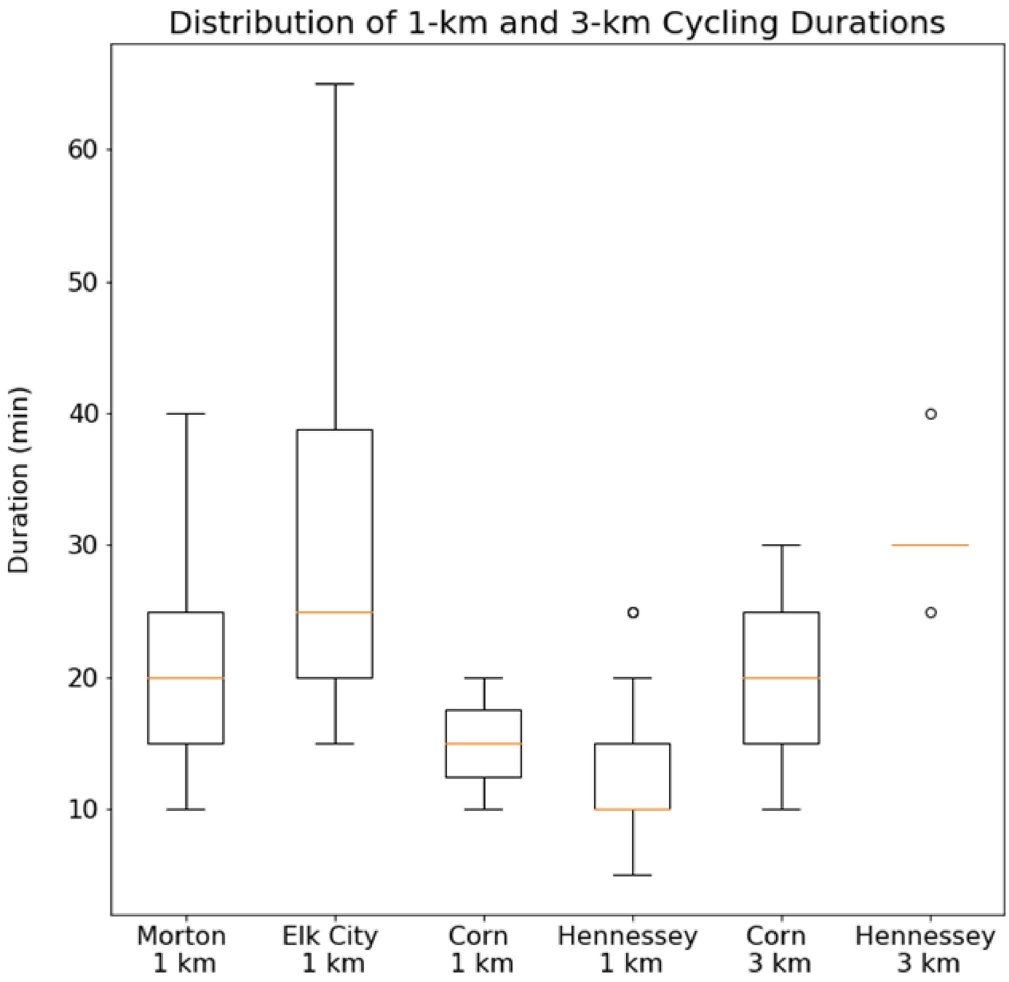

Figure 5.12: Box-and-Whisker plot for the cycling durations for all of the supercells at 1 km and the Hennessey and Corn supercells that cycled at 3 km. Circles represent outliers in the distributions. The gold line indicates the median or 50th percentile, the bottom of the box is the 25th percentile, and the top of the box is the 75th percentile. The lower whisker is calculated by taking 1.5 x IQR and subtracting that from the value of the first quartile (IQR is the Interquartile range). The higher whisker is calculated by taking 1.5 x IQR and adding it to the third quartile. The outliers are any values outside of whisker ranges.

To summarize, the cycles at 3 km for the Hennessey supercell is longer than that at 1 km. These longer durations may be attributable to the coarse grid spacing only able to resolve the broad-scale circulation or mesocyclone, and not the smaller-scale processes that influence cyclic mesocyclogenesis. At 1 km, there are many smaller circulations that occur where it is easier to see the occlusions of mesocyclones as they break away from the larger updraft. This is even seen in Fig. 5.4 where there are two cycles occurring at 1 km around the same time as one, large cycle at 3 km (Fig. 5.3). The 3-km grid is unable to resolve the smaller cycles, and so it translates it into a one, longer cycle. Additionally, the vertical velocities and vertical vorticities are weaker at 3 km compared to that at 1 km. Therefore, updrafts and downdrafts in the 3 km runs are weaker. If the 3-km RFD is weaker then it would take more time for it to wrap around the mesocyclone and fully occlude it. Therefore, cycling may take longer to complete because the RFD is weaker and slower than in the 1-km NEWS-e runs. However, the sample size being tested in this study is very small because there were not many forecast members that cycled at both the 3-km and 1-km resolutions. More cases would have to be observed where cycling occurs at both resolutions to see if the durations at 3 km are consistently longer than those at 1 km.

5.1.2.2 Cycling Frequency and Timing

Compared to their 3-km counterparts, the 1-km NEWS-e forecasts show more frequent cycling throughout the majority of the ensemble members. Even when cycling was observed in the 3-km forecasts, the 1-km forecasts for the same time and ensemble members produced more episodes of cycling. The NEWS-e 1-km members are better able to resolve the smaller-scale cycles than the 3-km members, which, as previously stated, are most likely only partially resolving broad-scale rotation and cycling. Also, the supercells that had more observed cycles (Morton and Hennessey) exhibited an overall (i.e. between all members and all forecast times analyzed) larger number of cycles (Fig. 5.13). The opposite was true for the cases that had fewer observed cycles (Elk City), which showed less frequent cycling as well as a smaller overall number of cycles.

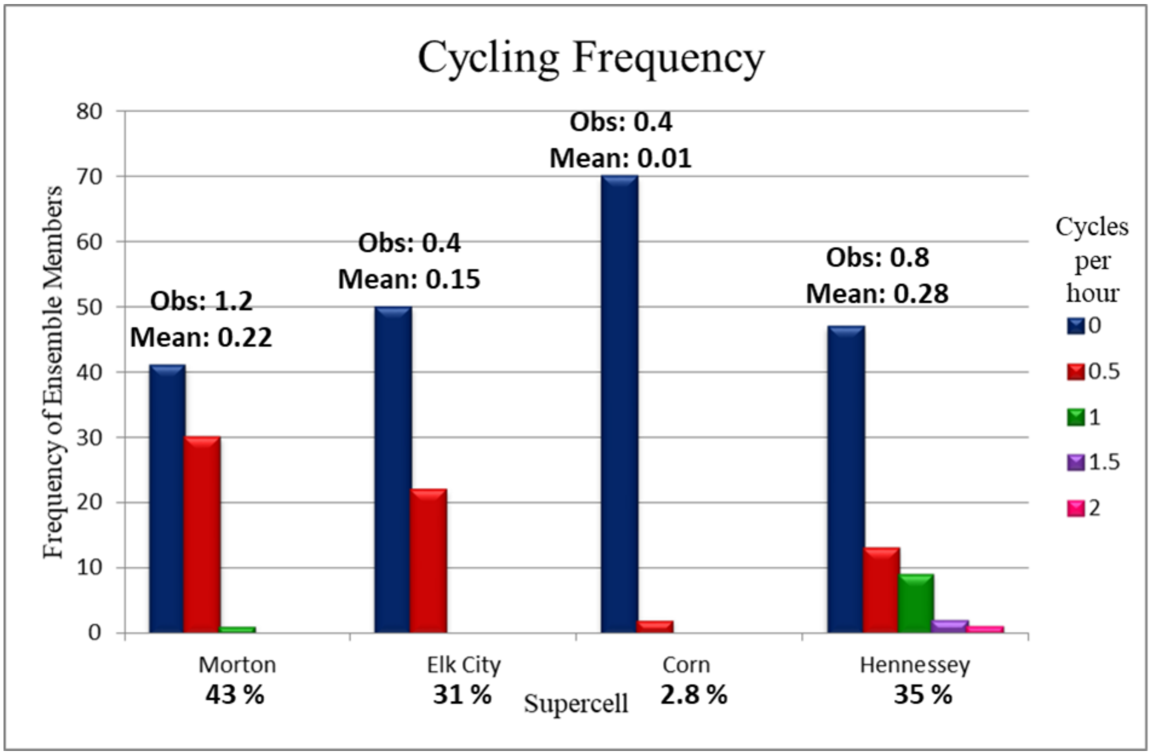

Figure 5.13: Cycling frequency for the four supercells at 1 km. The bars denote the cycles per hour observed with each supercell. The observation value and the mean above the bars represent the cycles per hour in the observations and the mean of the distribution for each supercell, respectively. The percentages below each supercell is the amount of cycling ensemble forecasts out of the total of 72 (18 forecast members multiplied by four forecasts available for each case) ensemble forecasts examined.

One supercell that was a high-cycling case is the Morton supercell of 9 May 2017 (Fig. 5.8). The Morton supercell had seven identified mesocyclones on WSR-88D data, and displayed six episodes of occluding cyclic mesocyclogenesis. However, the forecast times examined in this case (0000, 0100, 0200, and 0300 UTC forecasts) exhibited a variety of cycling types, like nonoccluding cyclic mesocyclogenesis that was not observed in radar.

There were four instances of nonoccluding cyclic mesocyclogenesis (members 5, 8, 9, and 10 in Fig. 5.8), all of which occurred before the occluding cycles (if there were any). This is similar to the observations for the Elk City and Corn supercells that displayed both forms of cyclic mesocyclogenesis, in which the nonoccluding cycles always took place before the occluding cycles (Figs. 4.5 and 4.11).

The majority of the cycles observed in the Morton supercell occur within the time frame of 0100–0315 UTC. For the NEWS-e forecast members, ten out of the eighteen members produced cyclic mesocyclogenesis for at least one forecast time during that time frame, with a total of 16 cycles across all members. While the majority of members only had one cycle occur within the 0100–0315 UTC time frame, four members displayed two or three cycles (members 6, 7, 10, and 16 in Fig. 5.8). Having a majority of ensemble members forecast at least one cycle within the time that there were 4 cycles identified in radar data does indicate the possibility for cycling. However, NEWS-e forecast members are unable to fully reproduce the frequency and timing of those cycles. Most of the members only have one cycle during the period of interest, whereas there are four in the observations.

From 0315–0545 UTC, there were only two observed cycles for the Morton supercell. During that time, there were 12 members that had cycles take place, which was more than that seen from 0100–0315 UTC. There were 16 total cycles that took place during this time. However, out of those 16 cycles there were three of them that matched with the two observed cycles. Those cycles belonged to member 1 (0300 UTC forecast) and member 8 (0200 and 0300 UTC forecasts; Fig. 5.8). Although NEWS-e forecast members are predicting the possibility for cycling, the timing is displaced from observations. For instance, the amount of cycles occurring in the NEWS-e forecasts during the period of many (0100–0315 UTC) and few (0315–0545 UTC) observed cycles is the same. Therefore, even if there are fewer cycles occurring in the observations, there is the same amount of cycles being produced than when there are many observed cycles occurring.

On the other hand, the Elk City supercell is an example of a infrequently cycling supercell because it only had two observed cycles on radar. The NEWS-e forecast members for this supercell have a total of 22 cycles (across all forecasts and all forecast members; Fig. 5.9). The NEWS-e forecast times that are examined for this supercell are the 2000, 2100, 2200, and 2300 UTC forecasts. The first observed cycle that occurs is a nonoccluding cycle. However, there is only one case of a nonoccluding cycle in the forecast members (i.e. member 4 during the 2200 UTC forecast in Fig. 5.9), and it happens an hour after the cycle occurs in the observations. There are only two instances of cycling that take place around the time of the first observed nonoccluding cycle (2245–2300 UTC; to be considered the cycle has to start within that time period). While those cycles begin near the same time as the observed nonoccluding cycle, the forecast cycles last up to 30–60 min while the observed cycle only lasted 15 min (members 16 and 17 in Fig. 5.9). This may be attributable to the nonoccluding mesocyclone taking longer to decay because it isn't moving to the left of storm motion and being surrounded by downdraft air, which would lead to its decay. Instead, the cycle travels down the gust front to the south of the storm and gets left behind as the new mesocyclone assumes control of the supercell. Once it is cut off from the storm, it slowly decays, but the dissipation is slower than for an occluding cycle that is in negatively buoyant air that is breaking down the circulation. To summarize, only two members capture a cycle around the same time as the observed nonoccluding cycle, but the duration of the cycle 15–45 min longer than the observed and the mode of cycling is wrong.

The second observed cycle happens around 0010–0025 UTC and belongs to the mesocyclone that produced a very clear occluding cycle on radar (Fig. 4.7). Out of the overall 22 cycles that were identified in the forecast members for this supercell, only 7 of them were within the time frame of the observed cycle (Fig.5.9). There are several cycles that occur just outside the 0010–0025 UTC window, and overall the forecasts did a decent job grouping the cycles around the second observed cycle.

Compared to the Morton supercell, the Elk City supercell had fewer observed cycles. NEWS-e forecast members also produced fewer cycles throughout all of the forecast times examined. This suggests the potential for environmental difference between the two cases to be influencing the frequency of cyclic mesocyclogenesis in a way that NEWS-e can predict.

For the Corn supercell of May 18 2017, there were only two cases of occluding cyclic mesocyclogenesis in two out of the eighteen ensemble members (i.e. members 1 and 6 in Fig. 5.10). Recall, the Corn supercell had a total of nine identified mesocyclones (Fig. 4.11) in WSR-88D data, but the timing of these mesocyclones was well before the first forecast of NEWS-e (initialized at 2000 UTC). The cycles that occurred after 2000 UTC but before 2100 UTC were also not included because as stated in Section 3.2 the first hour of each NEWS-e forecast was ignored due to imbalance from data assimilation. Therefore, only three out of the nine mesocyclones were considered for the Corn Supercell. This may also explain why predictions of the Corn supercell exhibited low cycling frequencies, when in fact it cycled 8 times in observations (Figs. 5.2 and 5.10). Only observations from the last 90 min of the supercell were assimilated into NEWS-e, and so only the dissipation stage of the supercell was predicted by NEWS-e. If the Corn supercell would have occurred later in time, NEWS-e may have had a better representation of its evolution and the amount of cycling that was present.

On the other hand, the Hennessey supercell had the most cycles present in the NEWS-e forecast members over all four supercell cases. The Hennessey supercell had 5 identified mesocyclones and 4 occluding cycles observed in WSR-88D radar data. There were a total of 42 cycles between all members for all forecast times analyzed (i.e. 2000, 2100, 2200, and 2300 UTC forecasts). All of the observed cycles occurred within the times of 2130–2245 UTC. Looking at that time frame (2000 and 2100 UTC forecasts were used) to see how many forecasted cycles occurred, there were 16 across 13 members (Fig. 5.11). There were four observed cycles for this supercell, but only 3 ensemble members (members 13, 15, and 18 in Fig. 5.11) had two cycles occurring within the window of the four observed cycles. Therefore, none of the ensemble members caught a total of four cycles in the exact time period of the observed ones.

However, member 18 has a unique 2000 UTC forecast compared to the other ensemble members for the Hennessey supercell (Fig. 5.11). During the 2000 UTC forecast, member 18 produces a total of 4 cycles, which is the same amount that the observed storm produced. The timing of the cycles is displaced, to the point where only two of the four cycles happen during the time period that all four of the observed cycles were occurring. However, it is the only forecast member that produces four cycles like the observed storm did. The duration of the four cycles nearly matches that of the observations, as well. The exact reason why this member did better than all the others is unclear, but this member may have had a more favorable environment than the other members to produce such frequent cycling.

By first glance at Fig. 5.11, there seems to be a lot of cycles clustered in the middle of the figure, which corresponds to about 2300 UTC when the observed storm was producing its last mesocyclone. Looking at the time window of 2245–0000 UTC, there were 19 cases of cycling over all the members and the forecast times. NEWS-e seems to be predicting more cycling at the end of the Hennessey supercell's life, rather than at the beginning when the observed cycles occurred. The 19 cases of cycling are dispersed over nine ensemble members. Out of those nine, five of them produce two or more cycles in that time window, with member 18 producing five cycles. Even though there are more cycles at the end of the supercell's life, there are also less members forecasting this increased frequency of cycling. Therefore, more members are forecasting cycles for the time window where all of the observed cycles are occurring, except they have the frequency and the timing of the cycles wrong.

The cycling frequency for all of the supercells and how they compare with each other is given in Fig. 5.13. The two more frequently cycling cases in observations are the Morton and Hennessey supercells, and the less frequently cycling case is the Elk City supercell.

The Corn supercell may be considered a low-cycling supercell with the caveat that this storm was close to dissipating once NEWS-e was able to resolve its storm evolution. For the rapid-cycling supercells, there are more predicted cycles per hour in the ensemble forecasts though fewer than the observed cycles per hour for each supercell. For instance, the Hennessey supercell has a few ensemble forecasts that have predicted cycles per hour of 1, 1.5, and 2 that surpass the observed cycling frequency of 0.8 cycles per hour. This means that some of the ensemble forecasts were able to predict that this was a rapid-cycling supercell. Also, the Morton and Hennessey supercells have higher percentages of forecasts that cycle than the Elk City and Corn supercells, which had fewer observed cycles. The low-frequency cycling supercells have a larger number of forecasts that do not predict cycling (the blue bars in Fig. 5.13).

To summarize, 1-km NEWS-e forecasts predict the possibility of cycling for all four of the supercells, but show little skill in predicting the exact timing of those cycles compared with observations. Rapid-cycling supercells like the Morton and Hennessey supercells had more forecasts of cycling than did the infrequent cycling supercells. This suggests that there is a signal that NEWS-e is able to distinguish between supercells that have high cycling frequencies compared to those with more infrequent episodes of cyclic mesocyclogenesis. Also, the shift from 3-km grid spacing to 1-km spacing seems necessary to observe cyclic mesocyclogenesis. Even though there were a couple of cases of cycling-like behavior at 3 km, those cases only occurred for one day out of the 3 days analyzed (18 May 2017). Therefore, it is possible that something in the environment of NEWS-e for this day is triggering cycling at 3 km and not for the other days. Overall, cyclic mesocyclogenesis becomes more apparent at 1 km and potentially provides a forecast of the potential for what storms may exhibit cycling and which may not.

5.1.3 Supercell Evolution

Changing horizontal grid resolution also had an effect on the forecasts for storm evolution and mesocyclone duration. For three of the four supercells cases (Hennessey, Corn, and Elk City), some of the forecast members over-forecasted the longevity of the supercells' mesocyclones. For instance, the Elk City supercell didn't develop a mesocyclone until approximately 2230 UTC and dissipated at 0100 UTC. There are differences between the 3-km and 1-km forecasts on when the first mesocyclone formed and when this storm decayed in NEWS-e. For the 1-km forecasts, all but two members forecast the presence of a mesocyclone at the beginning of the forecast period, which is earlier than observations. At 3 km, there are nine members that forecast the presence of a mesocyclone at the beginning of the forecast period when one is not present in the observations. Therefore, 3-km forecasts have a better potential in forecasting the lack of a mesocyclone at the beginning of the forecast period similar to observations (Fig. 5.14).

There are three other situations in which there is no mesocyclone present in the observations but the 1-km and 3-km NEWS-e forecasts are predicting the presence of a mesocyclone (Fig. 5.14). This over-forecasting happens for the Hennessey (Fig. 5.11), Corn (Fig. 5.10), and Elk City (Fig. 5.9) supercells when the supercell decays in the observations, but the forecast members are still predicting mesocyclones when there is no longer a storm present. In all of these situations, the 1-km forecasts over-predict the presence of mesocyclones more than the 3-km forecasts (Fig. 5.14).

However, the are a few limitations to this result. First of all, the thresholds that are used to define a mesocyclone in NEWS-e data could change the numbers in Fig. 5.14. A vertical vorticity threshold of 0.005 s^{-1} was used to define and identify mesocyclones at 1-km grid spacings. The threshold was lowered slightly for 3-km to 0.004 s^{-1} in vertical vorticites. The results from Fig. 5.14 may change when these thresholds change. The exact sensitivities of this result to different mesocyclone thresholds would have to be studied in future work. Lastly, when comparing the 3-km and 1-km forecasts of storm evolution, we

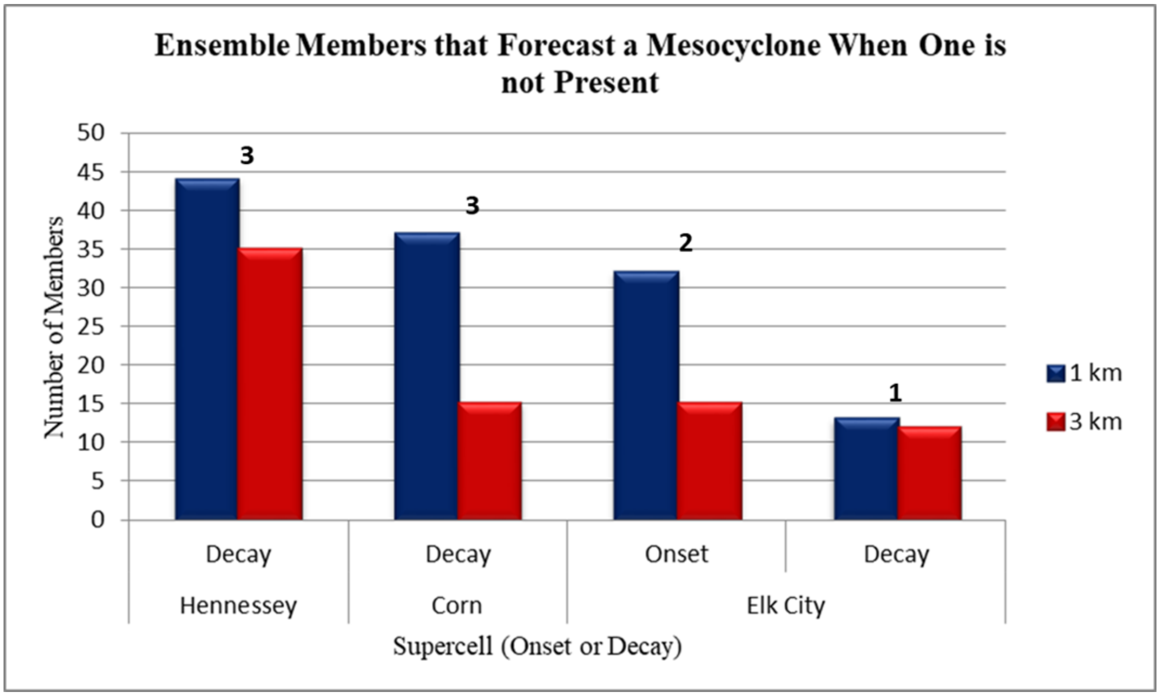

Figure 5.14: Bar chart of the ensemble members that forecast a mesocyclone when one is not present in observations. The numbers above the bars indicate the number of forecasts available (such as if the 2000 and 2100 UTC forecasts were available to look at the presence of a mesocyclone then there would be a 2). The higher the bars, the more forecast members that are over-predicting the presence of a mesocyclone. For all of the cases displayed, the 1-km forecasts over-predict the presence of a mesocyclone compared to 3-km forecasts.

are analyzing WSR-88D radar data that are assimilated into NEWS-e at 3 km and not 1 km. Therefore, it is not necessarily fair to say that 1-km forecasts perform worse than 3-km forecasts, unless we can analyze the results of assimilating 1-km WSR-88D on storm evolution. However, this result shows that when interpolating the 3-km analyses onto a 1-km grid, there may be an over-prediction of mesocyclones at 1 km compared to the same forecasts at 3 km.

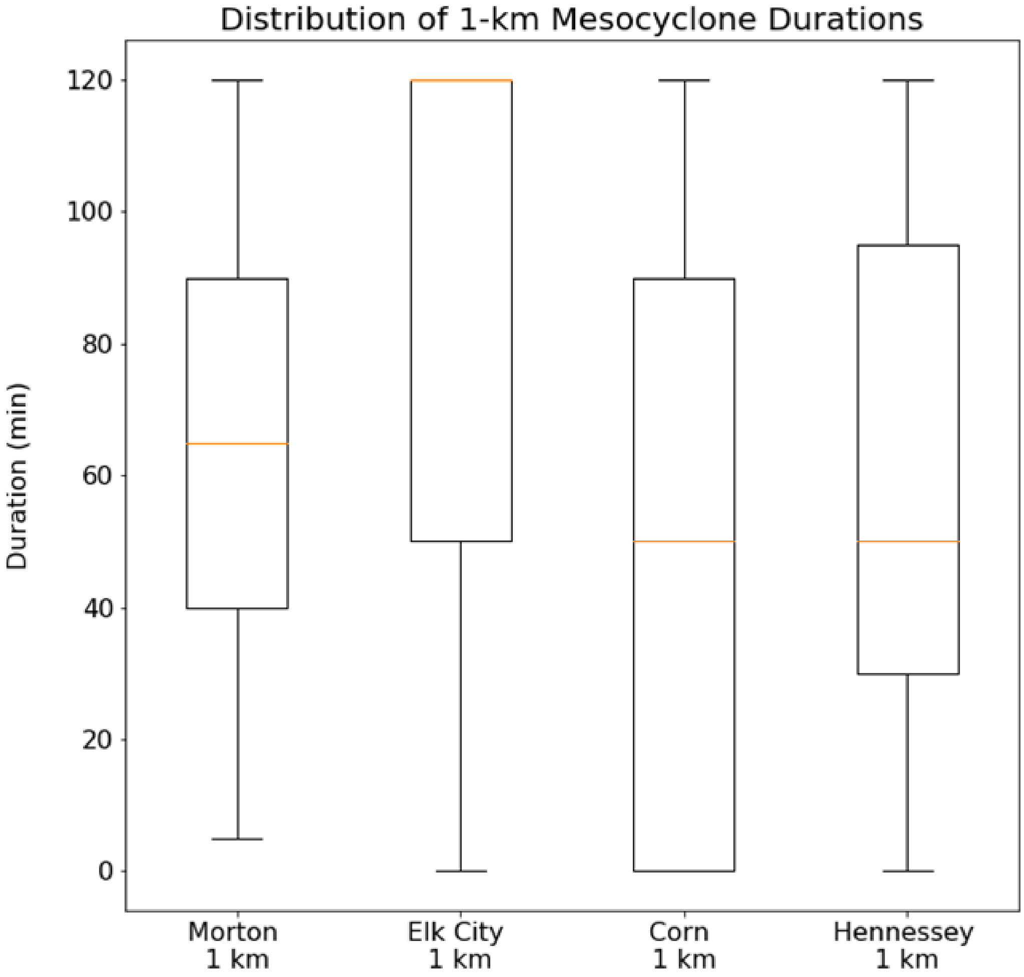

Figure 5.15: Similar to Fig. 5.12 but for mesocyclone duration for the 1-km NEWS-e forecasts.

Another factor sensitive to the horizontal grid spacing is mesocyclone duration. The 3-km summary figures show that usually a single, long-duration mesocyclone was predicted for the majority of the forecasts (Figs. 5.5, 5.6, 5.2, and 5.1). 1-km forecasts, on the other hand, were potentially able to resolve smaller-scale circulations than 3-km forecasts. This may be why the 1-km forecasts tended to predict more mesocyclones with shorter durations (Figs. 5.8, 5.9, 5.10, and 5.11). The distribution of all the mesocyclones' durations for the 1-km forecasts is given in Fig. 5.15). The Morton and Hennessey supercells that were considered rapid-cycling cases because they exhibited many cycles in both observations and in the forecasts, have lower medians for mesocyclone duration. On the other hand, the Elk City case that had only two cycles occurring in observations, has its median at 120 min. This means that the majority of the forecasts for the Elk City supercell are not cycling because they have the mesocyclone persisting for the full forecast time (120 min).

The Corn storm is an exception because it decayed early, so many of the forecasts were not predicting the presence of a mesocyclone (Fig. 5.10). Thus, this resulted in the median mesocyclone duration to be lower and the 25th percentile to be located at zero, which means there were many forecasts that did not predict the presence of a mesocyclone.

The Elk City supercell had the longest cycling durations (Fig. 5.12) and has the most forecasts that predict the presence of long-lived mesocyclones (Fig. 5.15). In observations, this supercell's second mesocyclone was long-lived and responsible for producing five tornadoes (Fig. 4.10), including the long-track, destructive Elk City tornado. Past research has found a balance between inflow and outflow that must exist to have favorable conditions for tornadogenesis (e.g. Dowell and Bluestein 2002b; Beck et al. 2006; French et al. 2008). When that balance does not exist, such as when the inflow dominates the outflow of the supercell, the storm usually has a faster cycling rate. In other words, if the storm is out of balance then the circulations are occluded much more readily. As a result, the mesocyclone is displaced from vorticity-rich air, causing it to lose the potential to produce long-lived tornadoes.

In WSR-88D radar observations, the Morton, Corn, and Hennessey supercells all produced many short-lived mesocyclones. This may have potentially contributed to fewer tornadoes than in the Elk City case. The tornadoes that were produced were weak and had very short durations. This fact also translates over to the NEWS-e 1-km forecasts, with the exception of the Corn storm. NEWS-e forecasts of the Morton and Hennessey supercells had shorter cycling durations (Fig. 5.12), higher cycling frequencies (Fig. 5.13), as well as shorter mesocyclone durations (Fig. 5.15). Hence, the majority of the predicted mesocyclones in these storms cycled, which is similar to storm observations. Forecasts of the Elk City supercell, however, had long cycle durations, long mesocyclone durations, and less cycles in general, and a majority of predicted mesocyclones that did not cycle. This, again, is similar to the observations for the Elk City storm. In conclusion, 1-km NEWS-e forecasts demonstrate the potential to discriminate between storms that cycle frequently versus infrequently or do not cycle in observations. If cyclic supercells that have lower cycling frequencies produce longer duration tornadoes, then NEWS-e may be helpful in determining which supercells have the potential for cycling and whether the cycling frequency of these storms may lead to an increased risk for long-track tornadoes.

5.2 Effects of PBL and Radiation Parameterizations

The second sensitivity experiment tested the effects of different physical parameterizations on both the 3-km and 1-km NEWS-e forecasts. There appeared to be no concrete relationships that would suggest a specific combination of PBL and radiation parameterizations would cause more or less cycling than another (Table 3.4). For example, there was no occurrence where using MYJ (or another parameterization) caused members to constantly be steady-state. A sample size of four supercells is also not sufficient enough to accurately test whether a combination of physical parameterizations will have the same effect (more, less, or no cycling) over all the forecasts with the same parameterizations. All forecast members went through equal periods of cycling and noncycling among all of the tested supercells. There was no PBL or radiation scheme that would consistently not cycle each time it was used. Therefore, there is no clear signal at this time that the parameterizations alone are impacting the forecasts of cyclic mesocyclogenesis. However, how the physical parameterizations modify the environment in conjunction with the initial and boundary conditions may have an impact. Future studies using idealized simulations may be needed to better test the relationship between parameterizations and cycling (if one exists).

5.3 Environmental Effects

Recalling from Adlerman and Droegemeier (2005), cyclic mesocyclogenesis was sensitive to environmental parameters, such as depth and magnitude of wind shear, and the curvature of the hodograph. One of the parameters analyzed in Adlerman and Droegemeier (2005) was SRH from 0–1 km (Fig. 2.6). According to this study, different values of SRH from 0–1 km were shown to have an impact on whether a storm cycles, and what mode of cyclic mesocyclogenesis occurs (Fig. 2.6). SRH in the 0–1 km layer is examined for both a frequent cycling (Hennessey supercell) and a infrequent cycling case (Elk City supercell) to analyze how the environments change between the cases if there is a resulting impact on cycling. The SRH values are taken from the near-storm and far-storm environments (Fig. 5.16) to estimate how the supercell is modifying the environment around it, as well as what the environment is like further away from the storm. The methodology being applied is a one-point system. In other words, only point in the model grid is chosen for the near- and far-storm environments. In the future, a method to pull all the data in the vicinity of the supercell should be used as to get a better representation of the distribution of the supercell environment. However, this method allows for a first examination of how the environments may affect both a frequent and infrequent cyclic supercell to see if there are any relationships.

First, the overall environments of the Elk City and the Hennessey supercells were compared to each other (Fig. 5.17). This was accomplished by taking three forecast times

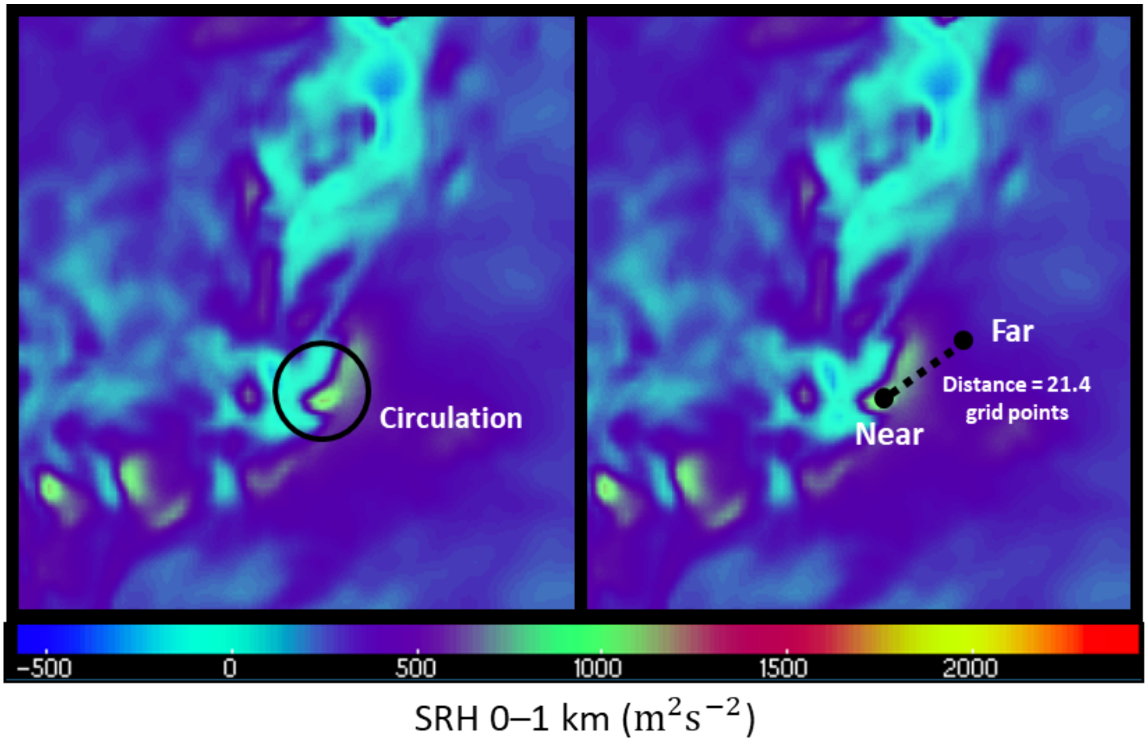

Figure 5.16: The black circle denotes the Hennessey supercell's circulation. These panels were taken from the 2100 UTC NEWS-e 1-km forecast at the time of 2200 UTC. The dots in the right panel show where the SRH values were taken to estimate the near-storm and far-storm environments. The near-storm point was in the circulation and the maximum value of SRH 0–1 km that occurred. The far-storm environment was chosen ahead of the expected path of the supercell and slightly to the south, which approximates the future inflow for the supercell.

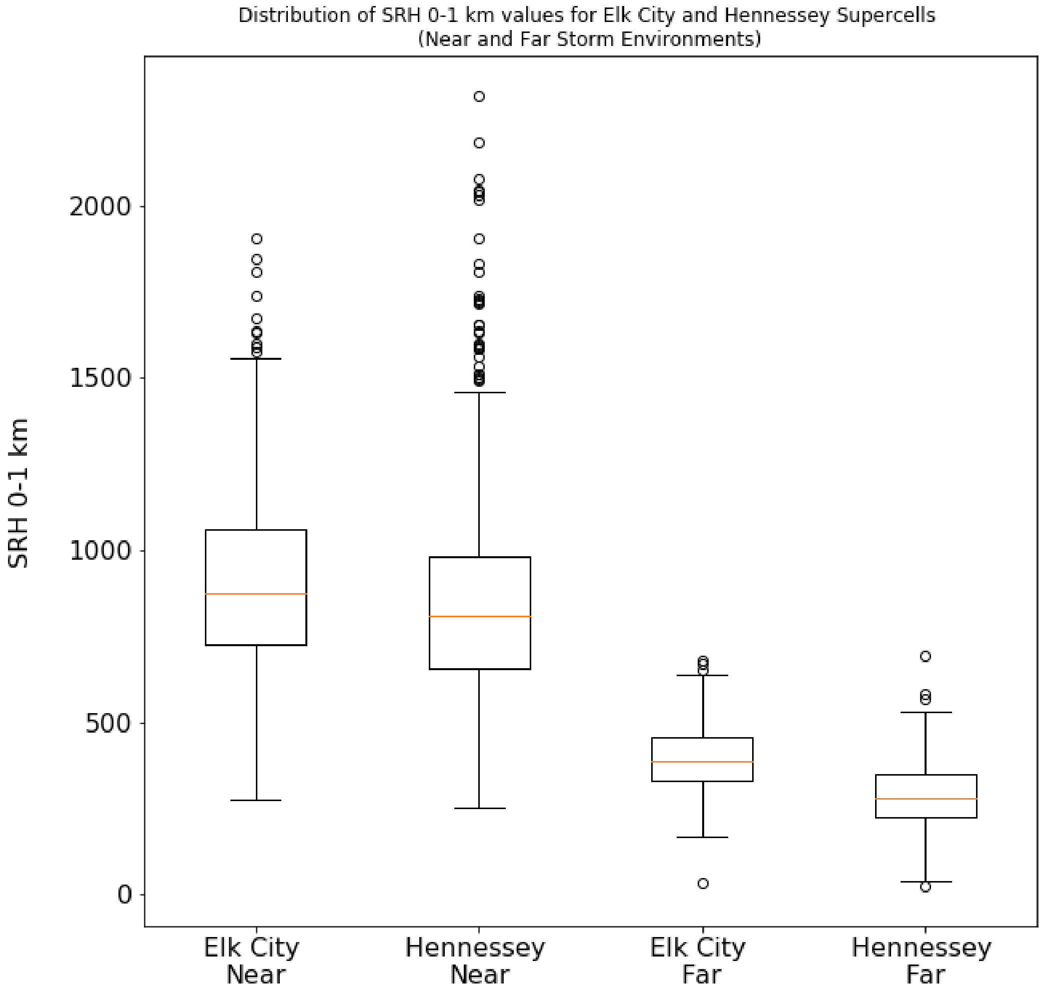

Figure 5.17: Box and whisker plots of the distribution of the SRH 0–1 km values in the near- and far-storm environments for both the Elk City and Hennessey supercells. The setup of the box and whisker plot is the same as in Fig. 5.12.

from each supercell and finding the SRH points. The forecast times used for the Hennessey supercell were the 2000, 2100, and 2200 UTC 1-km forecasts, while the 2100, 2200, and 2300 UTC 1-km forecasts were used for the Elk City supercell. The forecast times where chosen because that's when the most frequent cycling occurred and the supercell was still present during the forecast. For each forecast time, the first hour was ignored and then the SRH values were analyzed every 15 min. This method was performed for all 18 forecast members. The results of this process on the overall Elk City and Hennessey near- and far-storm environments are given in Fig. 5.17.

For the far-storm environment, the Elk City case has higher SRH 0–1 km values than the Hennessey case (Fig. 5.17). The Elk City supercell produced one long-lived mesocyclone that went on to produce five tornadoes (Fig. 4.10). The high SRH values in this supercell's environment are favorable for tornadogenesis to occur (Rasmussen and Blanchard 1998; Thompson et al. 2007). Higher values of SRH from 0–1 km coincided with storms that were noncycling in nature (Adlerman and Droegemeier 2005; Fig. 2.6). Hence, higher values of SRH 0–1 km may be why the Elk City storm cycled less frequently than the Hennessey supercell. The infrequent cycling may also suggest there was a balance between the inflow and outflow of the Elk City storm, which potentially led to the long-track second mesocyclone (Dowell and Bluestein 2002a; Beck et al. 2006; French et al. 2008). Having a balance between the inflow and outflow may have allowed the mesocyclone to become tornadic. Also, the large differences between the near- and far-storm environments means mesocyclones within these supercells were able to highly modify their immediate environments.

Similarly to examining the overall environment for each of the supercells, the SRH values were also broken down by cycling and noncycling members. Two forecast times were chosen for each supercell during the period of most frequent cycling. For the Hennessey supercell, the NEWS-e 1-km 2000 and 2100 UTC forecasts were used for both the near- and far-storm environments (Figs. 5.19 and 5.21). Comparably, the 2200 and 2300 UTC

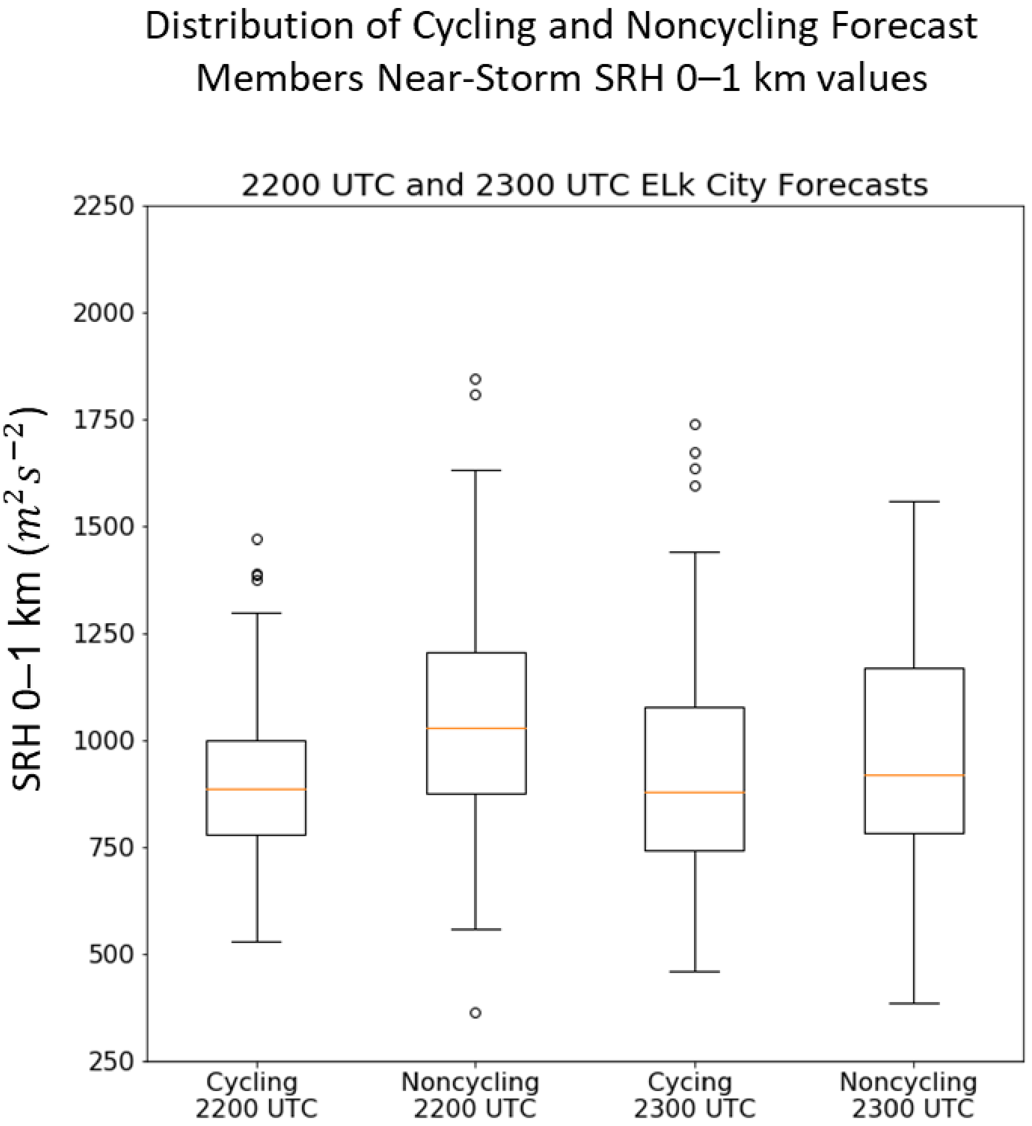

Total Members:	8	10	9	9
Total Cycles:	8		9	

Figure 5.18: Box and whisker plot with the same setup as in Fig. 5.17. The distribution of the SRH values for noncycling and cycling forecast members in the near-storm environment for the Elk City supercell. The total forecast members examined for each plot is given below the table. The total number of cycles observed in the 2100 and 2200 UTC forecasts are shown at the bottom of the figure.

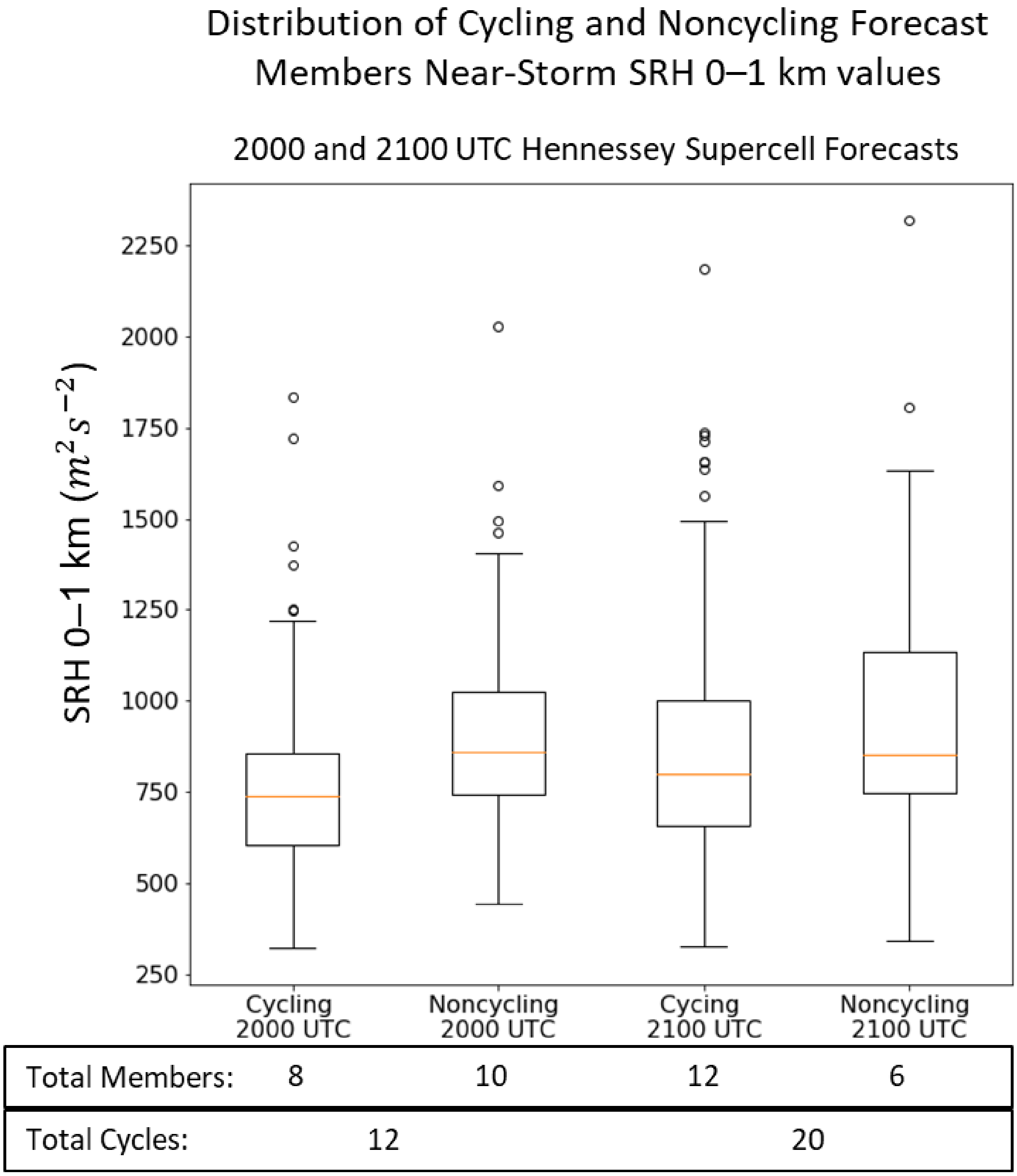

Total Members:	8	10	12	6
Total Cycles:	12		20	

Figure 5.19: Same as Fig. 5.18, but for the Hennessey supercell's near-storm environment in the 2000 and 2100 UTC forecasts.

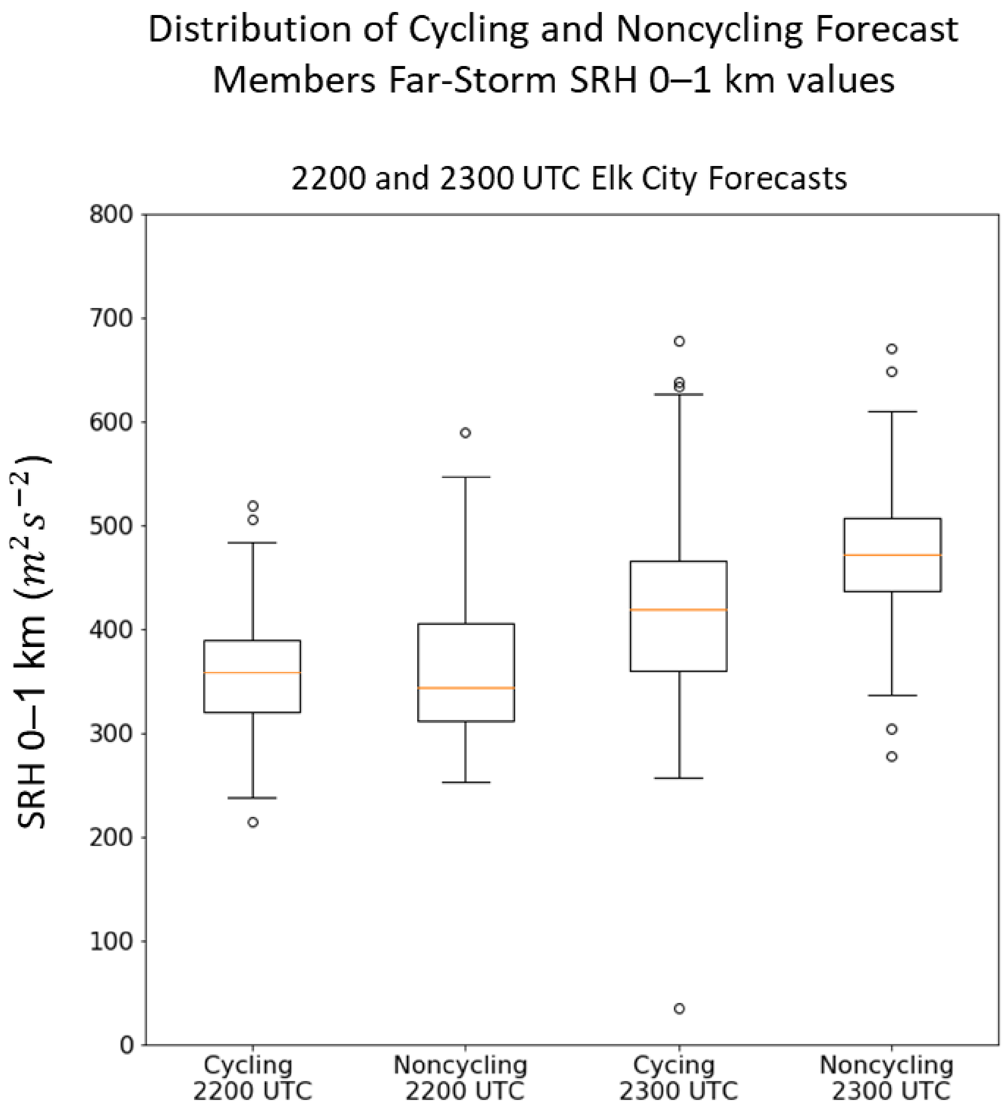

Total Members:	8	10	9	9
Total Cycles:	8		9	

Figure 5.20: Same as Fig. 5.18, but for the far-storm environment of the Elk City supercell.

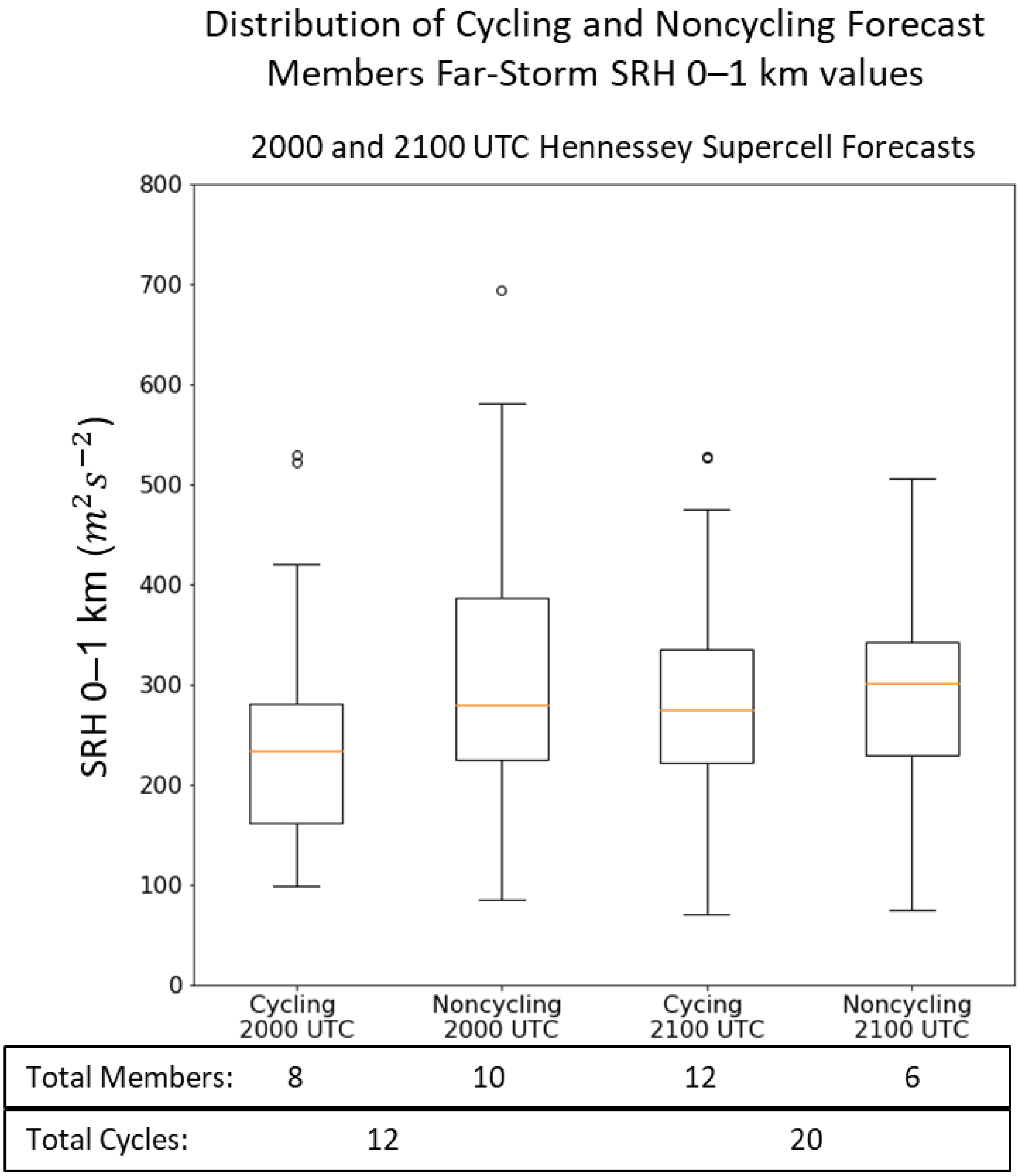

Total Members:	8	10	12	6
Total Cycles:	12		20	

Figure 5.21: Same as Fig. 5.19, but for the Hennessey supercell's far-storm environment.

forecasts were utilized for the Elk City supercell (Figs. 5.18 and 5.20). For the Elk City supercell, the near-storm (Fig. 5.18) and far-storm (Fig. 5.20) environments have higher SRH 0–1 km values for forecast members that do not cycle than those that exhibit cyclic mesocyclogenesis. The same is true for the Hennessey supercell (Figs. 5.19 and 5.21). This result suggests that the higher the SRH values, the more unlikely it is for the supercell to cycle.

In summary, environmental factors appear to impact whether or not a supercell goes through cyclic mesocyclogenesis. Examining the SRH 0–1 km values resulted in a relationship between SRH and whether a supercell cycles. The rapid-cycling Hennessey supercell had lower SRH values, whereas high SRH values was associated with the infrequently cycling Elk City supercell. Consequently, supercells in environments with higher SRH 0–1 km values appear to have a higher probability of less frequent cycling and potentially producing damaging tornadoes, such as in the case of the Elk City supercell. This result adds further evidence that frequently cycling supercells are less likely to produce long-lived tornadoes than infrequent cyclic supercells (Beck et al. 2006; French et al. 2008).

Chapter 6

Summary and Conclusions

The purpose of this study was to test the capability of a short-term (0–3 hr), storm-scale ensemble system (NEWS-e) to resolve and predict cyclic mesocyclogenesis, and whether this process is physically representative of the current understanding for cyclic supercells seen in past research (e.g. Burgess et al. 1982; Dowell and Bluestein 2002b; Adlerman et al. 1999). Cyclic supercells are a subset of supercells that produce multiple mesocyclones with similar life cycles through a process known as either occluding or nonoccluding cyclic mesocyclogenesis (Darkow and Roos 1970; Burgess et al. 1982; Adlerman et al. 1999; Adlerman and Droegemeier 2005). Simulating cyclic mesocyclogenesis has been found to be sensitive to the model's computational and physical parameters, as well as environmental conditions like depth and magnitude of wind shear (Adlerman and Droegemeier 2002, 2005). In Adlerman and Droegemeier (2002), the authors found that cyclic mesocyclogenesis was sensitive to horizontal grid resolution. They tested several grid spacings and found that any horizontal resolution coarser than 1 km did not exhibit cycling. This result suggested that the original 3-km grid spacing of NEWS-e would be too coarse to resolve or predict cycling, and would therefore need to be changed to a finer grid spacing of at least 1 km. Hence, the first sensitivity experiment in this study involved changing the horizontal resolution of NEWS-e from 3 km to 1 km. The second experiment dealt with examining whether NEWS-e physical parameterizations had any impact on cycling between the 18 ensemble members. The last experiment was based off Adlerman and Droegemeier (2005), and analyzed environmental impacts on cycling across different ensemble forecast members (Table 3.4).

Four cyclic supercells from three active severe weather days (all of which occurred in May 2017) were chosen to examine how NEWS-e resolved and predicted cyclic mesocyclogenesis. Radar reflectivity and radial velocities from WSR-88D data were analyzed to create an observational database for each of the four supercells to compare to the NEWS-e forecasts using subjective methods similar to Thompson et al. (2012) and Smith et al. (2012). The four supercells: Morton, Elk City, Corn, and Hennessey all exhibited multiple episodes of cyclic mesocyclogenesis, with the Elk City supercell being an example of a infrequent cycling case and the other three supercells being frequent cycling cases. The Elk City and Corn supercells were unique in that they exhibited both forms of cycling, with the nonoccluding cycles preceding all of the occluding cycles. The other two supercells only had occluding cycles.

Although results from the Adlerman and Droegemeier (2002) study suggested that cycling would not be observed at horizontal grid spacings of 3 km, NEWS-e did produce a few clear cases of cyclic mesocyclogenesis-like processes at 3 km (Fig. 5.3). The 3-km grid spacing is too coarse to fully resolve the small-scale processes attributed to cyclic mesocyclogenesis (e.g. the surging of the rear-flank gust front due to enhanced westerly momentum at the surface), but the evolution of predicted mesocyclones share many similarities to observed cyclic mesocyclogenesis. Those similarities include the mesocyclone being undercut and surrounded by downdraft air, and then being swept to the left of storm motion where it decays in the heavy precipitation region of the supercell (Fig. 5.3). This process is nearly identical to that seen in WSR-88D data of occluding cyclic mesocyclogenesis (Fig. 4.7).

When the grid spacing of NEWS-e was decreased to 1 km, cyclic mesocyclogenesis became more frequent. Forecast members exhibiting more than one cycle during a particular forecast time were more common than that seen at 3-km grid spacings. Supercells that had many observed mesocyclones tended to have more forecasted cycles throughout all their forecast members and forecast times (i.e. the Morton and Hennessey supercells).

Therefore, there was evidence that NEWS-e could distinguish between cases that generated many episodes of cyclic mesocyclogenesis and those that did not. Additionally, NEWS-e was able to forecast the possibility for cyclic supercells to occur for all three of the days analyzed. However, NEWS-e did not accurately predict the exact timing of the cycles compared to observations. From a predictability standpoint and for the cases examined, NEWS-e shows potential to provide forecasters with situational awareness on the potential for cyclic supercells on a given day, but it has little to no skill in predicting timing of those cycles.

Varying PBL and radiation parameterizations showed no correlation with cycling frequency. There were no cases in which the parameterizations caused ensemble members to consistently vary in cycling likelihood or frequency. Each combination of physical parameterizations had a roughly equal number of times were it would predict cycling (whether occluding or nonoccluding) and wouldn't cycle at all. However, the YSU and RRTM schemes seemed to have some repeated regeneration of cycles than the other schemes. The effects of physical parameterizations alone on the cycling process is unknown, but doesn't seem to have any notable implications.

Finally, Adlerman and Droegemeier (2005) also showed evidence of cyclic mesocyclogenesis being sensitive to environmental parameters such as wind shear and the curvature of the hodograph. In this study, environmental differences were also seen to have an impact on whether a supercell cycles. SRH 0–1 km was analyzed for the Elk City and Hennessey supercells to examine if environmental differences possibly caused two supercells to have different cycling frequencies. The infrequent cycling case of the Elk City supercell had higher overall SRH 0–1 km values than the rapid-cycling case of the Hennessey supercell. Also, when separating the SRH values for the noncycling and cycling forecast members, noncycling members for both supercells had higher SRH values than the members that cycled. This result suggests that cyclic mesocyclogenesis is indeed sensitive to environmental parameters, like SRH from 0–1 km, and could potentially be used to forecast which supercells may exhibit cyclic mesocyclogenesis and which do not.

6.1 Future Research

As with any research, this project has many limitations and caveats. First, there will always be errors when analyzing model simulations, due to data assimilation, parameterizations used, model equations, initial and boundary conditions, etc. Also, the sample size for this project was small, at just four cases of cyclic supercells owing to having to perform a manual analysis of both WSR-88D radar data and of the NEWS-e forecasts. A small sample size limits the conclusions we can confidently draw from this study, but provides insight on the direction for future studies that build on this work. Third, the number of mesocyclones identified may be sensitive to radar sampling resolution. Therefore, the number of mesocyclones may be under-sampled by WSR-88D, owing to its 1° beam width. There exists high-resolution observational studies of cyclic mesocyclogenesis (Beck et al. 2006; French et al. 2008) that are able to identify many smaller-scale mesocyclones that would not be seen on WSR-88D radar. A future study could examine the amount of mesocyclones seen on WSR-88D radar and compare them to what is observed in mobile radar data to analyze the extent at which information is lost. Additionally, the number of simulated mesocyclones may be sensitive to the thresholds that were set to define a mesocyclone, which may change the total number of mesocyclones and cycling that were forecasted. Thus, the extent of these sensitivities should be tested in the future.

Future studies testing a variety of aspects of this project will need to be conducted. For instance, due to time constraints, examination of the full environmental effects on cycling from the different ensemble member environments was limited. Environmental effects, such as the environmental wind profile, are shown to be very important in effecting cyclic mesocyclogenesis. Also, the PBL and radiation schemes alone did not show any strong signal of affecting cyclic mesocyclogenesis. However, how these parameterizations affect each member's environment which, in turn, affects cycling will need to be examined. One approach is to conduct a series of idealized simulations of the different combinations of PBL and radiation schemes used by NEWS-e. That way the direct impacts of changing combinations of physical parameterizations can be seen without all the effects from other aspects of the system.

As observed in WSR-88D radar data, there were two supercells (Elk City and Corn) that exhibited both modes of cyclic mesocyclogenesis. The cause of the transition between nonoccluding and occluding modes has not been studied, but could be examined more in the future.

One possible outcome for this research is to create an automated system that is able to detect and track supercells that exhibit cyclic characteristics. This will make it possible to analyze larger samples of supercells and identify any trends or relationships that may occur. Also, this research, as well as previous research (Dowell and Bluestein 2002b; Beck et al. 2006; French et al. 2008), have hinted at rapid-cycling supercells having lower probabilities for tornadogenesis. This is due to the fact that rapid-cycling supercells have many short-lived mesocyclones that occlude more rapidly. These circulations are disconnected from the updraft and source of vorticity-rich air, which makes them less likely to form long-lived tornadoes. For example, the Corn, Hennessey, and Morton supercells examined in this project were all rapid-cycling cases that produced few if any tornadoes. The tornadoes that were produced were often weak and did little damage to their surroundings (most rated EF0). On the other hand, infrequent cycling cases like the Elk City supercell have a higher probability in producing dangerous, long-lived tornadoes. These supercells often have longer-lived mesocyclones that move with storm motion and stay within the vorticity-rich air. If the conditions are favorable, this can lead to tornadogenesis. The Elk City supercell only produced three mesocyclones, the second of which produced five tornadoes that were relatively long-lived compared to the other supercells. Having an automated system to track these storms would allow a larger dataset of both frequent and infrequent cycling supercells to be examined. With a large dataset, it may be possible to see a significant relationship between cycling frequency and the number of tornadoes produced.

If a large sample size of cyclic supercells can be gathered, then there may be enough data to design a NEWS-e forecast parameter that can calculate the potential of cycling in supercells. If there is a relationship between cycling frequency and tornado production, then this forecast parameter may be able to offer guidance to forecasters on the tornado probability for cyclic supercells.

Bibliography

Adlerman, E. J. and K. K. Droegemeier, 2002: The sensitivity of numerically simulated cyclic mesocyclogenesis to variations in model physical and computational parameters. *Mon. Wea. Rev.*, **130**, 2671–2691.

Adlerman, E. J. and K. K. Droegemeier, 2005: The dependence of numerically simulated cyclic mesocyclogenesis upon environmental vertical wind shear. *Mon. Wea. Rev.*, **133**, 3595–3623, doi:10.1175/MWR3039.1.

Adlerman, E. J., K. K. Droegemeier, and R. Davies-Jones, 1999: A numerical simulation of cyclic mesocyclogenesis. *J. Atmos. Sci.*, **56**, 2045–2069.

Anderson, J., T. Hoar, K. Raeder, H. Liu, N. Collins, R. Torn, and A. Avellano, 2009: The Data Assimilation Research Testbed: A community facility. *Bull. Amer. Meteor. Soc.*, **90**, 1283–1296.

Anderson, J. L. and N. Collins, 2007: Scalable implementations of ensemble filter algorithms for data assimilation. *J. Atmos. Oceanic Technol.*, **24**, 1452–1463, doi: 10.1175/JTECH2049.1.

Beck, J. R., J. L. Schroeder, and J. M. Wurman, 2006: High-resolution dual-doppler analyses of the 29 May 2001 Kress, Texas, cyclic supercell. *Mon. Wea. Rev.*, **134**, 3125–3148, doi:10.1175/MWR3246.1.

Brooks, H. E. and R. B. Wilhelmson, 1993: Hodograph curvature and updraft intensity in numerically modeled supercells. *J. Atmos. Sci.*, **50**, 1824–1833.

Brown, R. A., V. T. Wood, R. M. Steadham, R. R. Lee, B. A. Flickinger, and D. Sirmans, 2005: New WSR-88D volume coverage pattern 12: Results of field tests. *Wea. Forecasting*, **20**, 385–393.

Bryan, G. H., J. C. Wyngaard, and J. M. Fritsch, 2003: Resolution requirements for the simulation of deep moist convection. *Mon. Wea. Rev.*, **131**, 2394–2416.

Bunkers, M. J., 2002: Vertical wind shear associated with left-moving supercells. *Wea. Forecasting*, **17**, 845–855.

Burgess, D. W., V. T. Wood, and R. A. Brown, 1982: Mesocyclone evolution statistics. *12th Conf. on Severe Local Storms*, **Preprints**, 422–424.

Craven, J. P., R. E. Jewell, and H. E. Brooks, 2002: Comparison between observed convective cloud-base heights and lifting condensation level for two different lifted parcels. *Wea. Forecasting*, **17**, 885–890.

Darkow, G. L. and J. C. Roos, 1970: Multiple tornado producing thunderstorms and their apparent cyclic variations in intensity. *14th Conf. on Radar Meteorology*, **Preprints**, 305–308.

Davies-Jones, R., 1984: Streamwise vorticity: The origin of updraft rotation in supercell storms. *J. Atmos. Sci.*, **41**, 2991–3006.

Dowell, D. C. and H. B. Bluestein, 2002a: The 8 June 1995 McLean, Texas, storm. Part I: Observations of cyclic tornadogenesis. *Mon. Wea. Rev.*, **130**, 2626–2648.

Dowell, D. C. and H. B. Bluestein, 2002b: The 8 June 1995 McLean, Texas, storm. Part II: Cyclic tornado formation, maintenance, and dissipation. *Mon. Wea. Rev.*, **130**, 2649–2670.

French, M. M., H. B. Bluestein, D. C. Dowell, L. J. Wicker, M. R. Kramar, and A. L. Pazmany, 2008: High-resolution, mobile doppler radar observations of cyclic mesocyclogenesis in a supercell. *Mon. Wea. Rev.*, **136**, 4997–5016, doi:10.1175/2008MWR2407.1.

French, M. M., H. B. Bluestein, I. PopStefanija, C. A. Baldi, and R. T. Bluth, 2013: Reexamining the vertical development of tornadic vortex signatures in supercells. *Mon. Wea. Rev.*, **141**, 4576–4601, doi:10.1175/MWR-D-12-00315.1.

Fujita, T. T., D. L. Bradbury, and C. F. V. Thullenar, 1970: PALM SUNDAY tornadoes of APRIL 11, 1965. *Mon. Wea. Rev.*, **98**, 29–69.

Heinselman, P. L., D. L. Priegnitz, K. L. Manross, T. M. Smith, and R. W. Adams, 2008: Rapid sampling of severe storms by the National Weather Radar Testbed Phased Array radar. *Wea. Forecasting*, **23**, 808–824, doi:10.1175/2008WAF2007071.1.

Heinselman, P. L. and S. M. Torres, 2011: High-temporal-resolution capabilities of the National Weather Radar Testbed Phased-Array radar. *J. Appl. Meteor. Climatol.*, **50**, 579–593, doi:10.1175/2010JAMC2588.1.

Jones, T. A., K. Knopfmeier, D. Wheatley, G. Creager, P. Minnis, and R. Palikonda, 2016: Storm-scale data assimilation and ensemble forecasting with the NSSL Experimental Warn-on-Forecast system. Part ii: Combined radar and satellite data experiments. *Wea. Forecasting*, **31**, 297–327, doi:10.1175/WAF-D-15-0107.1.

Klemp, J. B. and R. Rotunno, 1983: A study of the tornadic region within a supercell thunderstorm. *J. Atmos. Sci.*, **40**, 359–377.

Lemon, L. R. and C. A. Doswell, 1979: Severe thunderstorm evolution and mesocyclone structure as related to tornadogenesis. *Mon. Wea. Rev.*, **107**, 1184–1197.

Mansell, E. R., C. L. Ziegler, and E. C. Bruning, 2010: Simulated electrification of a small thunderstorm with two-moment bulk microphysics. *J. Atmos. Sci.*, **67**, 171–194, doi:10.1175/2009JAS2965.1.

Markowski, P. M., 2002: Hook echoes and rear-flank downdrafts: A review. *Mon. Wea. Rev.*, **130**, 852–876.

Markowski, P. M. and Y. P. Richardson, 2014: The influence of environmental low-level shear and cold pools on tornadogenesis: Insights from idealized simulations. *J. Atmos. Sci.*, **71**, 243–275, doi:10.1175/JAS-D-13-0159.1.

Markowski, P. M., J. M. Straka, and E. N. Rasmussen, 2002: Direct surface thermodynamic observations within the rear-flank downdrafts of nontornadic and tornadic supercells. *Mon. Wea. Rev.*, **130**, 1692–1721.

Marquis, J., Y. Richardson, P. Markowski, J. Wurman, K. Kosiba, and P. Robinson, 2016: An investigation of the Goshen County, Wyoming, tornadic supercell of 5 June 2009 using EnKF assimilation of mobile Mesonet and radar observations collected during VORTEX2. Part II: Mesocyclone-scale processes affecting tornado formation, maintenance, and decay. *Mon. Wea. Rev.*, **144**, 3441–3463.

Potvin, C. K., K. L. Elmore, and S. J. Weiss, 2010: Assessing the impacts of proximity sounding criteria on the climatology of significant tornado environments. *Wea. Forecasting*, **25**, 921–930, doi:10.1175/2010WAF2222368.1.

Potvin, C. K. and M. L. Flora, 2015: Sensitivity of idealized supercell simulations to horizontal grid spacing: Implications for Warn-on-Forecast. *Mon. Wea. Rev.*, **143**, 2998–3024, doi:10.1175/MWR-D-14-00416.1.

Rasmussen, E. N. and D. O. Blanchard, 1998: A baseline climatology of sounding-derived supercell and tornado forecast parameters. *Wea. Forecasting*, **13**, 1148–1164.

Rotunno, R. and J. Klemp, 1985: On the rotation and propagation of simulated supercell thunderstorms. *J. Atmos. Sci.*, **42**, 271–292.

Rotunno, R. and J. B. Klemp, 1982: The influence of the shear-induced pressure gradient on thunderstorm motion. *Mon. Wea. Rev.*, **110**, 136–151.

Schwartz, C. S., G. S. Romine, K. R. Fossell, R. A. Sobash, and M. L. Weisman, 2017: Toward 1-km ensemble forecasts over large domains. *Mon. Wea. Rev.*, **145**, 2943–2969, doi:10.1175/MWR-D-16-0410.1.

Skamarock, W., J. Klemp, J. Dudhia, D. Gill, D. Barker, W. Wang, X.-Y. Huang, and M. Duda, 2008: A description of the advanced research WRF version 3. Tech. rep., UCAR/NCAR. doi:10.5065/D68S4MVH.

Skamarock, W. C., 2004: Evaluating mesoscale NWP models using kinetic energy spectra. *Mon. Wea. Rev.*, **132**, 3019–3032, doi:10.1175/MWR2830.1.

Skinner, P. S., et al., 2018: Object-based verification of a prototype Warn-on-Forecast system. *Wea. Forecasting*, doi:10.1175/WAF-D-18-0020.1.

Smith, B. T., T. E. Castellanos, A. C. Winters, C. M. Mead, A. R. Dean, and R. L. Thompson, 2013: Measured severe convective wind climatology and associated convective modes of thunderstorms in the contiguous United States, 2003–09. *Wea. Forecasting*, **28**, 229–236, doi:10.1175/WAF-D-12-00096.1.

Smith, B. T., R. L. Thompson, A. R. Dean, and P. T. Marsh, 2015: Diagnosing the conditional probability of tornado damage rating using environmental and radar attributes. *Wea. Forecasting*, **30**, 914–932, doi:10.1175/WAF-D-14-00122.1.

Smith, B. T., R. L. Thompson, J. S. Grams, C. Broyles, and H. E. Brooks, 2012: Convective modes for significant severe thunderstorms in the contiguous United States. Part I: Storm classification and climatology. *Wea. Forecasting*, **27**, 1114–1135, doi:10.1175/WAF-D-11-00115.1.

Snyder, C. and F. Zhang, 2003: Assimilation of simulated doppler radar observations with an Ensemble Kalman Filter*. *Mon. Wea. Rev.*, **131**, 1663–1677, doi:10.1175//2555.1.

Stensrud, D. J. and J. Gao, 2010: Importance of horizontally inhomogeneous environmental initial conditions to ensemble storm-scale radar data assimilation and very short-range forecasts. *Mon. Wea. Rev.*, **138**, 1250–1272, doi:10.1175/2009MWR3027.1.

Stensrud, D. J., et al., 2009: Convective-scale Warn-on-Forecast System: A vision for 2020. *Bull. Amer. Meteor. Soc.*, **90**, 1487–1500, doi:10.1175/2009BAMS2795.1.

Stensrud, D. J., et al., 2013: Progress and challenges with Warn-on-Forecast. *Atmos. Res.*, **123**, 2–16, doi:10.1016/j.atmosres.2012.04.004.

Tanamachi, R. L. and P. L. Heinselman, 2016: Rapid-scan, polarimetric observations of central Oklahoma severe storms on 31 May 2013. *Wea. Forecasting*, **31**, 19–42.

Thompson, R. L., R. Edwards, J. A. Hart, K. L. Elmore, and P. Markowski, 2003: Close proximity soundings within supercell environments obtained from the rapid update cycle. *Weather and Forecasting*, **18**, 1243–1261.

Thompson, R. L., C. M. Mead, and R. Edwards, 2007: Effective storm-relative helicity and bulk shear in supercell thunderstorm environments. *Wea. Forecasting*, **22**, 102–115, doi:10.1175/WAF969.1.

Thompson, R. L., B. T. Smith, J. S. Grams, A. R. Dean, and C. Broyles, 2012: Convective modes for significant severe thunderstorms in the contiguous United States. Part II: Supercell and QLCS tornado environments. *Wea. Forecasting*, **27**, 1136–1154, doi:10.1175/WAF-D-11-00116.1.

Thompson, R. L., et al., 2017: Tornado damage rating probabilities derived from WSR-88d data. *Wea. Forecasting*, **32**, 1509–1528, doi:10.1175/WAF-D-17-0004.1.

Tong, M. and M. Xue, 2005: Ensemble Kalman Filter assimilation of doppler radar data with a compressible nonhydrostatic model: OSS experiments. *Mon. Wea. Rev.*, **133**, 1789–1807, doi:10.1175/MWR2898.1.

Weisman, M. L. and R. Rotunno, 2000: The use of vertical wind shear versus helicity in interpreting supercell dynamics. *J. Atmos. Sci.*, **57**, 1452–1472.

Wheatley, D. M., K. H. Knopfmeier, T. A. Jones, and G. J. Creager, 2015: Storm-scale data assimilation and ensemble forecasting with the NSSL Experimental Warn-on-Forecast System. Part I: Radar data experiments. *Wea. Forecasting*, **30**, 1795–1817, doi:10.1175/WAF-D-15-0043.1.

Wheatley, D. M., N. Yussouf, and D. J. Stensrud, 2014: Ensemble Kalman Filter analyses and forecasts of a severe mesoscale convective system using different choices of microphysics schemes. *Mon. Wea. Rev.*, **142**, 3243–3263, doi:10.1175/MWR-D-13-00260.1.

Wicker, L. J. and R. B. Wilhelmson, 1995: Simulation and analysis of tornado development and decay within a three-dimensional supercell thunderstorm. *J. Atmos. Sci.*, **52**, 2675–2703.

Wurman, J., J. Straka, E. Rasmussen, M. Randall, and A. Zahrai, 1997: Design and deployment of a portable, pencil-beam, pulsed, 3-cm Doppler radar. *J. Atmos. Oceanic Technol.*, **14**, 1502–1512.

Yussouf, N., E. R. Mansell, L. J. Wicker, D. M. Wheatley, and D. J. Stensrud, 2013: The Ensemble Kalman Filter analyses and forecasts of the 8 May 2003 Oklahoma City tornadic supercell storm using single- and double-moment microphysics schemes. *Mon. Wea. Rev.*, **141**, 3388–3412, doi:10.1175/MWR-D-12-00237.1.

Yussouf, N. and D. J. Stensrud, 2010: Impact of Phased-Array radar observations over a short assimilation period: Observing system simulation experiments using an Ensemble Kalman Filter. *Mon. Wea. Rev.*, **138**, 517–538, doi:10.1175/2009MWR2925.1.